Διιδρυματικό Πρόγραμμα Μεταπτυχιακών Σπουδών

«Μοριακή Κυτταρική Βιολογία και Βιοτεχνολογία»

Πανεπιστήμιο Ιωαννίνων

Εργαστήριο Βιολογίας, Τμήμα Ιατρικής, Πανεπιστήμιο Ιωαννίνων

Διατριβή Μεταπτυχιακής Ειδίκευσης

"Spindle organization through kinesin-dependent tubulin transport"

Student: **Symeon Georgios Nadalis - Molecular Biologist and Geneticist**

Supervisor: **Dimitris Liakopoulos, Assistant Professor, Biology, Dept. Medicine, University of Ioannina; Group Leader, CRBM, Montpellier**

Lab of spindle positioning and organization, Centre de Recherche en Biologie cellulaire de Montpellier (CRBM) – CNRS

Montpellier - France, 2021-2022

Contents

Acknowledgements

Περίληψη

Οι κινησίνες είναι "μοριακές μηχανές", οι οποίες κινούνται κατά μήκος των μικροσωληνίσκων και συμμετέχουν στη μεταφορά διαφόρων συστατικών (πρωτεΐνες, οργανίδια, χρωμοσώματα) μέσα στο κύτταρο. Εκτός από τη μεταφορά συστατικών, ορισμένες από αυτές μπορούν να ρυθμίζουν και τη δυναμική των μικροσωληνίσκων. Η ανάπτυξη μικροσωληνίσκων ευνοείται παρουσία συγκεκριμένων κινησινών, ωστόσο είναι σπάνιες οι περιπτώσεις στις οποίες η ανάπτυξη αυτή οφείλεται στη μεταφορά διμερών τουμπουλίνης στο αναπτυσσόμενο άκρο. Στη συγκεκριμένη μελέτη παρουσιάζεται ότι η κινησίνη Kip2 του *S. cerevisiae* προάγει την ανάπτυξη μικροσωληνίσκων μέσω μιας περιοχής στο Ν-τελικό άκρο, η οποία δε διαθέτει δευτεροταγή δομή και προηγείται της επικράτειας της ATPάσης. Όταν αυτή η περιοχή αφαιρείται, η ανάπτυξη των μικροσωληνίσκων παρεμποδίζεται. Επιπλέον, προκαταρκτικά δεδομένα δείχνουν ότι η περιοχή αυτή είναι σε θέση να προσδέσει και να μεταφέρει ελεύθερα διμερή τουμπουλίνης. Τα αποτελέσματα αυτά υποδεικνύουν ότι η Kip2 προάγει την ανάπτυξη των μικροσωληνίσκων μέσω μεταφοράς διμερών τουμπουλίνης στο (+) άκρο των μικροσωληνίσκων. Γνωρίζοντας ότι η συγκεκριμένη πρωτεΐνη συμμετέχει στην οργάνωση της μιτωτικής ατράκτου στον *S. cerevisiae*, τα αποτελέσματα αυτά πιθανό να αποκαλύψουν ένα καινούριο μηχανισμό για μια μιτωτική κινησίνη.

Abstract

Kinesins are molecular motors that facilitate transport of different components (proteins, organelles, chromosomes) across the cell, using microtubules as tracks. Apart from their role in cargo transportation, some kinesins also regulate microtubule dynamics. Microtubule growth can be favoured in presence of specific kinesins, but examples of kinesins promoting microtubule growth by transferring tubulin dimers to the growing end are very rare. Here, we report that the *S. cerevisiae* kinesin Kip2 promotes microtubule growth by an unstructured, N-terminus region, preceding the motor domain. When this region is removed, microtubule growth is impaired. Moreover, preliminary data show that this unstructured region can bind and transport free tubulin dimers. These results, combined, imply that Kip2 promotes microtubule growth by transportation of tubulin dimers to the plus end of growing microtubules. Since Kip2 participates in spindle organization of *S. cerevisiae*, these results may uncover a mechanism unprecedented for a mitotic kinesin.

Introduction

Cytoskeleton - brief reference at its constituents and functions

Cytoskeleton is defined as "a system of filaments or fibres that it is present in the cytoplasm of eukaryotic cells" (Britannica, 2021). Until recently, it was thought that the cytoskeleton was composed of three components, actin filaments, microtubules and intermediate filaments, as shown in **Figure 1** (Pollard et al., 2017). However, recent studies point out the existence of a fourth cytoskeletal component, the septins (**Figure 2**) (Mostowy & Cossart, 2012). Each cytoskeletal component is a polymer made of its distinct structural elements. For example, actin filaments occur from polymerization of globular actin (G-actin), as shown in **Figure 3**, and microtubules from polymerization of (mainly) αβ-tubulin heterodimers (Pollard et al., 2017). These polymers can depolymerize back to their structural elements. Cells take advantage of this property and dynamically control polymerization, depolymerization and stability of each cytoskeletal component, based on their needs (Lodish et al., 2016).
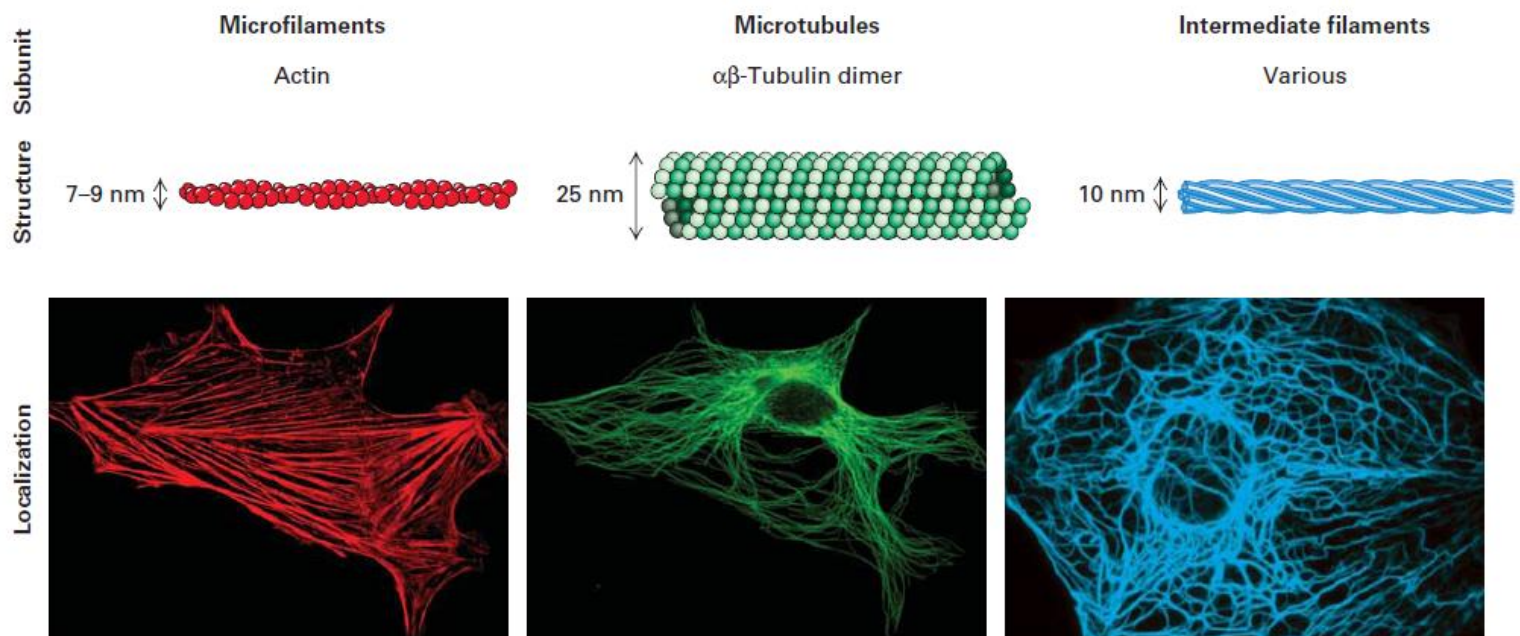
Figure 1. Top; Cartoons depicting the structure of the 3 cytoskeletal components. Bottom; Localization of each cytoskeletal component in cultured cells, using immunofluorescence microscopy. Actin filaments are shown in red, microtubules in green and intermediate filaments in blue. Figure adopted from Lodish et al. (2016).
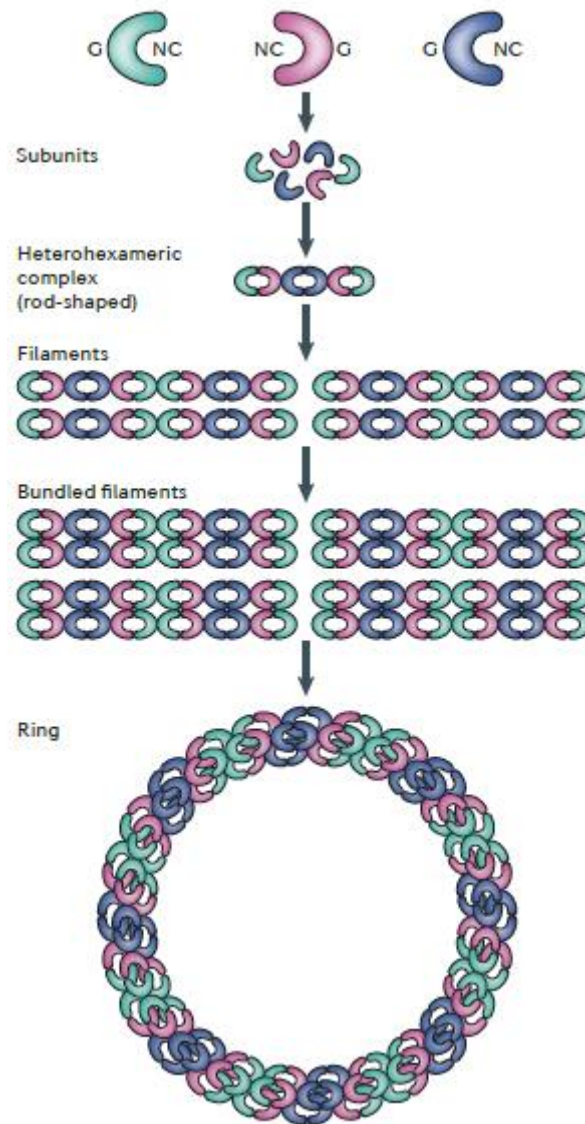
Figure 2. Assembly of septin cytoskeleton. Different septin proteins (top) interact with each other and assemble a heterohexameric complex (middle). That complex is the structural unit, which then polymerizes into filaments, bundled filaments or rings (middle and bottom). Figure adopted from Mostowy & Cossart (2012).
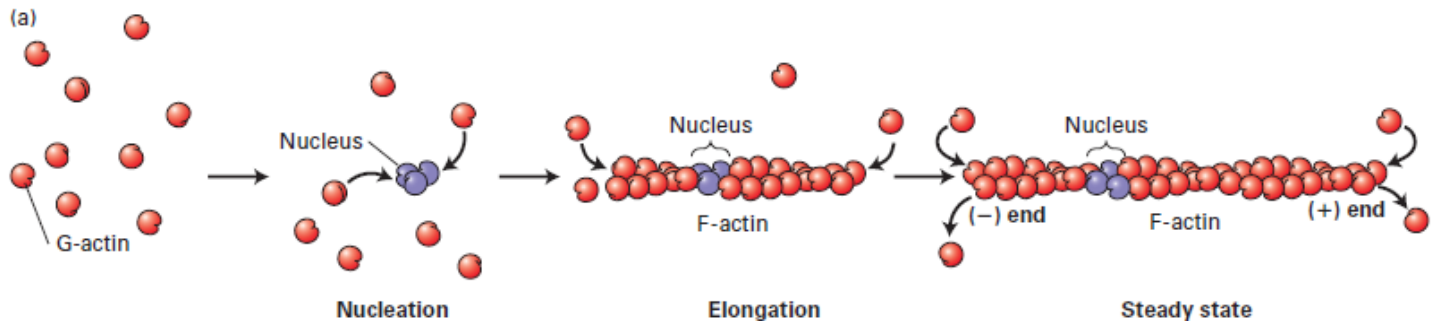
Figure 3. Assembly of actin filaments. G-actin; globular actin, F-actin; filamentous actin. Figure adopted from Lodish et al. (2016).

The cytoskeleton plays a pivotal role at cellular as well as at organismal level. It helps cells withstand and transmit mechanical forces, regulates cell shape, and participates in cell movements. Moreover, it has a major role in cell division, in intracellular cargo transport (for example mRNAs) and in distribution of various intercellular components (Pollard et al., 2017). Lastly, the cytoskeleton has been observed to create subcellular scaffolds as well as diffusion barriers (Mostowy & Cossart, 2012). As microtubules are the cytoskeletal component of interest in the current study, their structural elements will be further analyzed.

Tubulins, the structural elements of microtubules

Tubulin family evolution

Tubulins are globular proteins of approximately 50kDa. They are present in all studied eukaryotic organisms, whereas a structurally similar protein, named FtsZ, is present in prokaryotes and participates in procaryotic division (McKean et al., 2001; Pollard et al., 2017).

Tubulins form a protein family classified into 7 subfamilies; α-, β-, γ- δ-, ε-, ζ- and η-tubulins (McKean et al., 2001; Findeisen et al., 2014; Pollard et al., 2017). Amino acid sequence between subfamilies is well conserved, except from the C-terminus E-hook, which is highly divergent (see Tubulin Post Translational Modifications (PTMs)

for E-hook) (Findeisen et al., 2014). Tubulin proteins seem to be very old: an analysis of 3524 tubulins across 504 species, suggests that ancestors of all the 7 subfamilies were already present in the last common ancestor of eukaryotes (Findeisen et al., 2014). α-, β- and γ-tubulins have been identified in all eukaryotic organisms studied so far and are thought to be the minimal proteins required for microtubules assembly (McKean et al., 2001; Findeisen et al., 2014). δ-, ε-, ζ- and η-tubulins are present only in some eukaryotes. They are localized to centrioles and basal bodies, and their presence is thought to be correlated with these structures (McKean et al., 2001; Pollard et al., 2017).

Adding to tubulin diversity, genes encoding α-, β- and γ-tubulin have undergone duplication events, creating multiple variants or isotypes. For example, humans have at least eight α-tubulins and nine β-tubulins, while *S.cerevisiae* has two α-tubulins and one β-tubulin (Nsamba et al., 2021). In some cases, different isotypes participate in specific functions (McKean et al., 2001; Nsamba et al., 2021). In contrast, δ-, ε-, ζ- and η-tubulins have not undergone duplication events (Findeisen et al., 2014).

Tubulin structure

Microtubule assembly depends mainly a lot on tubulin structure. **Figure 4** shows α- and β-tubulin monomers interacting and forming an αβ-tubulin heterodimer. α- and β-tubulin monomers are almost identical in three-dimensional structure. Each monomer is composed of two β-sheets cores (B1-B6 and B7-B10), surrounded by α-helices. The loop connecting the α-helices H11 and H12 is crucial for interaction of one monomer with the next one along the protofilament (see **Figure 20** for the helices and Microtubule structure for protofilament). **Figure 5** shows that each monomer structure can be divided into three domains, namely the N-terminus domain, which has a nucleotide binding site for GTP (guanosine triphosphate) or GDP (guanosine diphosphate), an intermediate domain and a C-terminus domain. The latter is responsible for interactions with other proteins (Nogales et al., 1998).

Tubulins exist in cells in form of dimers. The structure of the tubulin dimer (**Figures 4, 6**) renders the nucleotide binding site of α-tubulin inaccessible for

nucleotide exchange and hydrolysis. Thus, α-tubulin is always bound to GTP. The nucleotide binding site of α-tubulin is named N-site (nonexchangeable site). The corresponding site at β-tubulin is named E-site (exchangeable site), as it is capable of switching between GDP and GTP when tubulin dimers are free in the cytoplasm (**Figure 6**) (Nogales, 2015).
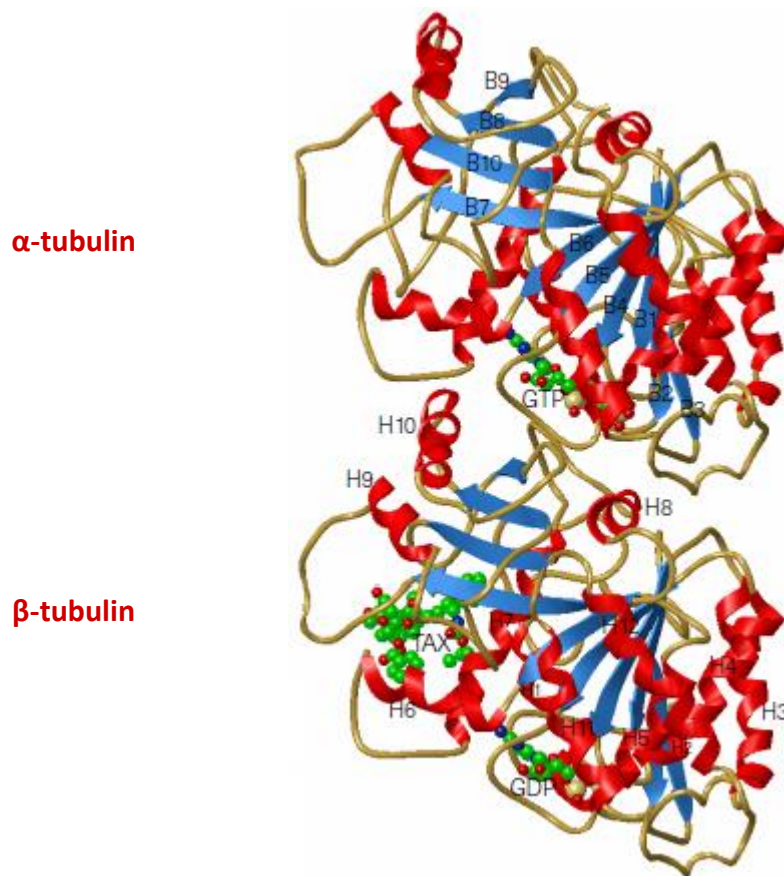
Figure 4. Pig brain αβ-tubulin dimer. α-tubulin is bound to GTP and β-tubulin to GDP and taxotere (a microtubule stabilizing drug). α-helices are in red, β-sheets in blue. GTP; guanosine triphosphate, GDP; guanosine diphosphate, TAX; taxotere. Modified figure from Nogales et al. (1998).
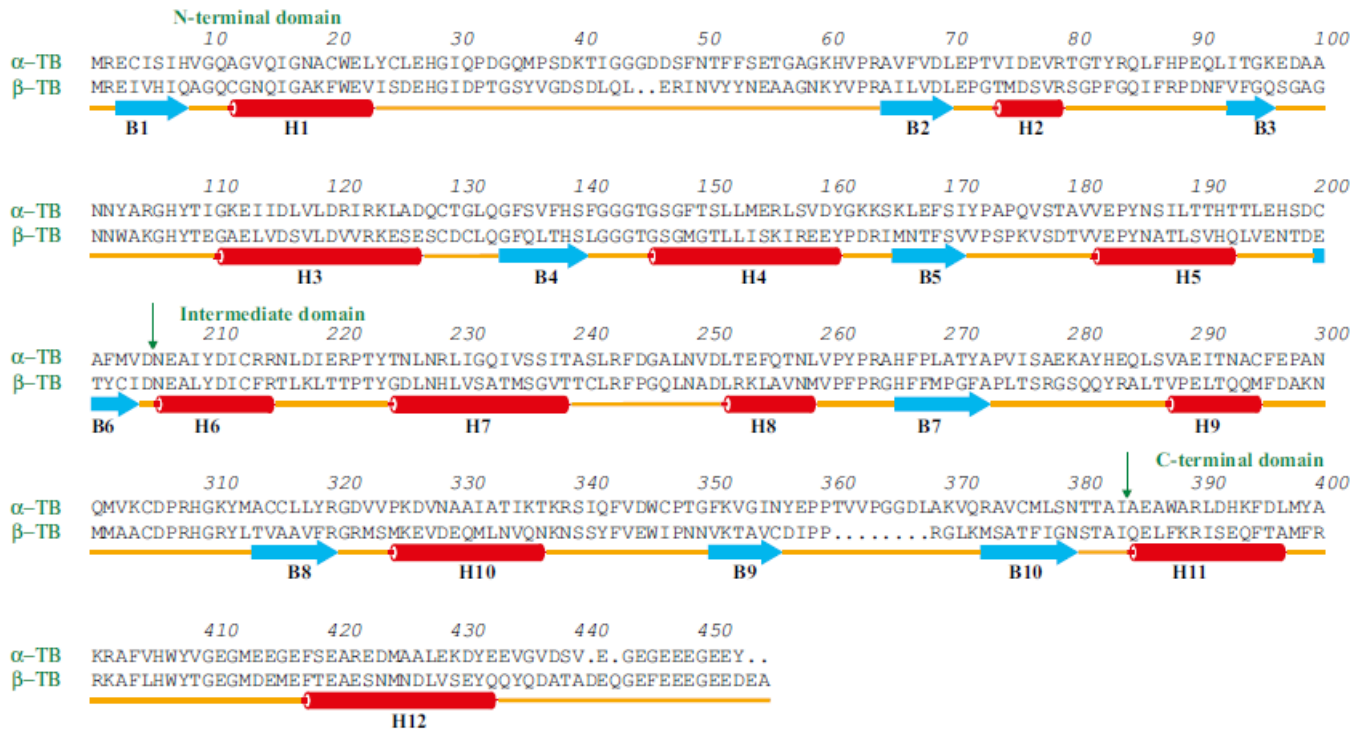
Figure 5. Pig brain α-, β-tubulin sequences. Green arrows flank each domain (N-terminus, intermediate, C-terminus). Colour code and numbering of secondary structures are same as in Figure 4. Figure adopted from Nogales et al. (1998).
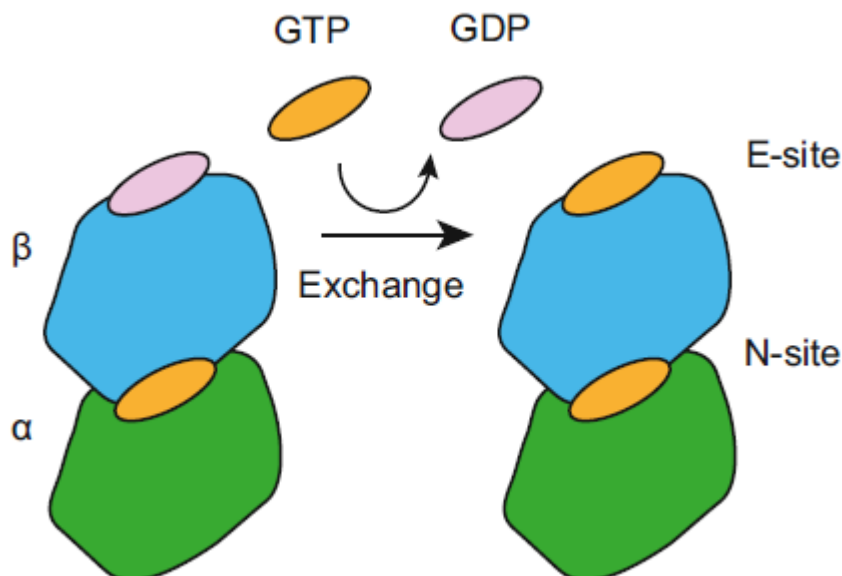
Figure 6. Nucleotide exchange (GDP to GTP) at αβ-tubulin dimer. Nucleotide exchange occurs only at E-site of β-tubulin. GTP in orange, GDP in light purple, α-tubulin in green, β-tubulin in blue. Figure adopted from Alushin et al. (2014).

Tubulin dimer conformation

From now on, the terms "GTP-tubulin" and "GDP-tubulin" will refer to the nucleotide state of β-tubulin in an αβ-tubulin heterodimer. α-tubulin is supposed to be always at the GTP state.

Scientists have been trying to determine the tubulin dimer structure since the late 90s. A relatively recent review sums up these tries (Brouhard & Rice, 2014). Briefly, initial cryo-EM microscopy experiments pointed out that free GTP-tubulin adopts a "straight" conformation (as in **Figure 6**) whereas free GDP-tubulin a "curved" conformation. However, subsequent structural and biochemical experiments questioned that hypothesis and today it is believed that free GTP-tubulin has also a "curved" conformation ("curved" conformation in the free GTP-tubulin is defined as a 12° rotation between α-, β-tubulins) (Brouhard & Rice, 2014). "Straight" conformation is adopted upon tubulin dimer addition to a microtubule (**Figure 7**, see also Microtubule assembly for curved-to-straight conformation transition). Experiments with proteins known to bind free GDP-tubulin showed that they can also bind free GTP-tubulin with the same affinity (Brouhard & Rice, 2014). Moreover, a structural study showed that free GTPγS γ-tubulin (GTPγS is a non-hydrolyzable or slowly hydrolysable GTP analog) has identical curvature with free GDP γ-tubulin (Rice et al., 2008). These studies suggest that free GDP-tubulin and free GTP-tubulin may have the same curvature angle.
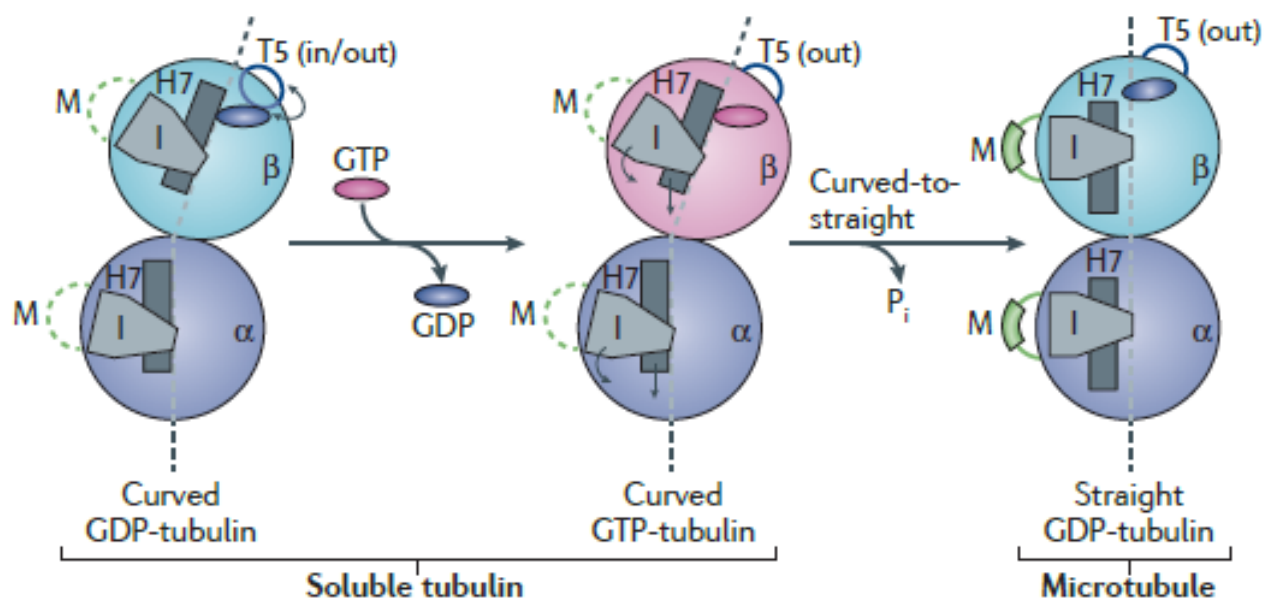
Figure 7. Free GDP- and GTP-tubulin in the cytoplasm are in "curved" conformation. Upon addition to a microtubule, tubulin dimer adopts the "straight" conformation. GTP α-tubulin is in dark blue, GTP β-tubulin is in purple and GDP β-tubulin is in light blue. Modified figure from Akhmanova & Steinmetz (2015).

Microtubules, a dynamic polymer

Microtubule structure

Microtubule structure and dynamicity are of particular interest for the current study. Microtubules are hollow, cylindrical structures, with a diameter of 25nm (**Figure 1**) and length varying from less than 1μm to more than 100μm (Goodson & Jonasson, 2018). Only GTP-tubulin can polymerize and give rise to microtubules (Nogales, 2015). All GTP-tubulin molecules incorporated to a microtubule have a specific orientation. Every β-tubulin of an αβ-heterodimer interacts always with the α-tubulin from the next heterodimer (on the longitudinal axis of the microtubule). That makes microtubules having a polarity. One end has free β-tubulin, grows fast and is called "plus end". The other end has free α-tubulin, grows very slow and is called "minus end" (**Figure 8**) (See Dynamic instability of microtubule for a comparison between the two speeds) (Cleary & Hancock, 2021).

Figure 8 shows that a tubulin dimer incorporated to a microtubule lattice interacts with other tubulin dimers and develops two types of interactions. First, it interacts with tubulin dimers from the same protofilament (which are ahead and behind of it). These interactions are called longitudinal. Second, it interacts with tubulin dimers from neighbouring protofilaments (which are on the left and on the right of it). These interactions are called lateral (Cleary & Hancock, 2021). It has been found that longitudinal interactions are stronger than lateral ones (Sept et al., 2003; Zhang et al., 2015).

A linear row of tubulin dimers is called protofilament (**Figure 9**). Often, microtubules are formed mainly by 13 laterally attached protofilaments (Goodson & Jonasson, 2018). However, the number of protofilaments can vary and microtubules made of 11, 15 or 16 can be also found in cells of different or even in the same species (Pollard et al., 2017).

Protofilaments attach laterally to create a microtubule. The point at which the "first" and the "last" protofilaments of a microtubule laterally attach is called seam (**Figure 9**). Generally, α-tubulins from one protofilament will interact with α-tubulins from neighbouring protofilaments. The same applies to β-tubulins. This type of interactions creates a B-lattice, where the position of every protofilament is slightly shifted relative to its neighbouring protofilaments (**Figure 9**). The impact of this shift is visible at the seam. At a 13-protofilament microtubule, shift results in 1.5-dimer translocation between the two protofilaments forming the seam (**Figure 10**). Therefore, at the seam α-tubulin interacts with β-tubulin creating an A-lattice (**Figures 9, 10**). The seam at 13-protofilament microtubules is considered to be a vulnerable spot (Katsuki et al., 2014). The shift between adjacent protofilaments at 15- or 16-protofilament microtubules results in 2-dimer translocation at the seam, making it indiscernable; these microtubules consist only of B-lattice (**Figure 10**) (Goodson & Jonasson, 2018).

Microtubule assembly

Because microtubules are hollow, cylindrical structures, one can think two models for their polymerization. One at which GTP-tubulin is added laterally, resulting in a helical polymerization and one at which GTP-tubulin is added longitudinally, resulting in a protofilament-based polymerization. Based on the observation that longitudinal interactions are stronger than laterals, it is believed that microtubules grow in a protofilament-based manner (Goodson & Jonasson, 2018). Free GTP-tubulin is incorporated to the plus end of a microtubule. The longitudinal interactions that take place during this incorporation are presented in **Figure 8**. The main outcome of these interactions is that the catalytically active residue E254 in the α-tubulin of the new tubulin dimer is placed near the β-tubulin E-site of the lattice-bound tubulin dimer, enabling GTP hydrolysis at this site (**Figure 8**, "Longitudinal interface" thumbnail) (Nogales et al., 1998; Cleary & Hancock, 2021). Moreover, the addition of the new dimer renders the E-site of the lattice-bound tubulin dimer inaccessible for nucleotide exchange. So, GDP cannot be exchanged for GTP (Nogales et al., 1998; Nogales, 2015).
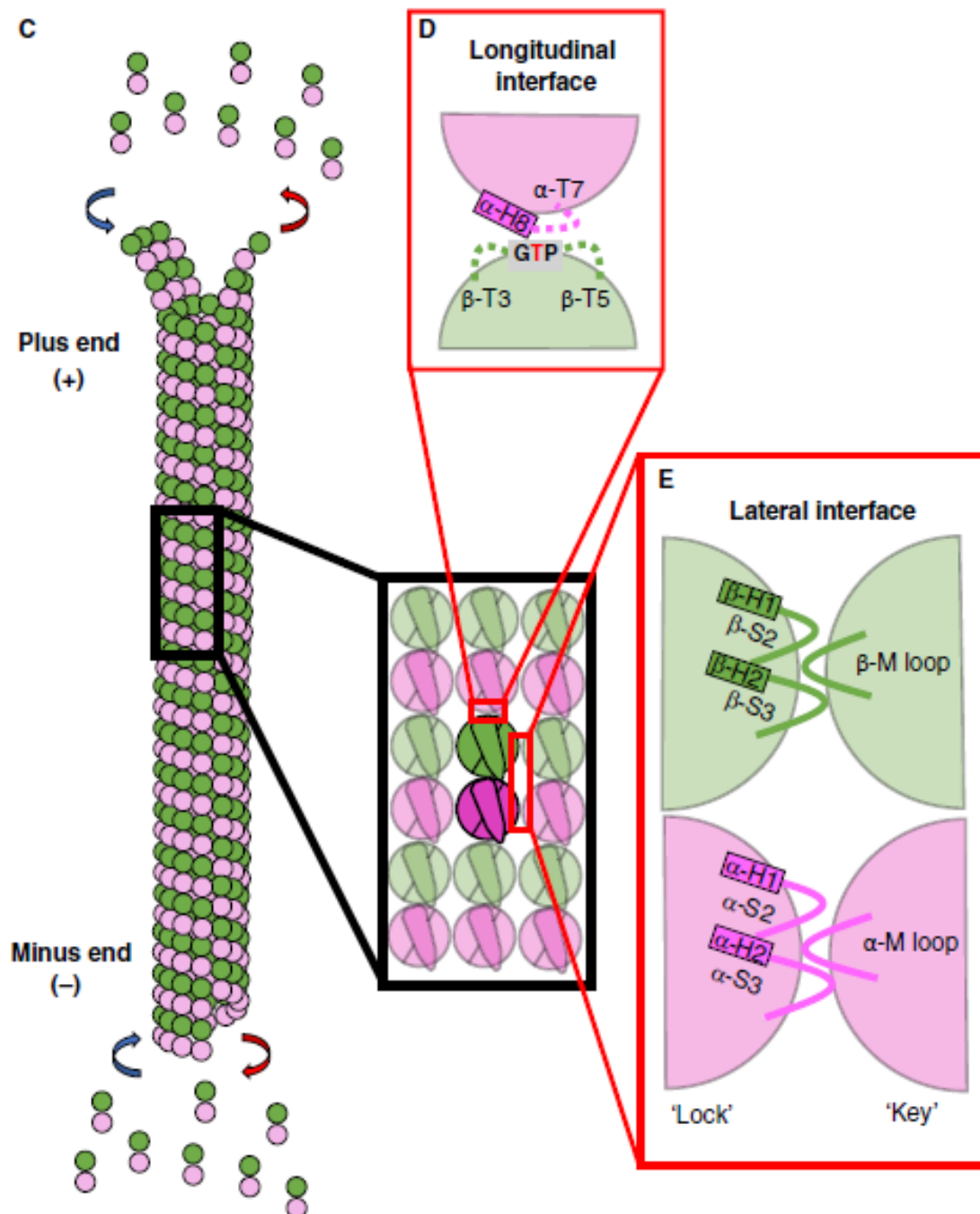
Figure 8. Cartoon depicting a growing microtubule (left). α-tubulin is in purple, β-tubulin is in green. Blue arrows indicate tubulin incorporation to the microtubule and red arrows dissociation from the microtubule. Thumbnails (right) showing the type of interactions between tubulin dimers. Modified figure from Cleary & Hancock (2021).
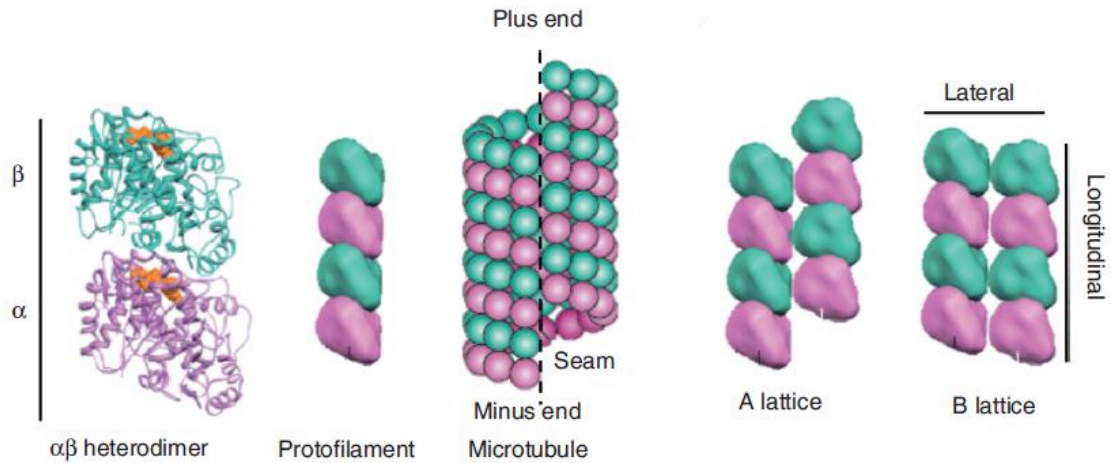
Figure 9. Far left; tubulin dimer, left; structure of a 2-dimers long protofilament, center; 13-protofilament microtubule (seam is indicated by the dotted line), right; structure of A-lattice, far right; structure of B-lattice. Modified figure from Goodson & Jonasson (2018).
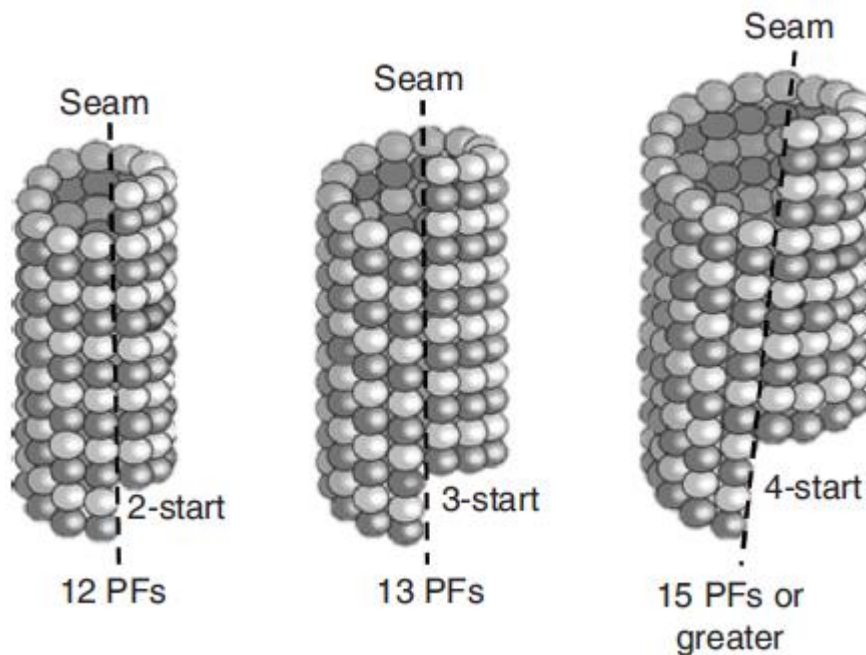
Figure 10. Impact of protofilaments shift at the seam of different microtubules. Seam at 15-protofilament microtubule is not discernable. Modified figure from Goodson & Jonasson (2018).

However, longitudinal interactions alone cannot promote microtubule formation. There are two problems; first, to create the cylindrical, hollow structure of microtubules, protofilaments need to interact with each other. Second, tubulins

making up the protofilaments are in the curved conformation: to create a microtubule, they must be straightened (**Figure 7**). Lateral interactions solve both problems (**Figure 8**, "Lateral interface" thumbnail).

During the curved-to-straight transition of tubulins, there are two opposing forces. One is the intrinsic tendency of GTP-tubulin to be curved and the second are the lateral interactions, which force GTP-tubulin to be straightened (Brouhard & Rice, 2018). In a recent review (Brouhard & Rice, 2018), authors proposed a model for the plus end structure of growing microtubules as well as for the curved-to-straight transition (**Figure 11**). According to this model, a part of a microtubule that is 2 tubulin dimers wide, is half straightened. When a part is 6 tubulin dimers wide, it is completely straight, whereas parts 3 to 5 tubulin dimers wide are progressively straighter.
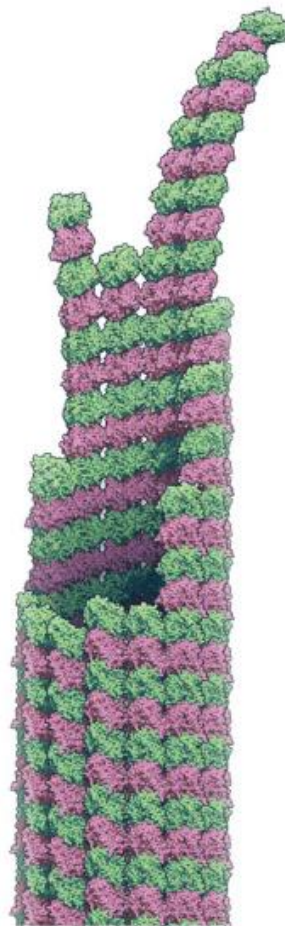
Figure 11. Model of the microtubule plus end. Microtubule end is tapered, "ragged" and presents variable curvature. Protofilaments are straightened up as lateral interactions increase. For more information see Brouhard & Rice (2018). Figure adopted from Brouhard & Rice (2018).

Dynamic instability of microtubule

As mentioned at the beginning, microtubules can polymerize as well as depolymerize. Polymerization rate depends on tubulin concentration. For example, *in vitro*, at 10µM of tubulin, polymerization rates of plus and minus ends are ~1.5 µm/min and ~0.5 µm/min respectively. Depolymerization rate is independent of tubulin concentration; plus end depolymerizes at a rate of ~27 µm/min, whereas minus end at ~34 µm/min *in vitro* (Walker et al., 1988). So, disassembly of a microtubule is much faster than its assembly. When microtubules grow in presence of GTP-tubulin only, they can polymerize and depolymerize stochastically **(Figure 12)**. The polymerization -> depolymerization transition is known as catastrophe. The exact opposite transition is known as rescue (**Figure 13**). The ability of microtubules to undergo consecutive cycles of growth and disassembly can be summed up in the term dynamic instability, described for first time by Mitchison & Kirschner (Mitchison & Kirschner, 1984). Plotting microtubule lengths according to time generates a kymograph diagram used to visualize microtubule dynamics as in **Figure 13**.
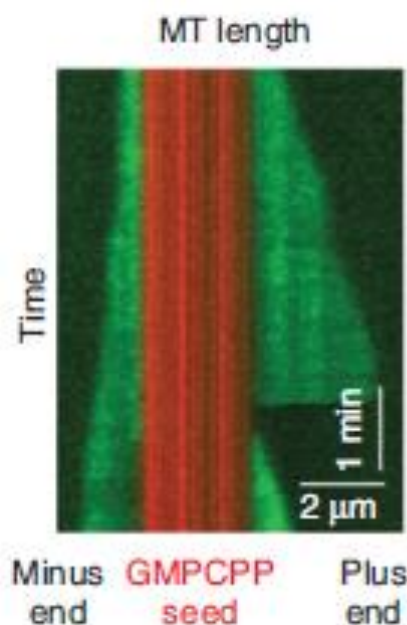
Figure 12. Kymograph (length/time plot derived from a movie, with length at x axis and time at y axis) of a microtubule undergoing dynamic instability *in vitro*. Note that both ends of microtubule grow, but plus end is more dynamic. Green represents Alexa488-labeled tubulin, and red represents tetra-rhodamine-labeled tubulin GMPCPP- (a slowly hydrolysable GTP analog) stabilized microtubule seeds. Modified figure from Goodson & Jonasson (2018).
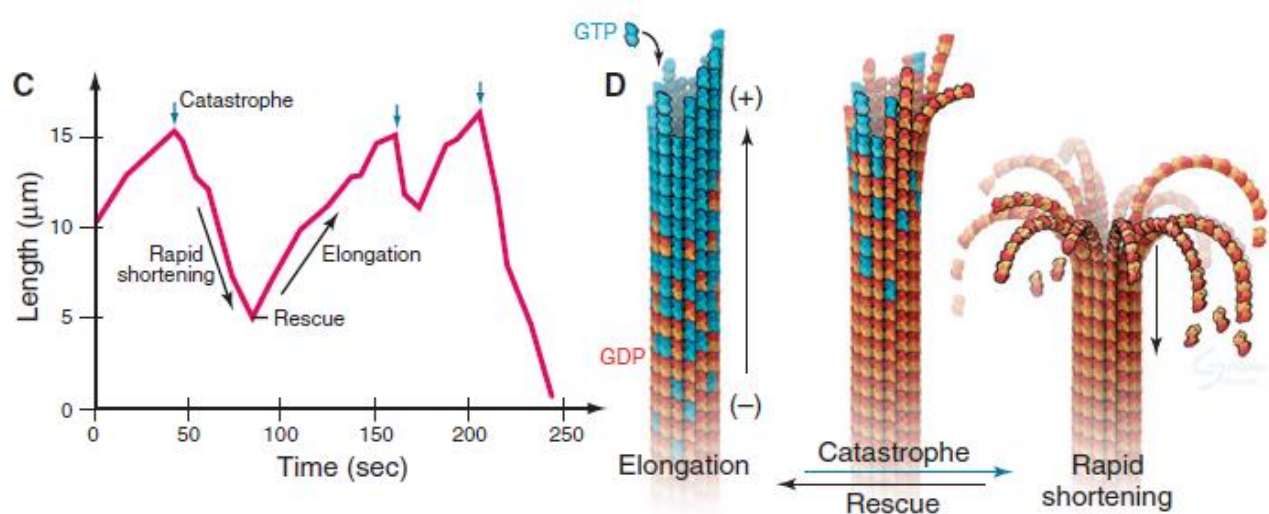
Figure 13. Left; Dynamic instability of a microtubule in presence of GTP-tubulin only. As diagram shows, a microtubule switches stochastically from growth to disassembly. Right; Growing microtubule with the GTP cap (left) and depolymerizing microtubule with the characteristic peeling of protofilaments (right). At the center an intermediate situation is presented. GTP-tubulin in blue-green and GDP-tubulin in red-yellow. Modified figure from Pollard et al. (2017).

Microtubule disassembly

GTP cap is crucial for microtubule stability

A catastrophe seems to be the result of GTP cap loss (Pollard et al., 2017). GTP cap occurs at the end of a growing microtubule, due to a delay in hydrolysis of GTP. It consists of GTP-tubulin and plays crucial role in the stability of the growing microtubule. When GTP-tubulin is not added, GTP is hydrolyzed to GDP and GTP cap is lost. This renders the microtubule unstable and promotes its catastrophe (see below) (Brouhard & Rice, 2018; Carlier, 1982; Erickson & O'Brien, 1992; Howard & Hyman, 2009; Mitchison & Kirschner, 1984).

How is GTP hydrolyzed, when this procedure requires addition of new tubulin dimers (see Microtubule assembly)? β-tubulin alone, without the aid of E254 from α-tubulin, can still hydrolyze GTP, but in a much slower rate (about 250 times slower) (Pollard et al., 2017). So, eventually, the GTP cap can be lost.

The size of GTP cap has been measured, but it is doubted if results reflect the reality (Akhmanova & Steinmetz, 2015; Roostalu et al., 2020). In a cleverly designed

series of experiments, Roostalu et al. (2020) showed that, at least *in vitro*, GTP cap size is less than 2µm.

GTP hydrolysis induces microtubule disassembly

Presence of GDP-tubulin is necessary for a catastrophe to happen, since microtubules growing in the presence of GMPCPP (Guanosine-5′-[(α,β)-methylene]-triphosphate, a slowly hydrolysable GTP analog) undergo catastrophe events less frequently (Hyman et al., 1992; Nogales et al., 2015). Goodson & Jonasson on their review (Goodson & Jonasson, 2018) made the exciting comment that, contrary to common sense, "energy of GTP is used to destroy the microtubule, not to build it".

A depolymerizing microtubule has a characteristic structure

How do microtubules depolymerize when the GTP cap is lost? Tubulin dimers in the lattice are in a straight conformation. However, because this is not their preferred conformation, tubulin dimers end up with "strain energy" (Brouhard & Rice, 2018). Moreover, because of GTP hydrolysis, they are compacted around 3 Å, due to rearrangements in α-tubulin and E-site of β-tubulin (**Figure 14**). Compaction leads to weakened lateral interactions, whereas longitudinal interactions are getting stronger (Alushin et al., 2014). Upon loss of the GTP cap, GDP-tubulin starts to adopt its favourable conformation (the curved one, due to weakened lateral interactions). That results in loss of lateral interactions between GDP-tubulins and creation of protofilaments that peel away (**Figures 13, 15**) (Cleary & Hancock, 2021). This structure is named "ram's horns" (Mandelkow et al., 1991). Interestingly, microtubules that peel away can apply pulling forces, which can move whole chromosomes during cell division (Koshland et al., 1988; Pollard et al., 2017).

Finally, it is not known whether compaction of GDP-tubulin is a common feature of all microtubules. Mammalian microtubules display compaction of GDP-tubulin (Alushin et al., 2014; Zhang et al., 2015), whereas yeast microtubules do not (Holy et al., 1997; Howes et al., 2017).

β-tubulin
α-tubulin Intermediate domain
α-tubulin Nucleotide-binding domain
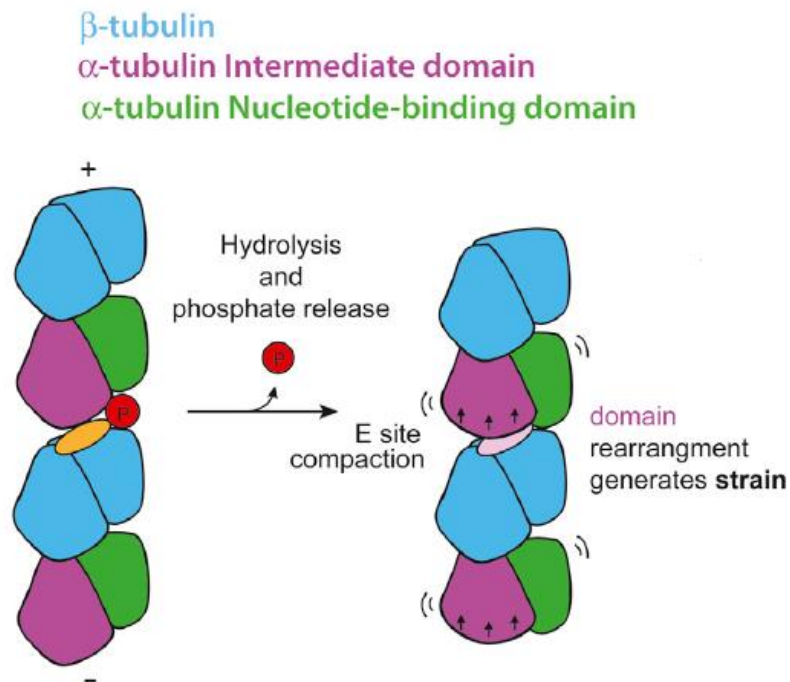
Figure 14. Cartoon representing tubulin compaction upon GTP hydrolysis. Figure shows that rearrangements in α-tubulin and E-site of β-tubulin, lead to tubulin dimer compaction. Modified figure from Alushin et al. (2014).
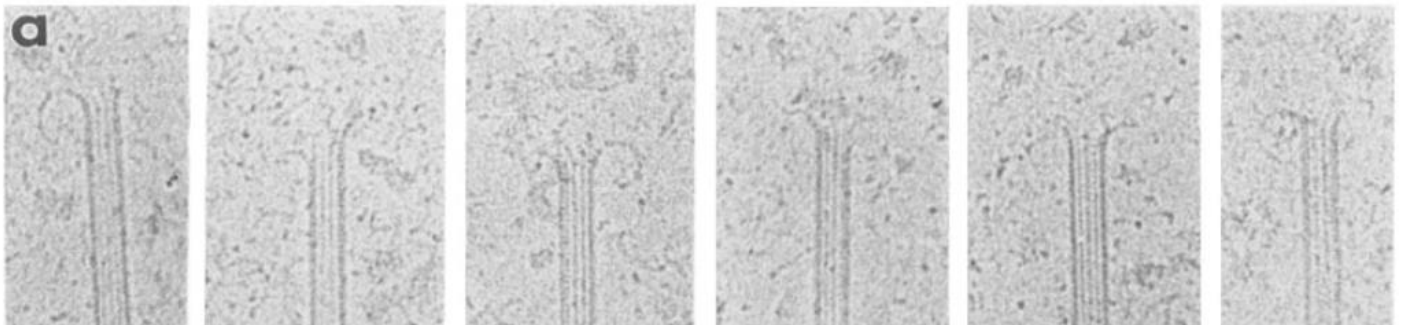
Figure 15. Cryo-EM of depolymerizing microtubules. Peeling of protofilaments, creating the so-called "ram's horns", can be observed. Modified figure from Mandelkow et al. (1991).

Nucleation of a microtubule

Nucleation of microtubules occurs either from spontaneous nucleation of αβ-tubulin heterodimers (**Figure 16**) or from specialized structures (Cleary & Hancock, 2021). The latter ones are called Microtubule Organizing Centers (MTOCs) (Pollard et al., 2017). Spontaneous nucleation will not be further analyzed, because it is not the theme of the current thesis. Note, however, that this process is not well understood and recently was questioned (Rice et al., 2021). MTOCs will be described very briefly, because they connect in a way with the theme of this study.
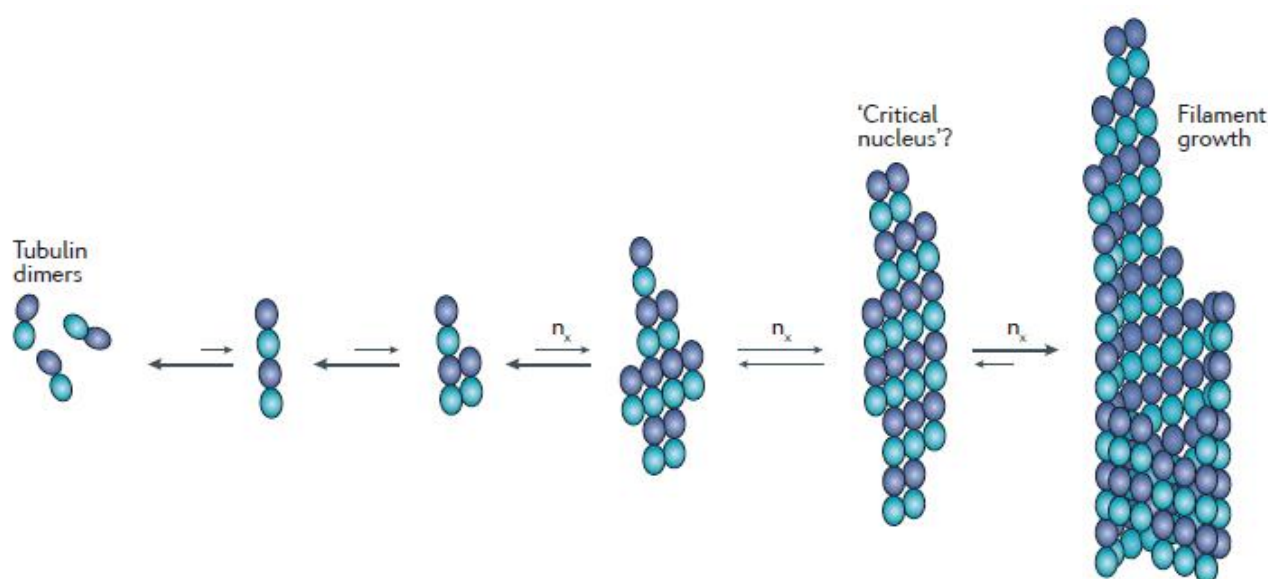
Figure 16. Microtubule spontaneous nucleation model. Size of arrows indicates the possibility of the reaction to happen, n_x; number of reaction steps. Modified figure from Roostalu & Surrey (2017).

There are three types of MTOCs, centrosomes, spindle pole bodies (SPB) and basal bodies. Centrosomes are the MTOCs in most animal cells. They are membraneless and can exist free in the cytoplasm. Microtubules emanating from centrosomes participate in cytoplasm organization during the cell cycle. During mitosis, they have the vital roles of organizing the mitotic spindle and segregating the chromosomes correctly. During cytokinesis, they orchestrate the contractile ring formation. Centrosomes consist of two cylindrical structures, named centrioles, which are surrounded by pericentriolar material, a protein mixture **(Figure 17)**. γ-tubulin is the most important protein of pericentriolar material, since it forms γ-tubulin ring

complexes (γ-TuRCs), the structure from which microtubules emanate. γ-TuRC consists of 14 γ-tubulins attached to accessory proteins, forming a characteristic structure of "a dislocated ring similar to a left-handed lock washer" according to Pollard et al. (2017) **(Figure 18).** It promotes the assembly of microtubules with 13 protofilaments and caps the minus end of microtubules (Pollard et al., 2017).
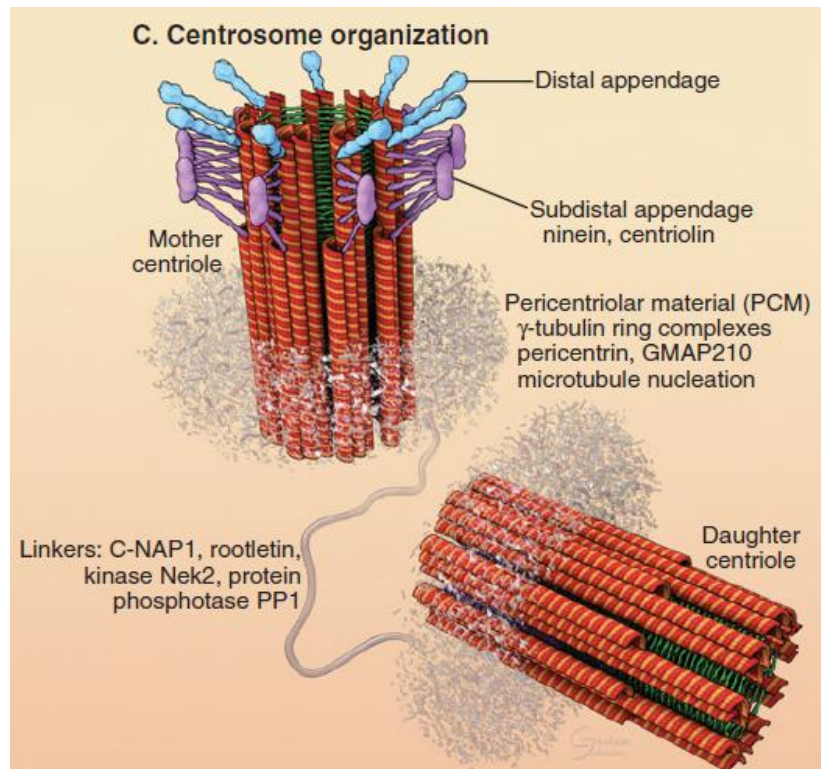
Figure 17. Centrosome structure. Centrioles are depicted as red cylindrical structures, surrounded by pericentriolar material (grey mesh). γ-TuRC is localized to pericentriolar material. Modified figure from Pollard et al. (2017).
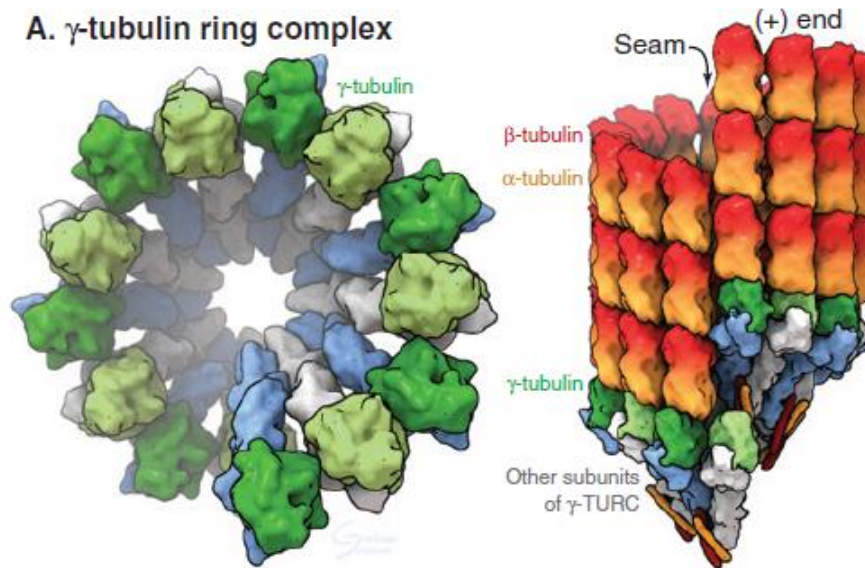
Figure 18. γ-tubulin ring complex (γ-TuRC) structure from the top (left figure) and from the side (right figure). γ-tubulin is in green, other γ-TuRC subunits in blue and grey, α-tubulin in orange and β-tubulin in red. Modified figure from Pollard et al. (2017).

SPBs are the centrosome counterparts on fungi. Although involved in basically the same processes, their structure is quite different from centrosomes **(Figure 19)**. More specifically, they lack centrioles and adopt a 3-layered plaque structure. Moreover, although γ-tubulin is present, protein composition seems to be different from that of centrosomes. Additionally, contrast to centrosomes that are free in the cytoplasm, SPBs are embedded in the nuclear envelope for the majority of the cell cycle. In *S. cerevisiae*, the SPB is embedded to the nuclear envelope during the entire cell cycle (Pollard et al., 2017).

Basal bodies are centriole-dependent structures that promote the assembly of cilia and flagella. These structures are important for cell movement (e.g., the flagella on the sperm cells) and for environment sensing (primary cilia) (Pollard et al., 2017).
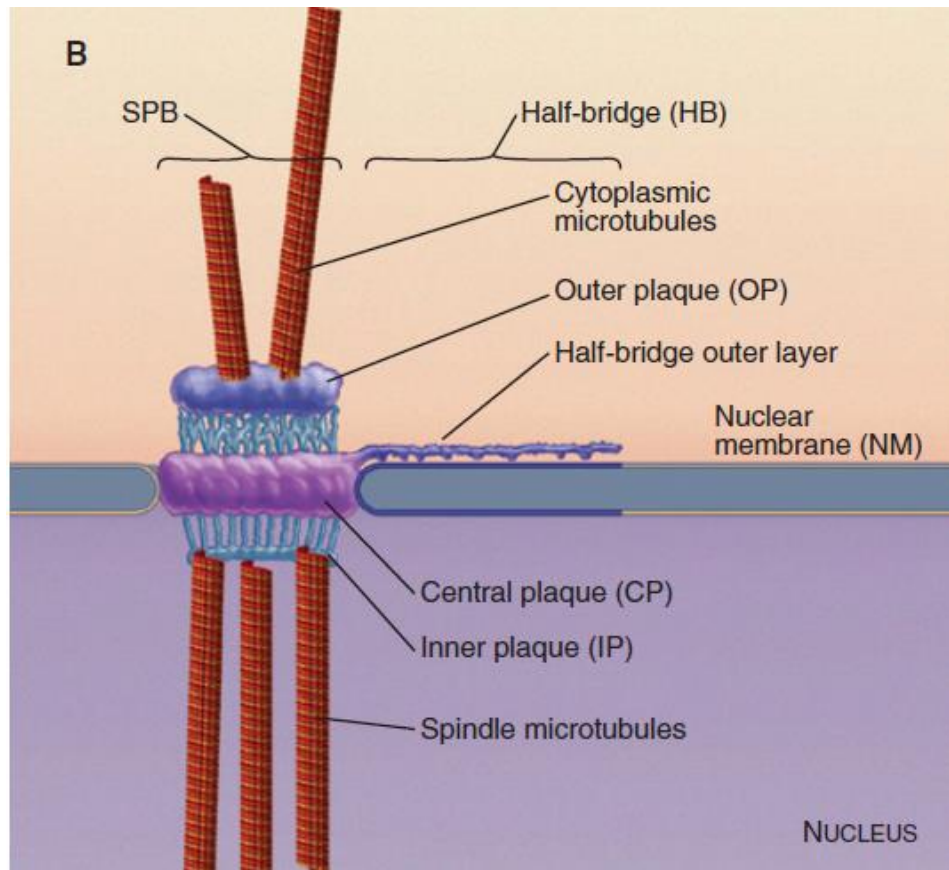
Figure 19. SPB structure. Note that SPB consists of 3 layers of plaques (outer, central, inner). Microtubules are in red. Modified figure from Pollard et al. (2017).

Tubulin Post Translational Modifications (PTMs)

The C-terminus of tubulins is quite acidic, due to the presence of many glutamic acid (E) residues (**Figure 5**). For that reason, it is called E-hook (Goodson & Jonasson, 2018). Electron crystallography experiments (Nogales et al., 1998) showed that the C-terminus of αβ-tubulin resides to the outer surface of the microtubule (**Figure 20**). Moreover, it participates in interactions between microtubules and Microtubule Binding Proteins (MTBPs) (Goodson & Jonasson, 2018; Hawkins et al., 2010; Magiera & Janke, 2014; Nogales et al., 1998). C-terminus has been found to be a target for PTMs, which in turn have been found to affect the binding of MTBPs (Magiera & Janke, 2014). This study focuses on the effect of a kinesin (a MTBP) on *S. cerevisiae* microtubule dynamics. Since microtubules in *S. cerevisiae* do not present

any PTMs (Janke, 2014), PTMs of tubulin will not be further analyzed. For more information about this topic, see Magiera & Janke (2014) and Janke (2014).
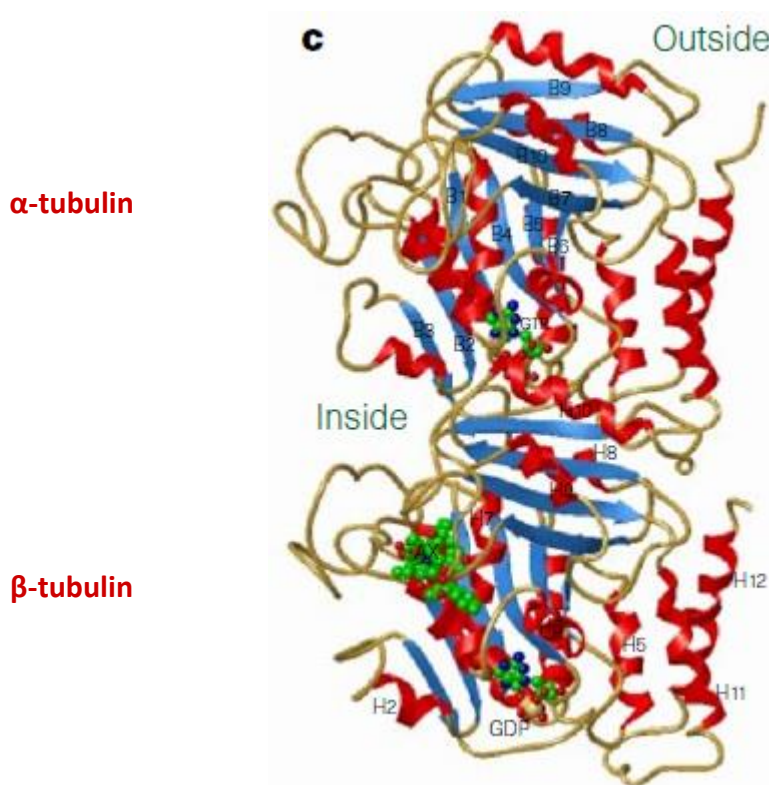
Figure 20. Orientation of pig brain αβ-tubulin dimer in the microtubule lattice. "Inside" corresponds to the lumen of the microtubule and "Outside" to the cytoplasm. As picture shows, the C-terminus of tubulins (H11 - H12) faces the cytoplasm. α-tubulin is bound to GTP and β-tubulin to GDP and taxotere (a microtubule stabilizing drug). α-helices are in red, β-sheets in blue. Colour code and numbering are same as in Figures 4, 5. TAX; taxotere. Modified figure from Nogales et al. (1998).

Microtubule Binding Proteins (MTBPs)

Cells can regulate the dynamicity of microtubules according to their needs by MTBPs (Goodson & Jonasson, 2018). MTBPs can be categorized either by their activity or by their localization (Goodson & Jonasson, 2018). Here, two categories of MTBPs, relevant to the purpose of this study (stabilizers and destabilizers), will be briefly analyzed. For more information, see Goodson & Jonasson (2018).

"Stabilizers" describe the proteins that enhance polymerization and/or weaken depolymerization of microtubules (Goodson & Jonasson, 2018). An example

of a microtubule polymerase is the protein XMAP215, which attaches to microtubule plus end and promotes microtubule growth by adding tubulin dimers (Brouhard et al., 2008). A subset of kinesins (a molecular motor) has also been found to act as stabilizers by inducing microtubule growth (see Kinesin-2, -5).

"Destabilizers" can be sorted into three main categories, "sequestering proteins", "tip destabilizers" and "microtubule severing proteins" (Goodson & Jonasson, 2018). Proteins from the first category bind to free tubulin dimers and impair their incorporation to microtubules (Goodson & Jonasson, 2018). Proteins that specifically affect the tip of a microtubule fall into the second category; depolymerizing kinesins (see Kinesin-8, -13) are the best studied proteins of this group (Goodson & Jonasson, 2018). Microtubule severing proteins describe the set of proteins that destabilize microtubules by shredding them (Goodson & Jonasson, 2018).

Molecular motors - Kinesin

Molecular motors are a subset of MTBPs that attach to microtubules and move onto them. There are two types of molecular motors: kinesins and dyneins. Common feature of both is the ATP-dependent movement; they use the hydrolysis of ATP to move (Pollard et al., 2017; Schliwa & Woehlke, 2003). As this study focuses on the effect of the kinesin Kip2 on *S. cerevisiae* microtubule dynamics, kinesins will be introduced here in more detail.

Kinesins are motors that can move towards the plus or the minus end of microtubules [see Kinesin Superfamily Proteins (KIFs)]. As **Figure 21** shows, kinesins have generally 4 domains. A head domain, bearing the ATP binding site and motor activity, a coiled-coil that plays role in dimerization, a neck which connects the head and the coiled-coil and a tail, where various cargoes are attached. Functional kinesin molecules occur from homodimerization of monomers. However, there are exceptions [see Kinesin Superfamily Proteins (KIFs)]. Kinesins are responsible for intraflagellar transport (Taschner & Lorentzen, 2016) and transport of organelles (e.g., mitochondria, lysosomes, synaptic vesicles in neuronal cells) (Pollard et al., 2017).

They also play a crucial role during the mitosis, by transferring chromosomes and regulating mitotic spindle dynamics (Pollard et al., 2017). Lastly, they have been implicated into normal embryo development, and they are crucial for nervous system function (Hirokawa et al., 2009a; Konjikusic et al., 2021).
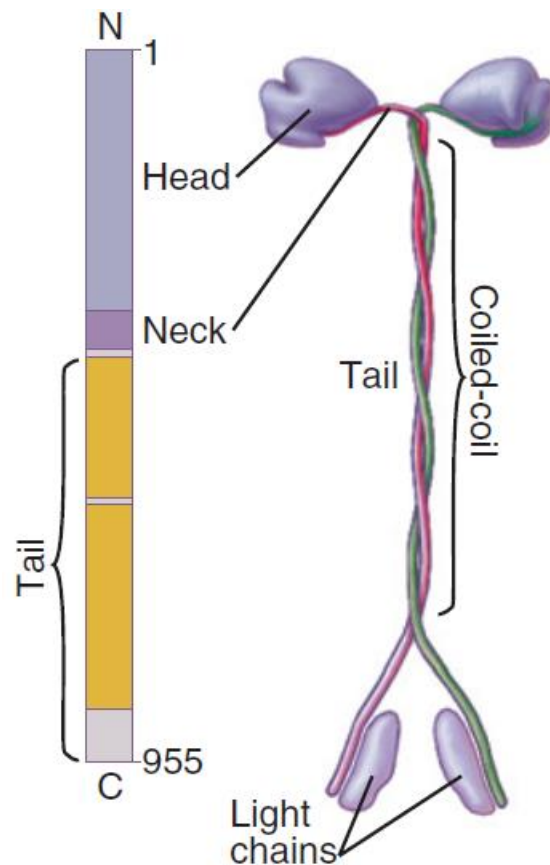
Figure 21. Cartoon depicting the domains (left) and the structure of kinesin-1. Light chains are responsible for attaching cargoes to the kinesin. Modified figure from Pollard et al. (2017).

How do kinesins move on microtubules?

There are two ways by which kinesins move on microtubules, by "walking" on them and by diffusing along them. Generally, they "walk". Kinesins belonging to the kinesin-3, and -5 families can also diffuse, whereas members of kinesin-13 can only diffuse [see Kinesin Superfamily Proteins (KIFs)] (Hirokawa et al., 2009b).

So, it is believed that kinesins move on microtubules by a conserved mechanism. The best studied model on how a kinesin moves comes from KIF1A, a

monomeric kinesin-3 protein. KIF1A, being a monomer, moves on microtubules by diffusion. Here, a brief description of the diffusion-based as well as the "hand-over-hand" model will be given. The latter explains how kinesins "walk" on microtubules by using information encoded in the microtubule structure (Hirokawa et al., 2009b). Diffusion-based movement model is described in detail at Hirokawa et al. (2009b) and Nitta & Hirokawa (2013).

Figure 22 sums up the diffusion-based model for KIF1A and proposes how "hand-over-hand" model on KIF5, a kinesin-1 protein, works. On the diffusion-based model, after ATP hydrolysis weak interactions between K-loop (a KIF1A region) and E-hook restrict KIF1A to 1D diffusion. Interactions between the microtubule binding domain of the kinesin and the top of the tubulins enhance this 1D diffusion and might promote the biased movement towards plus end (not shown in the figure). When ADP is exchanged for ATP, KIF1A binds strongly to microtubules (Hirokawa et al., 2009b; Nitta & Hirokawa, 2013).

The "hand-over-hand" applies to dimeric kinesins (so it refers to the majority of the kinesins, see below). There are two heads, the leading and the trailing. When ATP binds to the empty leading head, it is hydrolyzed (ADP + Pi state; Pi: inorganic phosphate). Hydrolysis causes a conformational change that pulls the trailing head forward. This movement is known as "power stroke". The new leading head finds the next binding site by diffusional search. Binding to microtubule leads to the dissociation of ADP from the new leading head. Pi is removed from the new trailing head (ADP state) and the trailing head detaches from the microtubule. The cycle is repeated. (Hirokawa et al., 2009b; Pollard et al., 2017). After each cycle, kinesin has moved 8nm forward (Pollard et al., 2017). "Hand-over-hand" model explains how kinesins "walk" on microtubules. From now on, instead of saying that a kinesin "walks", the term "processive kinesin", will be used. This term is used extensively across bibliography.
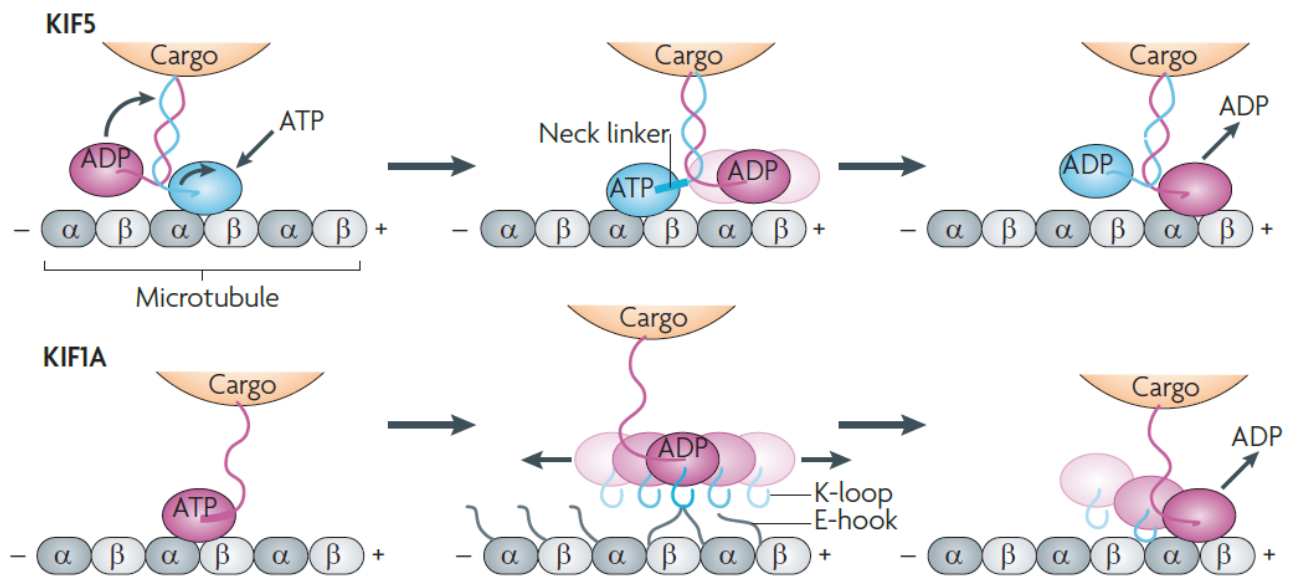
Figure 22. Top; "Hand-over-hand" model for KIF5. Bottom; Diffusion-based model for KIF1A. Modified figure from Hirokawa et al. (2009b).

Kinesin Superfamily Proteins (KIFs)

With latest data, Kinesins Superfamily Proteins (KIFs) consist of 15 different families. In **Figure 23**, all these families are presented (Miki et al., 2005; Miki & Hirokawa, 2013). Kinesins belonging to Kinesin-1 till Kinesin-12 families have the motor domain at the N-terminus and move towards the plus end of microtubules (**Figures 21, 24**). Members of the Kinesin-14 family have the motor domain at the C-terminus and move towards the minus end of microtubules, whereas Kinesin-13 family members have the motor domain in the middle of the protein (**Figures 24**) (Miki & Hirokawa, 2013). There have been done many tries to classify each kinesin to the right family (Kim & Endow, 2000; Lawrence et al., 2004; Miki et al., 2001; Miki et al., 2005;). The classification presented in **Figure 23** is based on a phylogenetic tree created by alignment of motor domains from 623 kinesins and has been adopted as the foundation for kinesin classification (Miki et al., 2005; Miki & Hirokawa, 2013). Classification of Kip2 seems not to be robust: in some studies, it is classified to Kinesin-7 family (Lawrence et al., 2004; Miki et al., 2001; Miki et al., 2005;), while in other is classified closer to Kip3 (Kinesin-8 superfamily) (Kim & Endow, 2000).

Below, a brief description of kinesin families known to affect microtubule dynamics will be done. For more information about kinesin families see Miki & Hirokawa (2013).

Family	Founding member(s)	Representative members	Reported function/structural features	Member no.[a]
Kinesin-1	LpKHC DmKHC	KIF5B, KHC, NKin, KLP1, KinA, DdK5	Vesicle transport, conventional	3/1/1/4/3
Kinesin-2	MmKIF3A StrPuKRP85/95	KIF3A/3B, KIF17, Krp85/95, Osm3, Fla10	Vesicle-intraflagellar transport/ heterotrimeric	4/3/3/0/0
Kinesin-3	CeUnc104 MmKIF1B	KIF1A, KIF1B, KIF13A, KIF16B, UNC104	Organelle transport/monomeric	8/4/2/0/1
Kinesin-4	MmKIF4A	KIF4A, KIF21A/B, chromokinesin	Organelle transport, chromosome movement	5/3/2/3/1
Kinesin-5	AnBimC SchPoCut7	KIF11, Eg5, BimC, CIN8, KIP1, Cut7	Spindle formation/ homotetrameric, bipolar	1/1/1/4
Kinesin-6	CgCHO1	KIF20, KIF23, Rab6Kinesin, CHO1, MKLP1, Zen4, MPP1	Cytokinesis, spindle polarity	5/2/1/0/1
Kinesin-7	ScKip2 HsCENP-E	KIF10, CENP-E, CMET, CANA, KIP2	Kinetochore microtubule capture	1/2/0/14/2
Kinesin-8	DmKLP67A	KIF18A/18B KIF19A, KLP67A, KIP3	Nuclear migration, mitochondrial transport	3/2/1/2/0
Kinesin-9	CrKLP1	KIF6, KIF9, KRP3, CrKLP1	Unclear	2/0/0/0/0
Kinesin-10	DmNod	KIF22, KID, Nod	Chromosome segregation/ Helix-hairpin-Helix DNA-binding motif	1/1/0/1/0
Kinesin-11	ScSmy1	KIF26A, KIF26B, VAB8, SMY1	Signal transduction/divergent catalytic core	2/1/1/2/0
Kinesin-12	XlXklp2	KIF12, KIF15, HKLP2, KLP54D, Xklp2, PAKRPd	Organelle transport/ homologous tail	2/1/0/6/0
Kinesin-13	MmKIF2A CgMCAK	KIF2A, MCAK, XKCM1, PfKinI	Microtubule depolymerizing/ central motor	4/3/2/1/1
Kinesin-14A	ScKAR3 DmNCD	KIFC1, CHO2, Ncd, Kar3, KatA	Chromosome segregation/C-terminal motor	1/1/4/4/1
Kinesin-14B	AtKCBP	KIFC2, KIFC3, KatD, KCBP, KIF25	Organelle transport/C-terminal motor	3/0/1/16/0

Figure 23. All the 15 kinesin families. Classification of a kinesin into a family is based on a phylogenetic tree created by alignment of motor domains from 623 kinesins. Modified figure from Miki & Hirokawa (2013).

Kinesin structures

N-terminal motor	Example	Heavy chain domains	Architecture
Kinesin-1	Hs Kif5B	Head — Coiled-coil — Tail	
Kinesin-2	Sp Krp85/95		85 / 95
Kinesin-3	Mm Kif1b		
Kinesin-4	Xl Klp1		
Kinesin-5	Dm Klp61f		
Kinesin-7	Hs CENP-E		
Internal motor			
Kinesin-13	Xl MCAK		
C-terminal motor			
Kinesin-14	Dm Ncd		
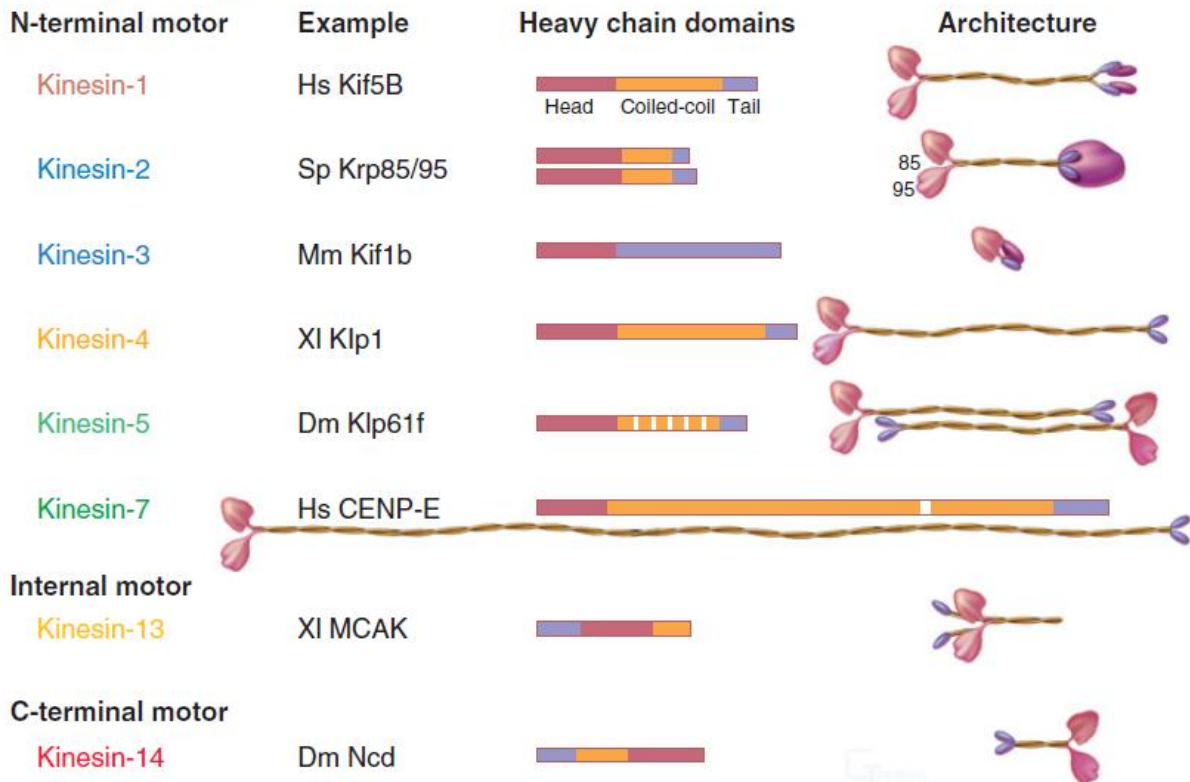
Figure 24. Cartoons depicting the domains and the structure of kinesins from different families. Kinesin-1 to Kinesin-12 families have the motor domain at the N-terminus. Members of the Kinesin-14 family have the motor domain at the C-terminus and kinesin-13 members have the motor domain in the middle of the protein. Kinesin families 8 to 12 are not presented but, generally, they have the same structure as kinesins from families 1 to 7. See Miki et al. (2005) for more information. Modified figure from Pollard et al. (2017).

Kinesin-2

Members of this family can homodimerize, heterodimerize (Miki & Hirokawa, 2013) or even heterotrimerize (Pollard et al., 2017; Taschner & Lorentzen, 2016). They participate in organelle as well as in intraflagellar transport (Miki & Hirokawa, 2013). In *Chlamydomonas reinhardtii* and *Caenorhabditis elegans*, two organisms used for intraflagellar transport studies, it has been proved that kinesins of this family can promote flagellar microtubules growth. They do so, by transporting tubulin dimers into flagella/cilia. However, they do not directly interact with tubulin: instead, tubulin dimers are attached to a complex of proteins, which in turn attaches to the kinesin (Taschner & Lorentzen, 2016).

Kinesins falling into this family form homotetramers (**Figure 24**) that participate in cell division. Their most known feature is the bundling of interpolar microtubules present at the mitotic spindle (**Figure 25**) (Miki & Hirokawa, 2013; Pollard et al., 2017). Interpolar microtubules have antiparallel polarity so, during anaphase, the plus end directed movement of the kinesin leads to the elongation of the spindle (Pollard et al., 2017). Except from being processive, kinesins of this family are also capable of diffusing along microtubules (Kapitein et al., 2008).

A major discovery was that kinesin-5 is a microtubule polymerase. It exerts its polymerizing activity by accumulating to the plus end of microtubules. There, it stabilizes the newly incorporated tubulin dimers and prevents their dissociation from the plus end (**Figure 26**) (Chen and Hancock, 2015). Interestingly, Cin8, the kinesin-5 homolog in *S.cerevisiae*, has ionic strength-dependent directionality *in vitro* (Gerson-Gurwitz et al., 2011).
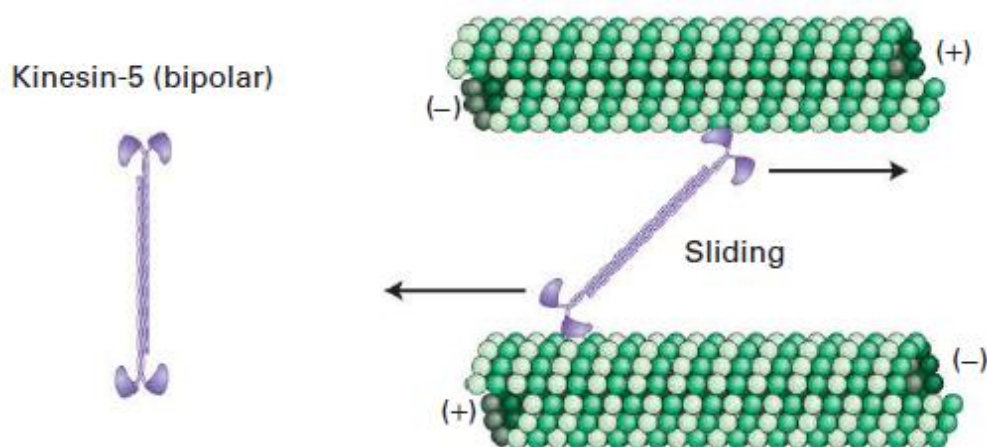
Figure 25. Kinesin-5 forms homotetramers that bundle antiparallel microtubules. Its plus end directed movement leads microtubules to move away from one another. Modified figure from Lodish et al. (2016).
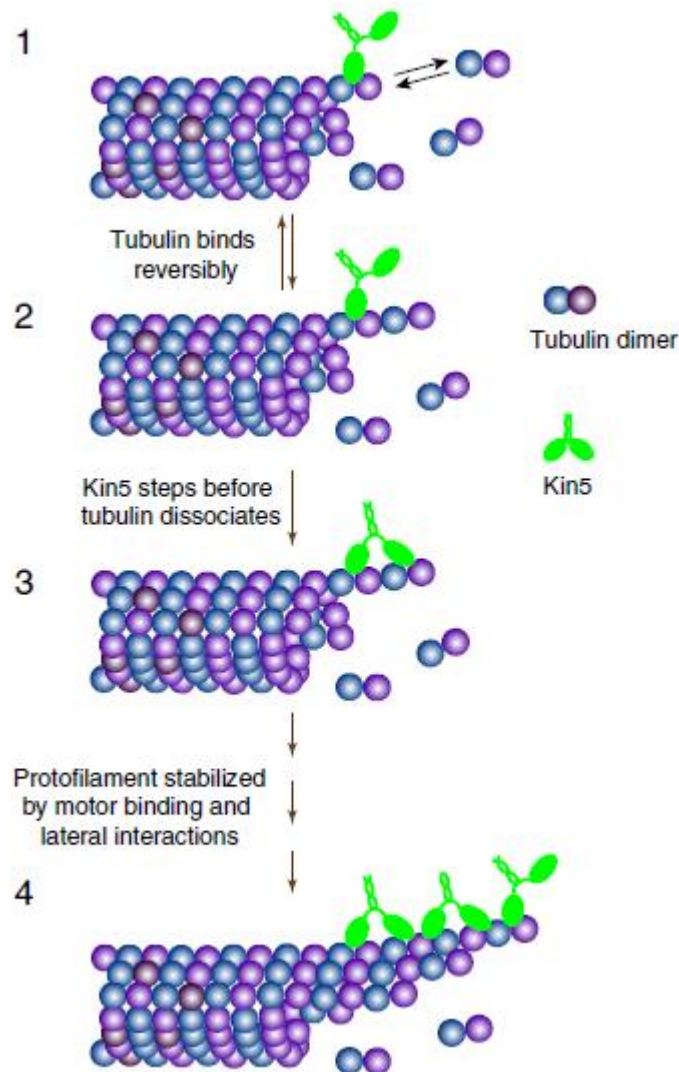
Figure 26. Kinesin-5 accumulates to the plus end of microtubules. There, it promotes microtubule elongation by stabilizing the newly incorporated tubulin dimers and preventing their dissociation from the plus end. Modified figure from Chen & Hancock (2015).

Kinesin-8

Proteins making up this family promote microtubule disassembly. Like most of the kinesins, they move processively towards the plus end of microtubules. There, they depolymerize microtubules by a not well-established mechanism. On the one hand, human Kif18A is believed to block microtubule dynamicity and maybe promote the curved conformation of the tubulin, like kinesin-13s (see below) (**Figure 27**). On the other hand, the yeast homolog of kinesin-8, Kip3 actively removes tubulin dimers

from the plus end. However, Kip3 depolymerizing activity seems to depend on arrival of "trains" of Kip3 (**Figure 27**) (Walczak et al., 2013).

Kinesin-13

Kinesins belonging to this family possess the head domain in the middle of the molecule (**Figure 24**) (Miki & Hirokawa, 2013). This family consists of non-processive kinesins. They diffuse along microtubules and attach to ends with higher affinity than the lattice. Unlike kinesin-8 family members, these kinesins can bind to both ends (**Figure 27**). There, they promote microtubule disassembly in an ATP-dependent manner. They attach to the ends and favour the curved conformation of the tubulin (**Figures 7, 27**). Then, with the aid of ATP hydrolysis, they remove one tubulin dimer at a time (Howard & Hyman, 2007).

Kinesin-13 family members participate into cell division. Probably, the most known feature is during anaphase, where MCAK (mitotic centromere-associated kinesin), a kinesin-13, simultaneously depolymerizes the plus end of kinetochore microtubules and drags chromosomes to the poles of the spindle (Maney et al., 1998).
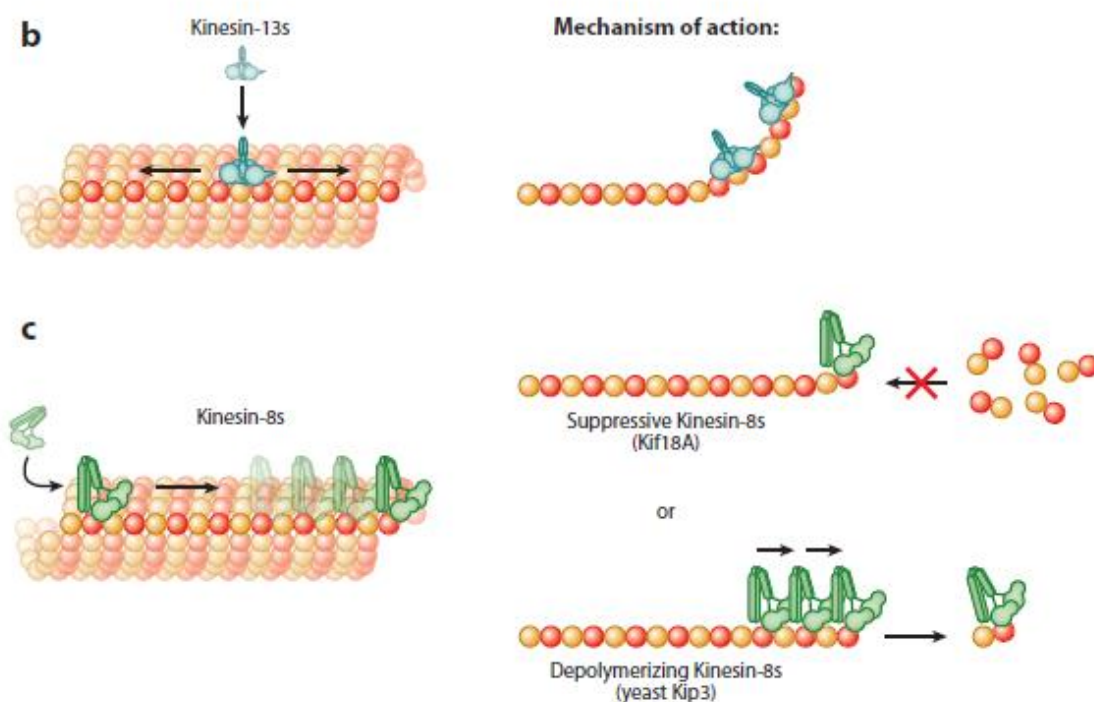
Figure 27. Models for microtubule depolymerizing activity of kinesins-8 and -13. Top; Kinesin-13s diffuses along microtubule lattice and attaches to microtubule ends. There in an ATP-dependent process, it induces the curved conformation of tubulin and removes one tubulin dimer at a time. Bottom; Kinesin-8s move towards the plus end of microtubules. There, they depolymerize microtubules by a not well-established mechanism. Kif18A seems to block microtubule dynamicity and maybe promote the curved conformation of the tubulin, whereas Kip3 actively removes tubulin dimers from the plus end. Its activity seems to depend on arrival of "trains" of Kip3. Tubulin dimers are in red-yellow. Modified figure from Walczak et al. (2013).

In vitro reconstitution experiments

The aim of cellular biology is to decipher the mechanisms underlying various cellular procedures. Even though *in vivo* studies are a straightforward approach to that, they are not always informative. Cells are very complex structures with thousands of proteins interacting with each other, making the study of a particular mechanism challenging. A solution to that are the *in vitro* studies. In these, cellular extracts or purified proteins are isolated, to be studied out of the complex environment of the cell. *In vitro* studies can further support procedures observed into live cells and uncover new functions of cellular constituents, not observed into the complex environment of the cell. Additionally, due to their simplicity, they allow for modelling of mechanisms (Liu & Fletcher, 2009). The challenge with *in vitro* studies is to find the optimal conditions for the system to work as inside the cell.

In vitro reconstitution experiments have shed light on major biological processes. They led the way on what are the minimum elements required for DNA replication. In the field of cytoskeleton, they showed how muscles contract, that a mitotic spindle can be reconstituted without the presence of centrosomes or kinetochores and that cytoskeletal elements in prokaryotes play a more important role in cellular functions than previously thought. Finally, they have been utilized in experiments for interactions taking place on the plasma membrane, such as the immunological synapse (Liu & Fletcher, 2009). These and other *in vitro* reconstitution experiments are analyzed further in Liu & Fletcher, (2009).

Total Internal Reflection Microscopy (TIRF)

To carry out the experiments in this study, TIRF microscopy was used. The basic principles of it are mentioned below. Fluorescence microscopy is a type of light microscopy that uses fluorescent molecules (named fluorophores) "tagged" to a molecule of interest. Photons of a specific wavelength, produced by a light source, excite the fluorophores. After a few nanoseconds, fluorophores emit photons that have longer wavelengths (less energy) than the excitation photons (Lichtman & Conchello, 2005). Here, a brief reference to the physical basis of fluorescence microscopy and TIRF microscopy will be done. In **Figure 28**, a simplified fluorescent microscope is presented. As it is depicted, in "classical" fluorescence microscopy the excitation beam (in green) passes through the objective lens and the sample (**Figures 28 bottom left, 29**). The excited fluorophores emit photons (in red), which are collected by the objective and sent to the eye or detector (Lichtman & Conchello, 2005). There are many drawbacks of this setup. First, because the whole sample is excited, signal/noise ratio is not good. Moreover, when imaging live cells for long time, excitation photons can cause phototoxicity to cells (Martin-Fernandez et al., 2013; Mattheyses et al., 2010).
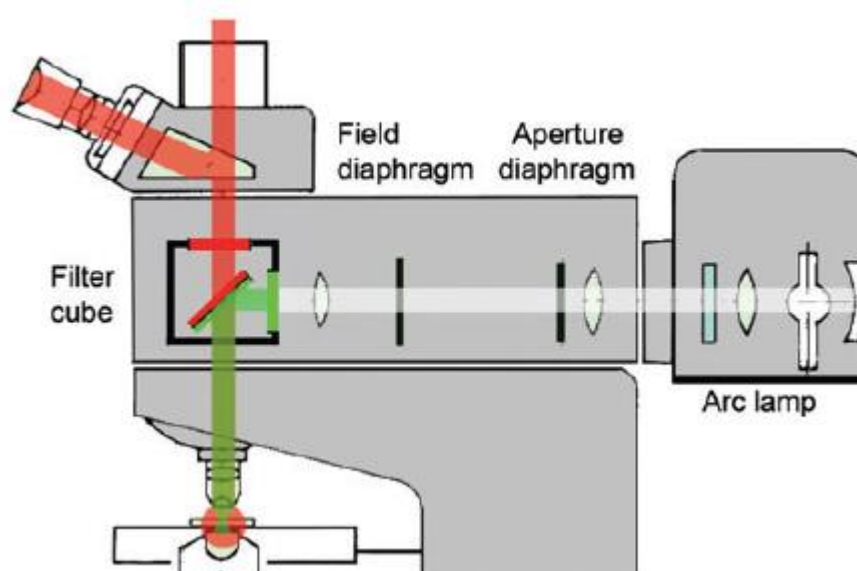
Figure 28. Light path in a simple fluorescence microscope. Excitation light (in green) emitted from a source (arc lamp in this case) is driven to the sample (bottom left) through the objective. Fluorophores

absorb the excitation photons and after a few nanoseconds emit photons of different (longer) wavelength (in red). Emitted light is collected from the objective and sent to the detector or the eye. Modified figure from Lichtman & Conchello (2005).
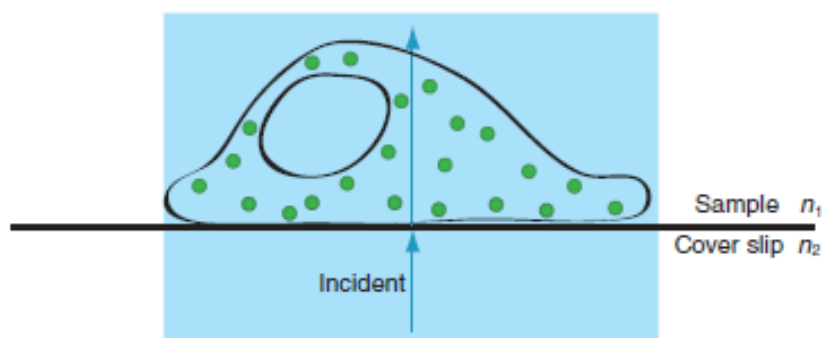
Figure 29. Cartoon showing that in "classical" fluorescence microscopy excitation beam (in light blue) passes through the sample (cell) and excites all the fluorophores (green). Modified figure from Mattheyses et al. (2010).

To understand the principle of TIRF microscopy, one must know Snell's law. Think of a ray of light propagating into a medium (glass) with refractive index n_1. Glass contacts with a second medium (air), having a refractive index n_2, where $n_1 > n_2$ (**Figure 30**). When the ray of light hits the interface between glass and air (incident ray) at an angle θ_1, part of it is reflected to the glass (reflected ray) whereas another part of it is refracted (refracted ray), while it starts to propagate in the air, with an angle θ_2. Snell's law is an equation connecting the two angles and the refractive indices of the two media (**Figure 30**) (Keiser, 2016).

In cases like the above, when light goes from an optically denser media (glass) to an optically less dense media (air), there is a critical angle of incidence (named θ_{crit}) at which the refracted rays do not propagate to the air anymore but are parallel to the interface between the two media (**Figure 31, left**). Rays of light with an incident angle greater than θ_{crit} do not propagate to air and are exclusively reflected into the glass. This physical phenomenon is called Total Internal Reflection (**Figure 31, right**) (Keiser, 2016).

Snell's law: $n_1 \sin\theta_1 = n_2 \sin\theta_2$
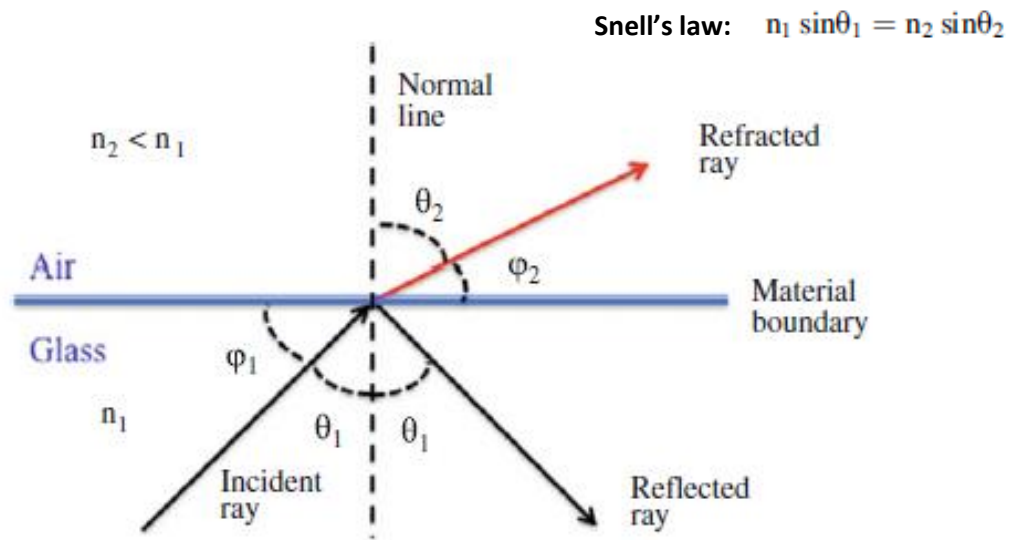
Figure 30. A ray of light can be reflected and refracted when going from an optically denser media to an optically less dense media. Modified figure from Keiser (2016).
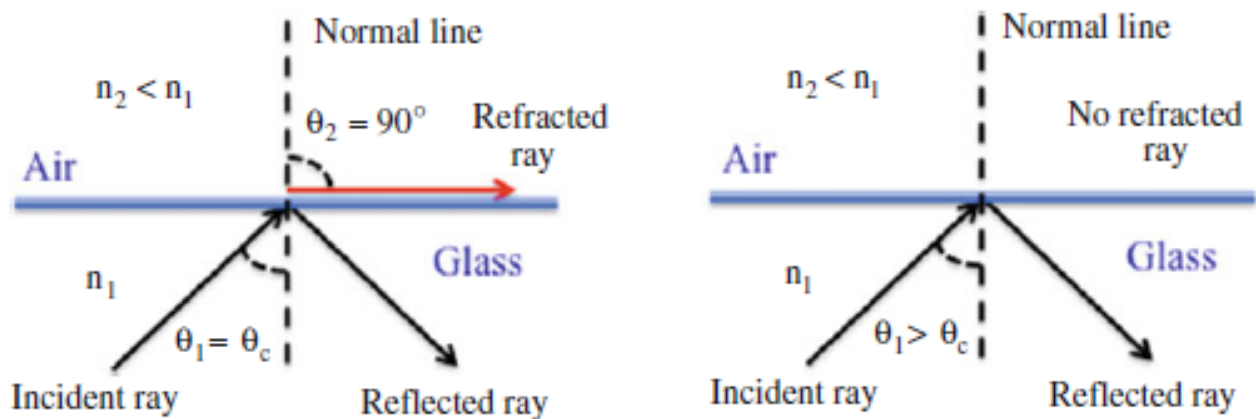
Figure 31. When the incident angle is greater than θ_{crit}, total internal reflection occurs (right figure). Modified figure from Keiser (2016).

Martin-Fernandez et al. (2013) state that "light is energy emitted by charged particles and manifests itself, as it travels through space, in the form of particles (photons) and electromagnetic waves". In Total Internal Reflection, even though the

rays of light are totally internally reflected, energy is transferred to the second media (air in the case above), creating an "evanescent" wave. The intensity of this wave is maximum at the interface between the two media and decays exponentially with distance from this interface. The distance at which "evanescent" wave can reach, depends mainly on the incident angle, the wavelength of the light and the refractive indices of two media. Typical values are 60-100nm, whereas it does not exceed 200nm (Martin-Fernandez et al., 2013; Mattheyses et al., 2010). For the mathematical approach to this phenomenon, see Martin-Fernandez et al. (2013).

TIRF microscopy uses exactly this property (**Figure 32**). Excitation beam hits the coverslip - sample interface at an angle greater than θ_{crit} [dashed line, note that refractive index of coverslip (n_2) must be greater than the refractive index of the sample (n_1)]. Because the coverslip is optically denser than the sample, total internal reflection happens. However, as mentioned above, an "evanescent" wave is created. The intensity of this wave decays exponentially with distance. That means that fluorophores (small circles) that are closer to the coverslip - sample interface will be excited strongly than those being further. Moreover, because penetration depth does not exceed 200nm, fluorophores beyond that distance will not be excited (green vs grey fluorophores). That gives TIRF microscopy an extremely good singal/noise ratio (**Figure 33**). Additionally, when imaging live cells, this technique reduces phototoxic effects as only a small portion of the cell is exposed to excitation beam (Mattheyses et al., 2010).
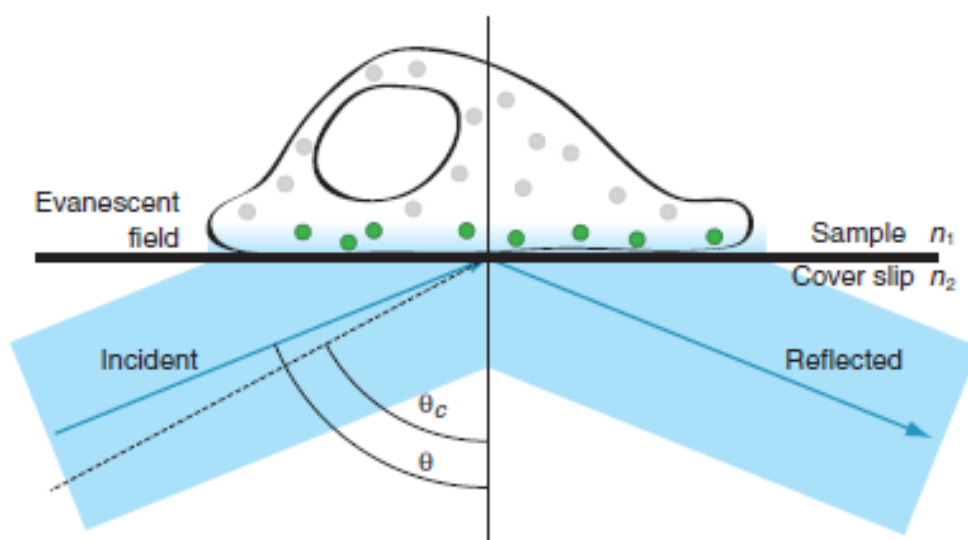
Figure 32. Cartoon showing the principle of TIRF microscopy. Excitation beam (in light blue) hits the coverslip - sample interface at an angle greater than θ_{crit} (dashed line) and total internal reflection occurs. "Evanescent" wave is created and only fluorophores proximal to the coverslip - sample interface are excited (green). Modified figure from Mattheyses et al. (2010).
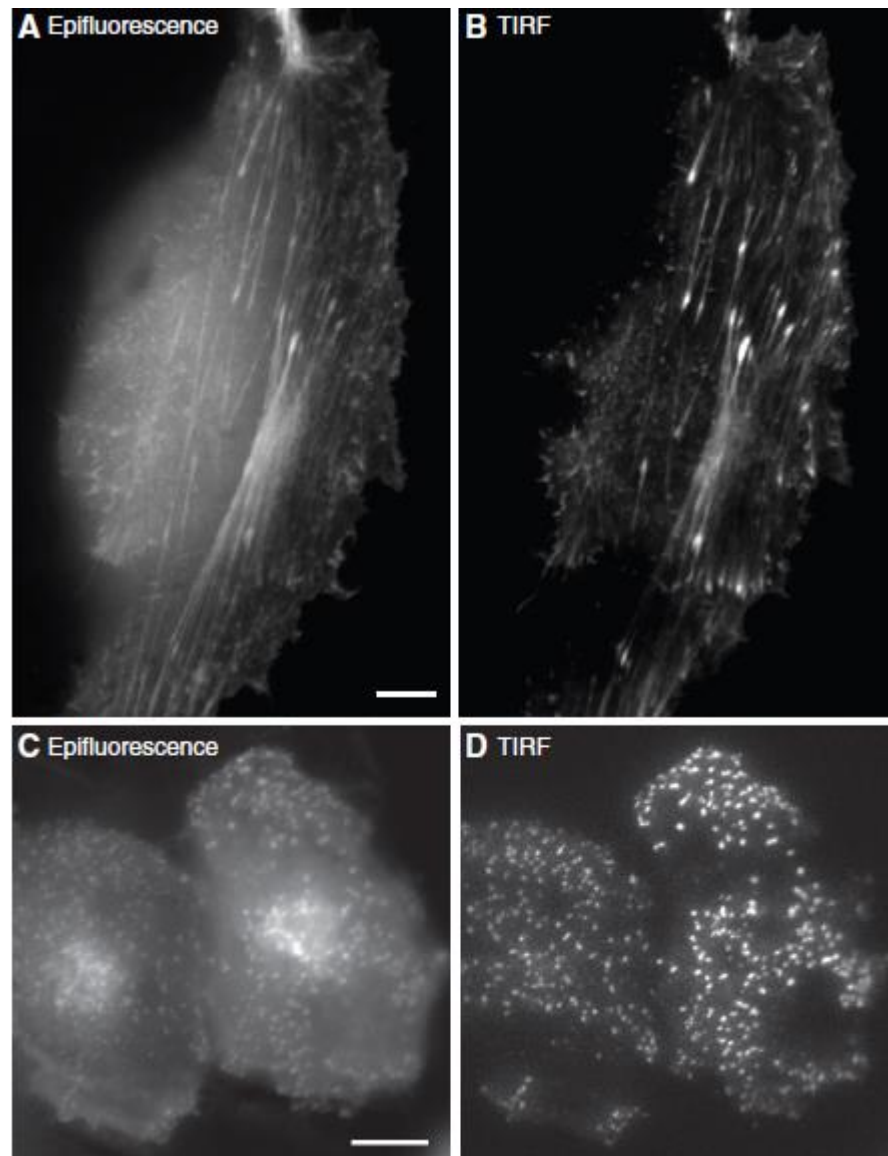

Figure 33. Differences between Epifluorescence and TIRF microscopy. Top row panels; Actin (LifeAct-GFP) in a migrating cell. Bottom row panels; Clathrin (clathrin light chain–GFP) in cell. Modified figure from Mattheyses et al. (2010).

There are two approaches for a TIRF microscope setup, the prism- and the objective-based (**Figure 34**). In the prism-based approach (**Figure 34, left**), a prism is placed above the coverslip. Some advantages of this setup are the cost and that it allows a wide range of incident angles; very big incident angles can be achieved, reducing the "evanescent" wave depth and resulting in better signal/noise ratio. Moreover, unwanted photons are not collected by the objective. However, because excitation and emission happen on the opposite site of the objective lens, focus through the specimen is necessary. That makes this setup unsuitable for thick samples. Additionally, calibration may be required each time a new sample is added, making this setup time-consuming (Martin-Fernandez et al., 2013; Mattheyses et al., 2010).

In the objective-based approach (**Figure 34, right**), the excitation beam passes through the objective lens, as in a typical fluorescence microscope. However, because the light beam needs to hit the sample in an angle and not pass through it (compare **Figures 29, 32, 34**), light is focused on back focal plane of the objective; that allows light to hit the sample in an angle. A major advantage of this approach is the ease of access to the sample; one can intervene or change his samples without having to remove a prism first. However, unwanted photons are collected by the objective, making the use of special filters necessary (Martin-Fernandez et al., 2013; Mattheyses et al., 2010).

In the second approach, there are some more things to take into consideration. One is the NA (numerical aperture; describes the light gathering power of the lens) of the lens. Objectives with NA>n_{sample} are required (n_{sample} is the refractive index of the sample). Moreover, because the objectives are immersed into media (oil), the lens, the oil and the coverslip must have the same refractive index (Martin-Fernandez et al., 2013; Mattheyses et al., 2010). This will allow excitation light to propagate till it hits the coverslip - sample interface, without changes in its direction. In this study, the objective-based approach for TIRF microscopy was used.
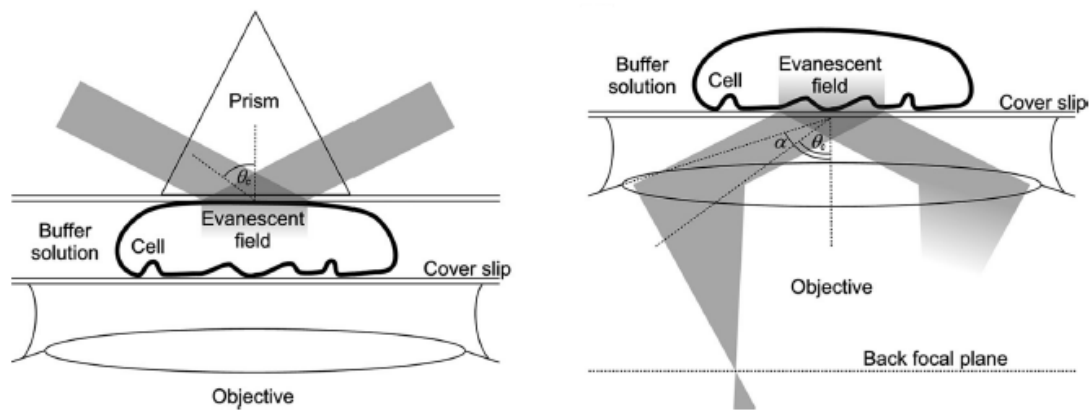
Figure 34. Prism-based (left) and objective-based (right) approach for TIRF microscope setup. Modified figure from Martin-Fernandez et al. (2013).

TIRF microscopy has been used in to study dynamic procedures such as endocytosis, exocytosis, cell-substrate adhesion, intracellular signaling, single molecule tracking and the dynamics of the cytoskeleton (Martin-Fernandez et al., 2013; Mattheyses et al., 2010).

Spindle positioning in *S. cerevisiae*

Before presenting the already published data about Kip2 and its effect on microtubule dynamics, a mention to its cellular functions is necessary. *S. cerevisiae* is a model organism in cellular biology. It is the one at which the cell cycle was first studied (Hartwell, 1974). *S. cerevisiae* has three discernible characteristics about its division. First, it undergoes closed mitosis, meaning that the nucleus does not break apart, as in higher eukaryotes (**Figure 35**) (Boettcher & Barral, 2013; Güttinger et al., 2009). Second, it duplicates through asymmetric division. In brief, a bud starts growing from the mother cell. As the cell cycle proceeds, this bud is getting bigger. Finally, it is separated from the mother cell (**Figure 36**) (Hartwell, 1974). Third, whereas in other organisms cell division is done in the plane of mitotic spindle, in *S. cerevisiae* it is the spindle that must be oriented towards the mother-bud axis (**Figures 36, 37**) (McNally, 2013).
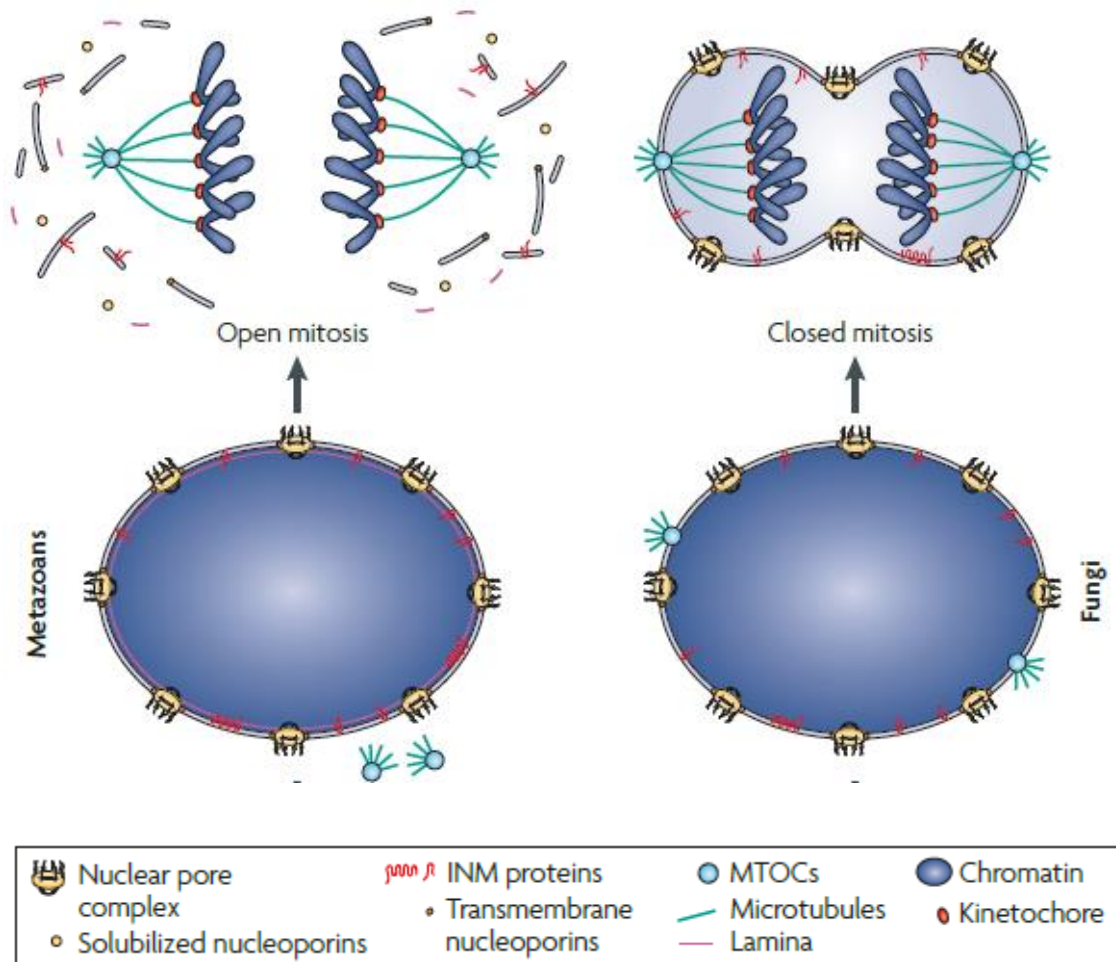
Figure 35. Differences between open and closed mitosis. The egg-like structures on the bottom as well as the structure on top right represent the nucleus of a eukaryotic cell. Left; during open mitosis, nuclear envelope (double-layered membrane surrounding the nucleus) breaks apart. The DNA or chromatin (dark blue in the figure) is exposed to the cytoplasm and mitosis proceeds at it. Right; during closed mitosis, nuclear envelope does not break apart and mitosis takes places into the nucleus of the cell. Modified figure from Güttinger et al. (2009).
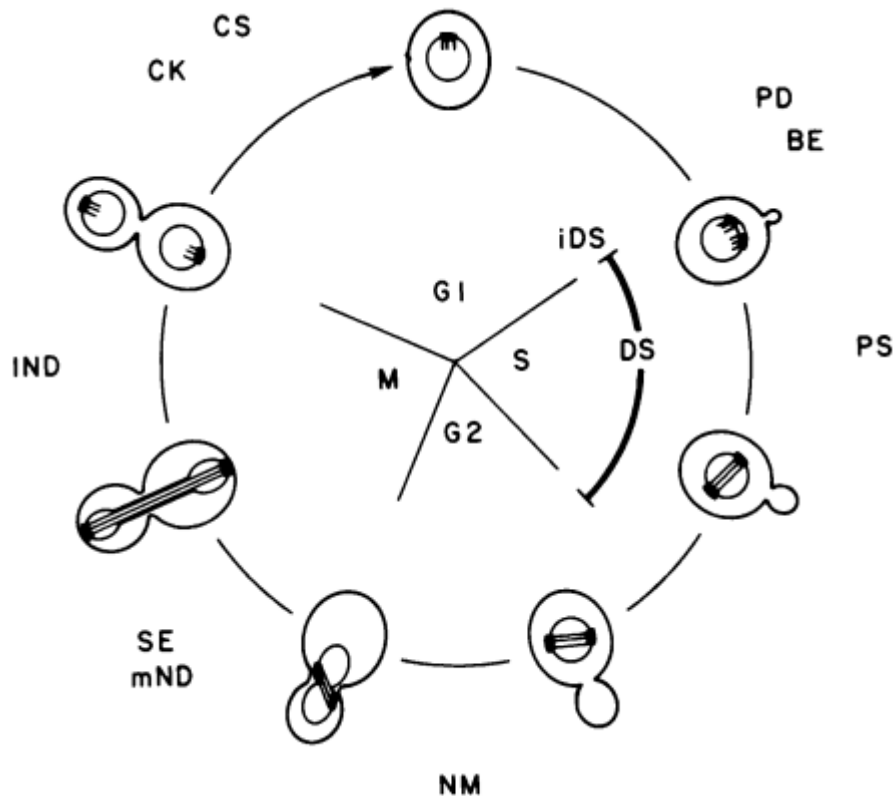
Figure 36. *S. cerevisiae* cell cycle scheme. The cell is represented by the oval shape. The small circle inside the cell represents the nucleus. The rectangular structure embedded into the nucleus represents the SPB (Spindle Pole Body; MTOC of *S. cerevisiae*, see above). Parallel lines represent microtubules of the spindle. BE; bud emergence, NM; nuclear migration, SE; spindle elongation, CK; cytokinesis, CS; cell separation. Abbreviations that are more relevant to the aim of this section are mentioned. For full explanation, see Hartwell (1974). Modified figure from Hartwell (1974).

The correct spindle positioning and the subsequent chromosome segregation is achieved through two partially redundant pathways, named the Kar9 and the dynein pathway (**Figure 37**). Briefly, Kar9 is transported to the plus end of astral microtubules and there, through interaction with Myo2, crosslinks astral microtubules with actin filaments. Myo2 is a myosin (molecular motor that moves along actin filaments), which transports the whole nucleus (and thereby the spindle) at the bud neck and places the spindle in parallel to the mother-bud axis (**Figure 37**) (McNally, 2013).

A little bit later, dynein is transported through astral microtubules to cortical sites of the bud. There, during anaphase, dynein moves along astral microtubules. Its

minus end movement pulls half of the spindle to the bud, leading to delivery of half of the genetic information into the bud (**Figure 37**) (McNally, 2013).
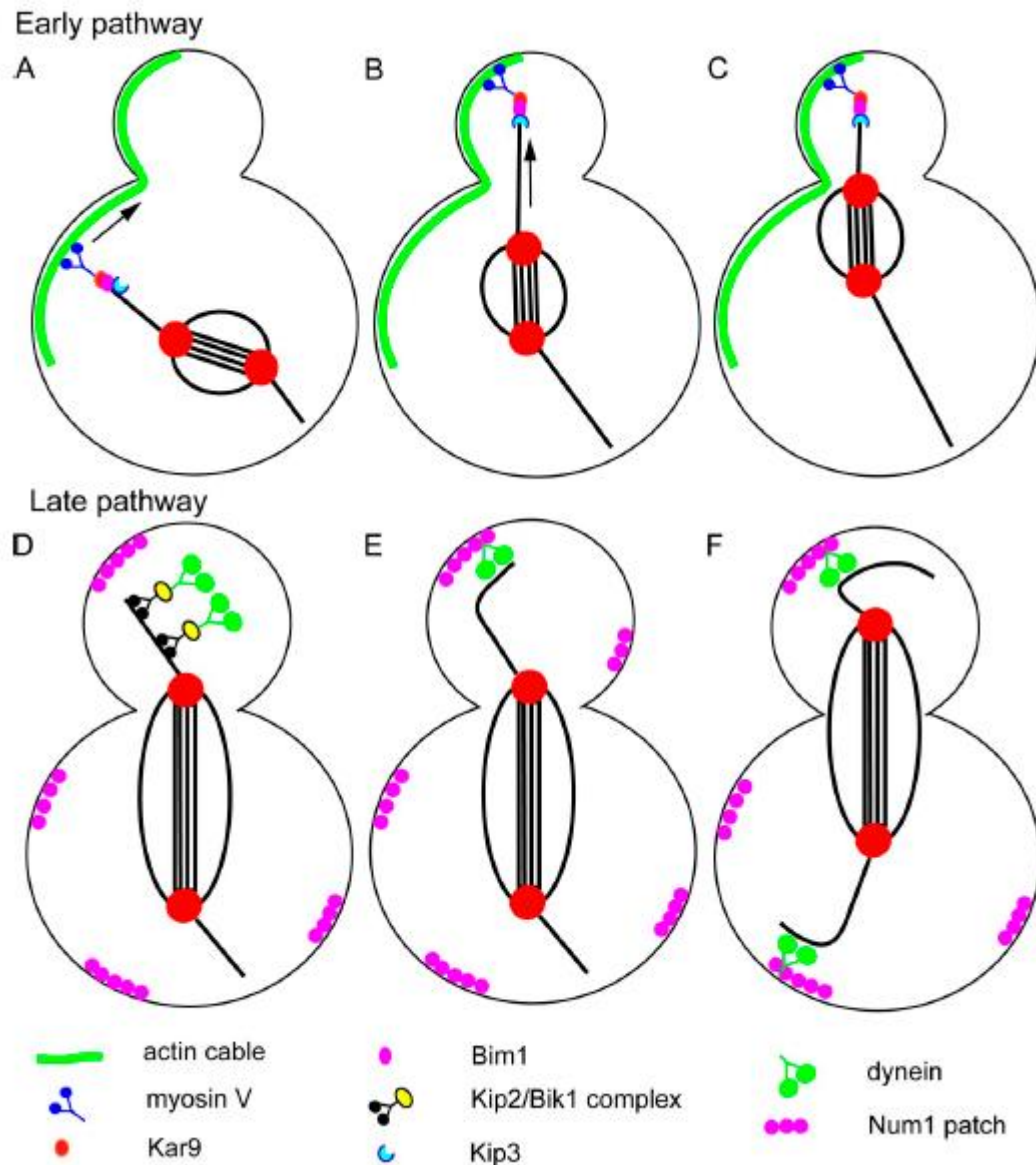
Figure 37. The spindle positioning mechanism in *S. cerevisiae*. Early pathway corresponds to the Kar9 pathway and late pathway to the dynein pathway. Big red dots correspond to the SPBs. Straight black lines connecting the SPBs correspond to spindle microtubules. The two curved black lines connecting the SPBs correspond to the nuclear envelope. The straight black lines protruding to the cytoplasm correspond to the astral microtubules. Modified figure from McNally (2013).

Cellular functions of Kip2

Kip2 participates in the spindle positioning mechanism by transporting dynein (McNally, 2013) (**Figure 37**) and Kar9 (Drechsler et al., 2015; Maekawa et al., 2003; Miller et al., 1998) to the plus end of astral microtubules. Moreover, its presence is restricted only to astral microtubules (**Figure 38**) (Carvalho et al., 2004; Chen et al., unpublished data; Miller et al., 1998).
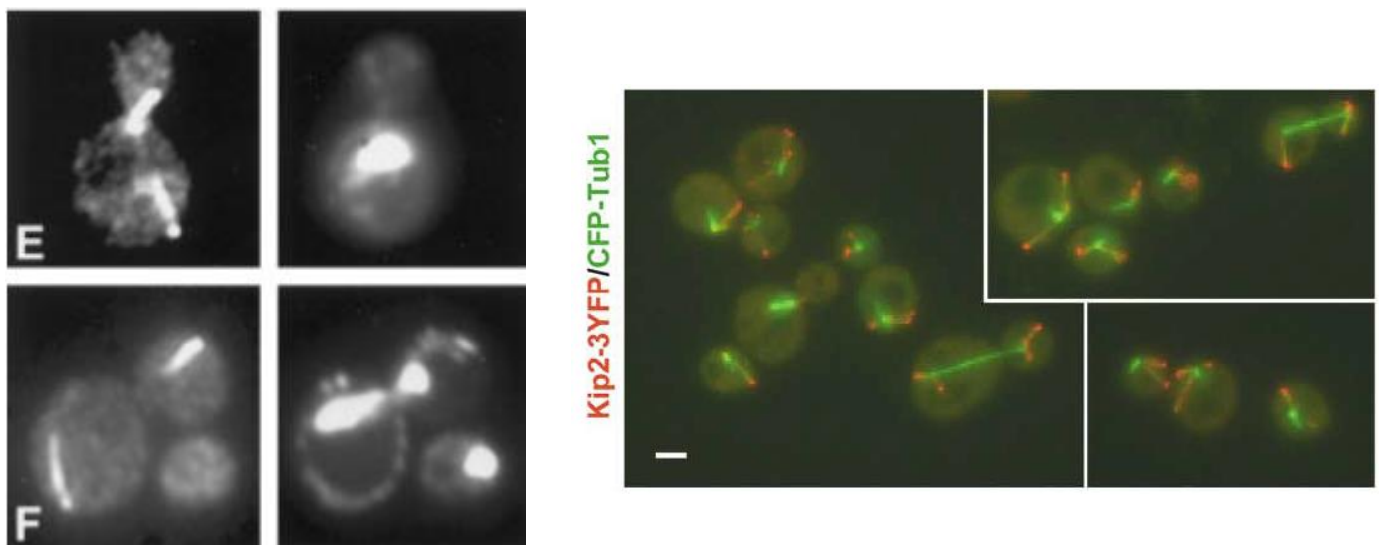
Figure 38. Localization of Kip2 in *S. cerevisiae*. Left figure; first row panels show GFP-Kip2 signal (left panel) and DAPI stained DNA (right panel) at a metaphase cell. Second row panels show Kip2 signal (left panel) and DAPI stained DNA (right panel) at an anaphase cell. Modified figure from Miller et al. (1998). Right figure; Kip2-3YFP (red) localizes to the plus ends of astral microtubules, labeled with CFP-Tub1 (green). Spindle microtubules appear as a straight line, whereas astral microtubules appear as short extensions at one or both ends of the spindle. Modified figure from Carvalho et al. (2004). Compare with Figure 37, to see that Kip2 indeed localizes to astral microtubules.

Experiments in cells lacking the Kip2 gene pointed out two results. The first was that Kip2 is not the only protein responsible for proper localization of Kar9 and dynein. That's because, cells lacking Kip2 were able to grow as normal cells, although they were a little bit more prone to nuclear migration defects. (Miller et al., 1998). The second was that cells lacking Kip2, did not have astral microtubules or if they had, they were very short (**Figure 39**) (Chen et al., unpublished data; Miller et al., 1998). So, it

was proposed that Kip2 has a microtubule stabilizing or assembling effect (Miller et al., 1998).
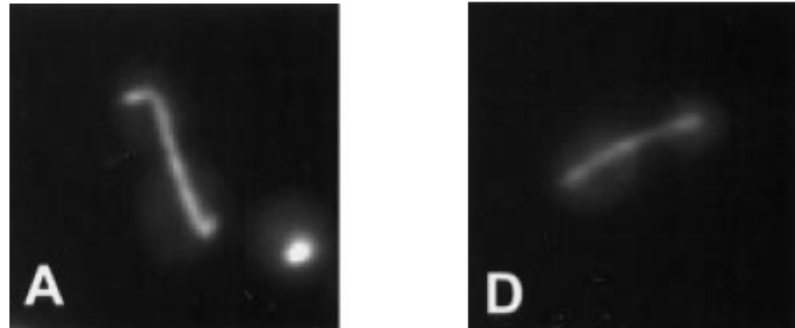
Figure 39. Kip2 deletion leads to absence or presence of very short astral microtubules. Left figure; microtubule morphology of wild type cells. Right figure; microtubule morphology of *kip2Δ* cells. Spindle microtubules appear as a straight line, whereas astral microtubules appear as short extensions at one or both ends of the spindle. Cells were stained with anti-tubulin YOL1/34 antibody. Modified figures from Miller et al. (1998).

Kip2 and microtubule growth

The question was clear; how does Kip2 stabilize microtubules? Some years later, researchers studying Kip2 and Bik1 (a microtubule plus end binding protein), showed that overexpression of Kip2 in wild type cells, led to over-elongated astral microtubules (**Figure 40**). Subsequently, they did the same experiment in cells lacking Bik1 (*bik1Δ* cells). In these conditions, cells were lacking over-elongated astral microtubules. So, the study concluded that Kip2 regulates microtubule dynamics by transferring Bik1 to the plus ends. There, Bik1 stabilizes and promotes microtubule growth (**Figure 40**) (Carvalho et al., 2004).
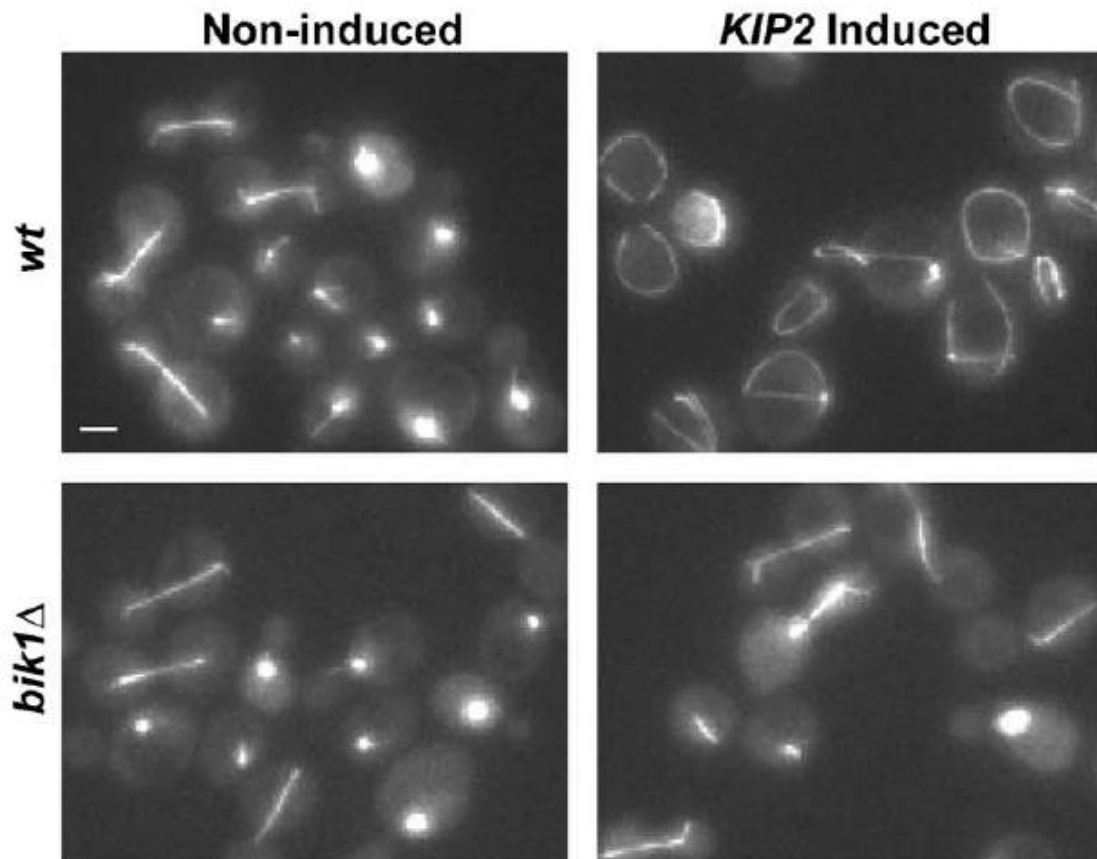
Figure 40. Effect of Kip2 normal levels and Kip2 overexpression in wild type cells and cells lacking Bik1 (*bik1Δ*). The signal comes from GFP-Tub1 (α-tubulin). Spindle microtubules appear as a straight line, whereas astral microtubules appear as short extensions at one or both ends of the spindle. In Kip2 induced, wild type cells, the very long and curved microtubules observed, are astral microtubules. Modified figure from Carvalho et al. (2004).

However, an important experiment was missing. Bik1 can also accumulate to the plus end of microtubules by Kip2-independent mechanisms. In kip2Δ cells, Bik1 fluorescence can still be observed at the plus ends of microtubules, even though in lower levels (Carvalho et al., 2004, Caudron et al., 2008). The missing experiment was observing the length of astral microtubules in kip2Δ cells, that overexpress Bik1. This, based on the proposed mechanism, would have a phenotype similar to overexpression of Kip2 in wild type cells (**Figure 40**).

A paper published in 2015 (Hibbel et al., 2015) studied *in vitro* the properties of Kip2. When researchers added Kip2, free tubulin and GMPCPP-stabilized microtubule seeds, they observed that Kip2 could promote microtubule growth, reduce the catastrophe frequency and act as nucleation factor (**Figures 41, 42**). The

first two features were concentration-dependent and did not require any other protein (Hibbel et al., 2015).

The study concluded that, at least *in vitro*, "Kip2 is a microtubule polymerase and an anti-catastrophe factor". As for how it promotes microtubule growth, researchers came up with two models. In the first one, Kip2 transports free tubulin dimers to the plus end of microtubules. This results to local increase of tubulin concentration at the plus end, leading to microtubule growth. In the second, Kip2 accumulates to the plus end of microtubules. There, it actively incorporates free tubulin dimers and promotes growth (Hibbel et al., 2015).
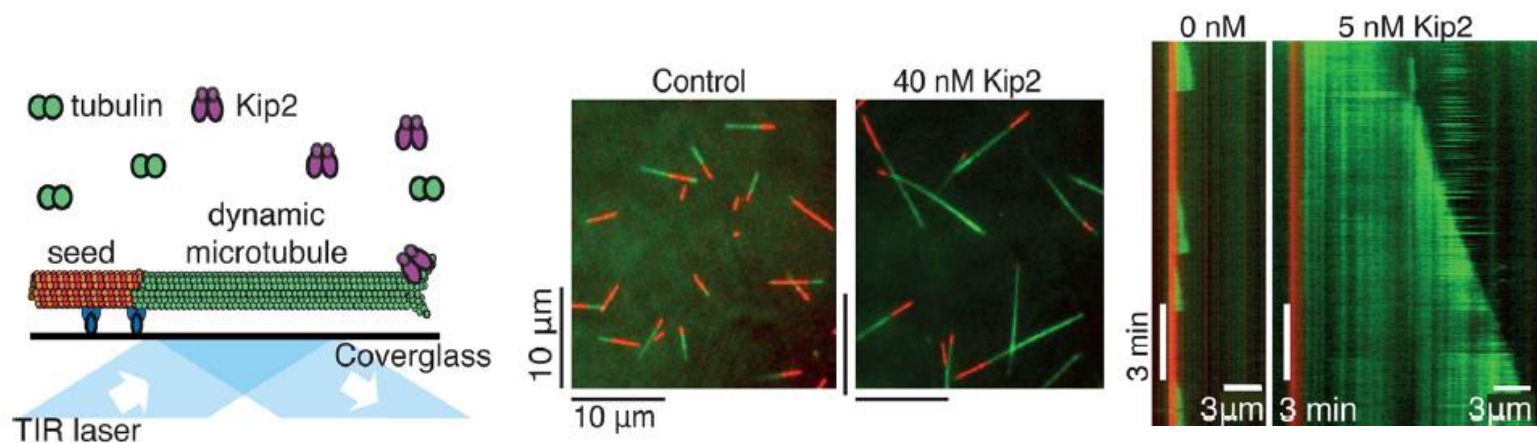
Figure 41. Left; cartoon of the experiment: free tubulin in green, GMPCPP-stabilized microtubule seeds in red, Kip2 in purple. Stabilized microtubule seeds are attached to the coverslip with antibodies (blue). Center; TIRF microscopy images of dynamic microtubules grown from stabilized seeds without and with 40 nM Kip2. Right; Kymograph (length/time plot derived from a movie, with length at x axis and time at y axis) of a microtubule in presence and in absence of Kip2. Modified figures from Hibbel et al. (2015).
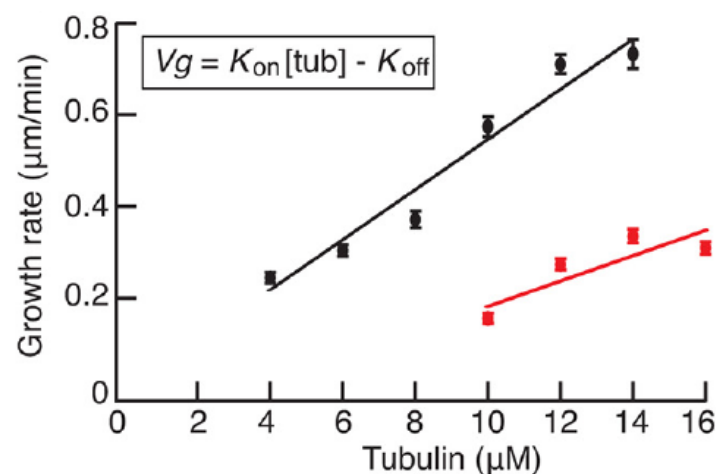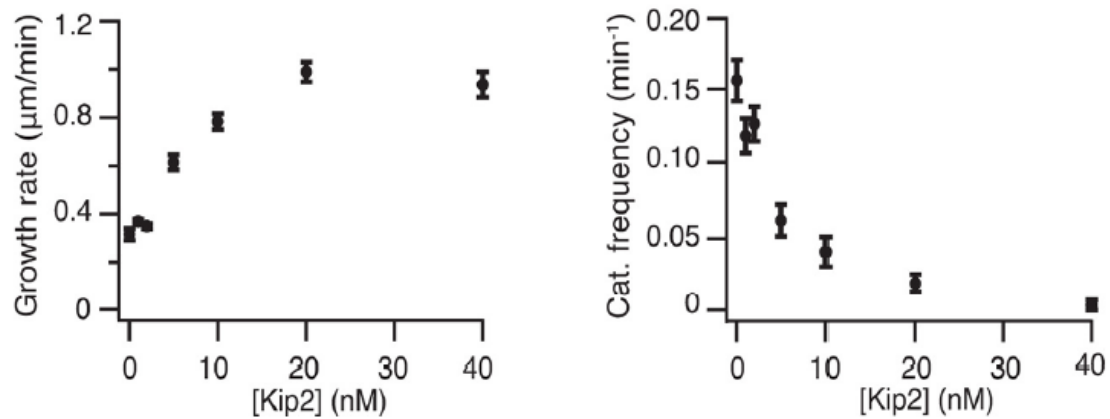
Figure 42. Previous page; Kip2 acts as a nucleation factor. Microtubule growth rate as a function of tubulin concentration in ATP, without Kip2 (red) and with 40 nM Kip2 (black). In absence of Kip2, microtubules grow when tubulin concentration is 10µM, whereas in presence of Kip2 microtubule growth is observed with 4µM of tubulin. Current page; Left; Microtubule growth rate plotted against Kip2 concentration. Right; Catastrophe frequency plotted against Kip2 concentration. Modified figures from Hibbel et al. (2015).

In a recently submitted paper (Chen et al., unpublished data), researchers found that Kip2 can promote microtubule growth through a positively charged area or "patch" (named P1), which is found near the motor domain. Mutation of P1 region (K294A, R296A) led to short astral microtubules *in vivo*. Moreover, *in vitro* experiments with Kip2P1 mutant, free tubulin and GMPCPP-stabilized microtubule seeds [same experiment as in Hibbel et al. (2015)], showed that the mutant could not promote microtubule growth as wild type Kip2 (Chen et al., unpublished data).

Based on these results, researchers proposed that Kip2 accumulates to the plus end of microtubules and promotes microtubule growth, by incorporating free tubulin dimers, through its patch 1 region (Chen et al., unpublished data).

Preliminary experiments in the lab

In our lab, preliminary experiments have shown that Kip2 is able to transfer tubulin to the plus end of microtubules. More specifically, when Kip2, free GDP-tubulin dimers and GMPCPP-stabilized microtubules are mixed (**Figure 43**), a result like in **Figure 44** is observed. Kip2 (in red) processively moves along stabilized

microtubule and accumulates to the plus end. However, the same is true for free GDP-tubulin dimers (in green). They move onto microtubules (green diagonal lines, which seem to overlap with the corresponding of Kip2) and accumulate over time to the plus end (green signal at the plus end is getting brighter). GDP-tubulin was selected because it cannot be incorporated to the microtubule lattice.
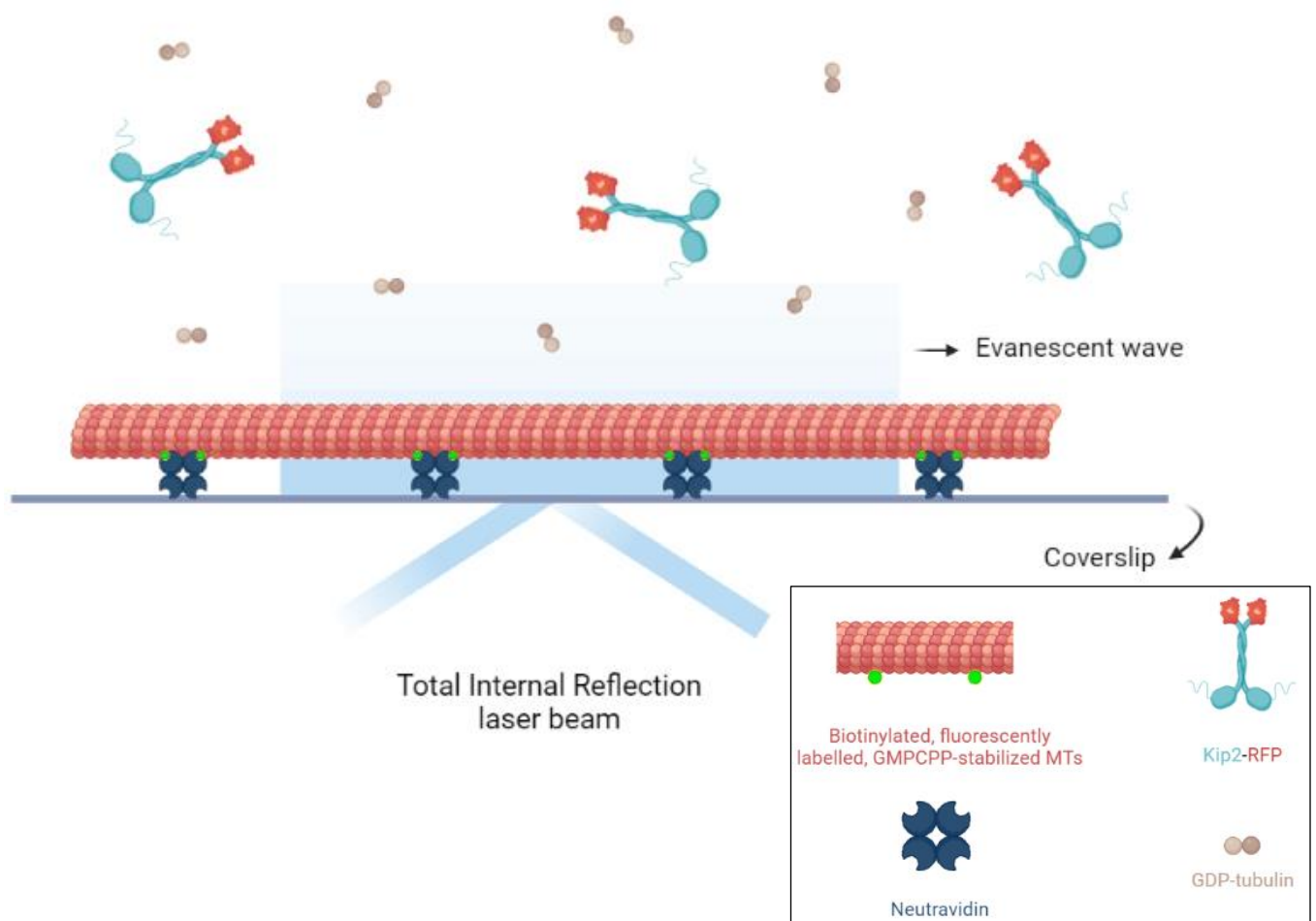
Figure 43. Stabilized microtubules were mixed with GTP-tubulin and Kip2 and observed using TIRF microscopy. Created with BioRender.com

| Stabilized microtubule | Kip2 | GDP-tubulin | Merged |
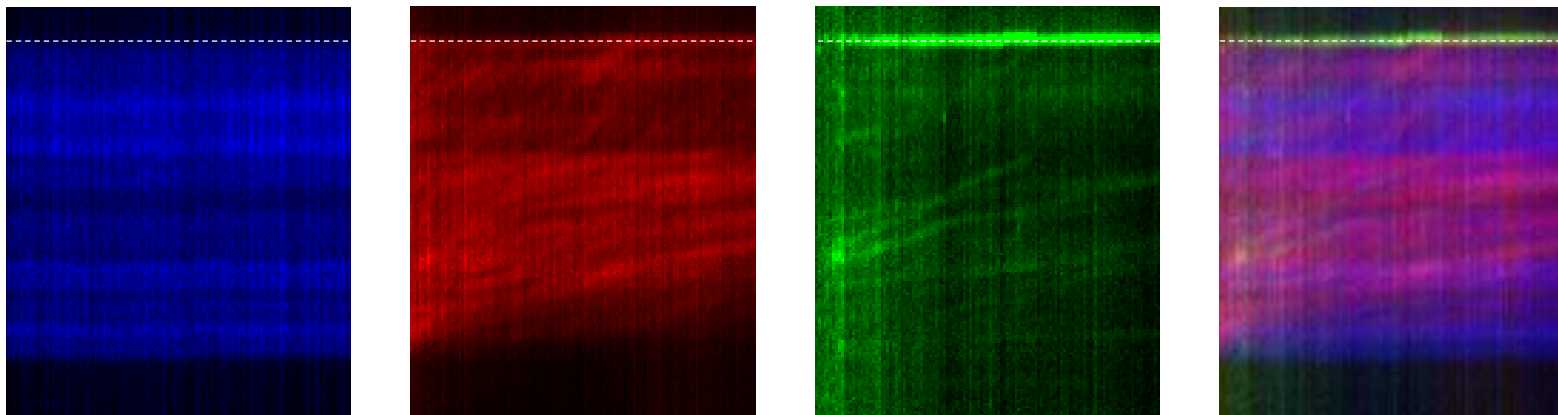
Figure 44. Kymograph (length/time plot derived from a movie, with length at x axis and time at y axis) from the experiment presented in Figure 49. GMPCPP-stabilized microtubule in blue, Kip2 in red, free GDP-tubulin in green. White dotted line marks the plus end of the microtubule. Preliminary experiments in the lab.

The Kip2 structure has not been determined experimentally yet, but a prediction of it is available on AlphaFold (access number in UniProt: P28743, **Figure 45**). Motor domain and α-helices (which seem to promote dimerization by formation of coiled coils) can be seen. Studying the structure further, one can observe something unusual for the majority of kinesins: Kip2 has its motor domain on the N-terminus, but before the this, a sequence of 97 amino acids precedes. Moreover, this area is predicted to be unstructured (**Figure 45**), it has a lot of positively charged or polar amino acids (**Figure 46**) and its pI (isoelectric point; the pH at which this polypetide is neutrally charged) is around 12 (calculated using the "Compute pI/Mw" tool from Expasy). This data predicts that, in the *S. cerevisiae* cytoplasm, the 1-97 amino acids of Kip2 is unstructured and positively charged.
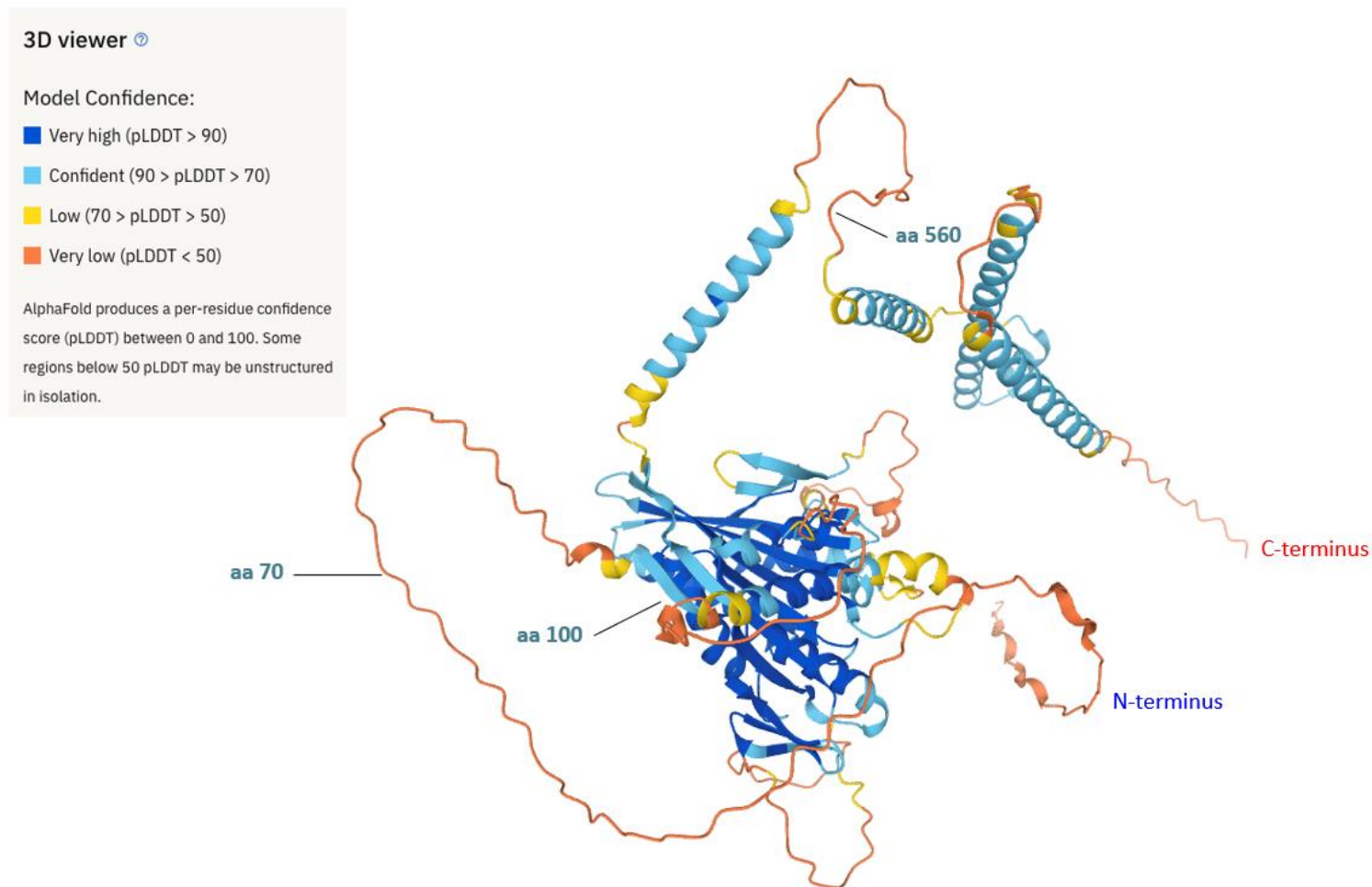
Figure 45. Structure of Kip2 protein. N- and C-terminus and some important residues (see below) are indicated. Kip2 is coloured based on the confidence of each domain. The N-terminus residues preceding the motor domain (1-97) are predicted to have very low confidence, meaning that this area may be unstructured.
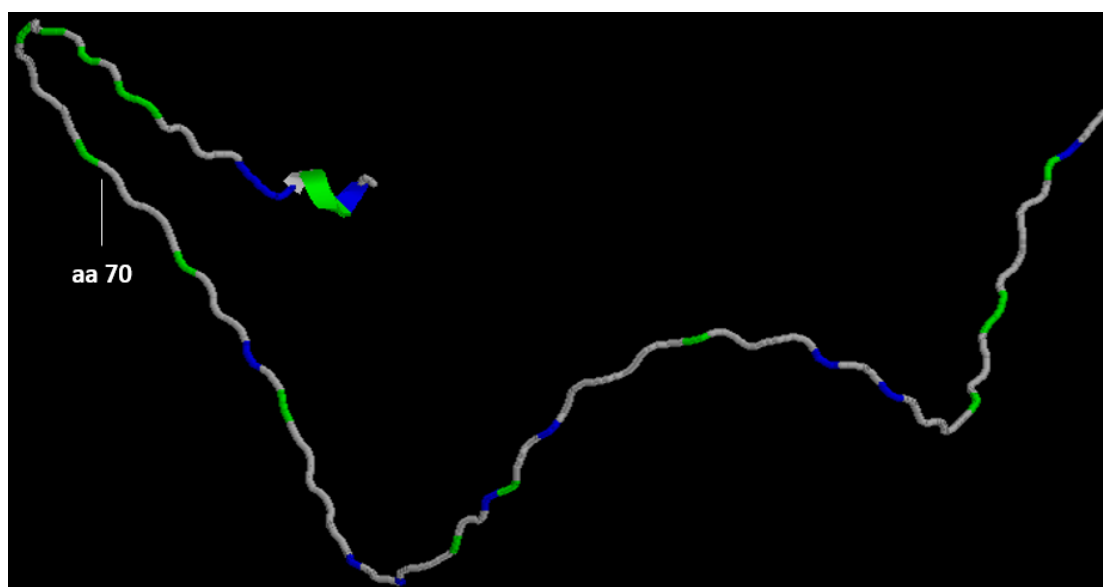
Figure 46. Structure of Kip2 residues 1-97. Positively charged residues (Lysine, Arginine, Histidine) are coloured in green, whereas in blue are Asparagine and Gluatamine. Figure obtained from RasMol.

We therefore wondered if these 97 amino acids could interact with the negatively charged tubulin dimers. For that reason, Kip2Δ70, a mutant lacking the first 70 amino acids of N-terminus, was created (**Figures 45, 46**). *In vitro* experiments showed that removal of these residues, heavily impaired microtubule growth (**Figure 47**). Moreover, Kip2Δ70 mutant could not transfer GDP-tubulin to the plus end of microtubules, although it could reach the plus end (**Figure 48**, compare it with **Figure 44**; experimental procedure as for Kip2, **Figure 43**). We thus hypothesize that the unstructured N-terminus area of Kip2, is capable of transferring free tubulin dimers.
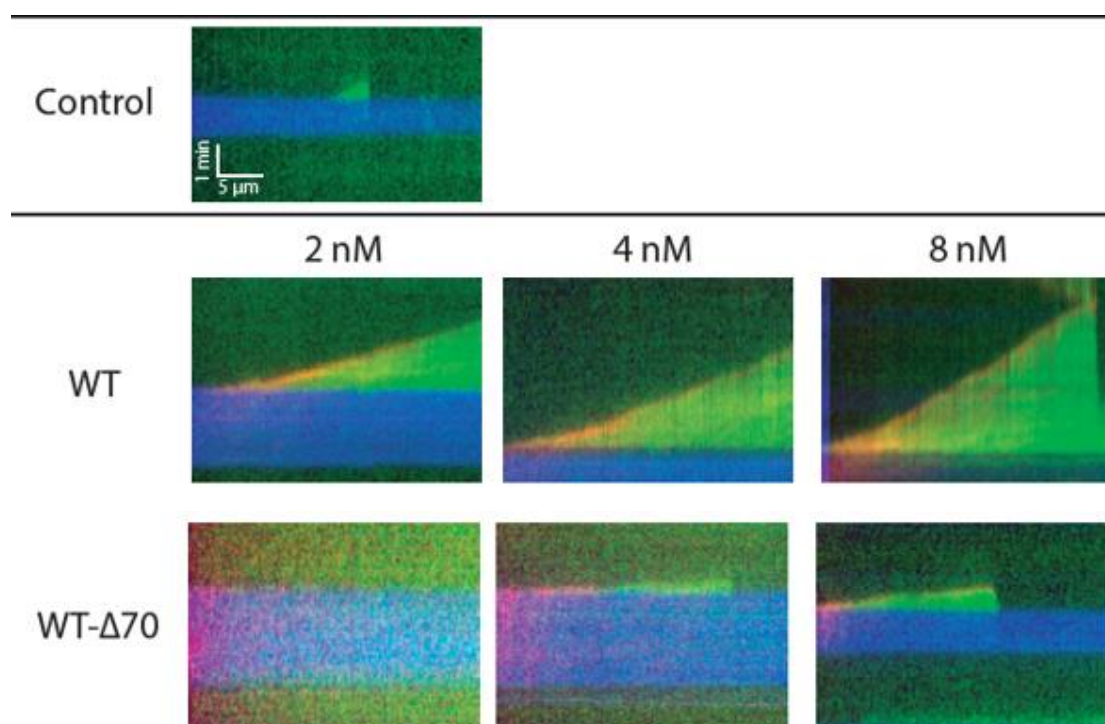
Figure 47. Kymograph of a microtubule growth in presence of Kip2 or Kip2Δ70. Free tubulin in green, GMPCPP-stabilized microtubule seed in blue, Kip2 in red. Preliminary experiments in the lab.
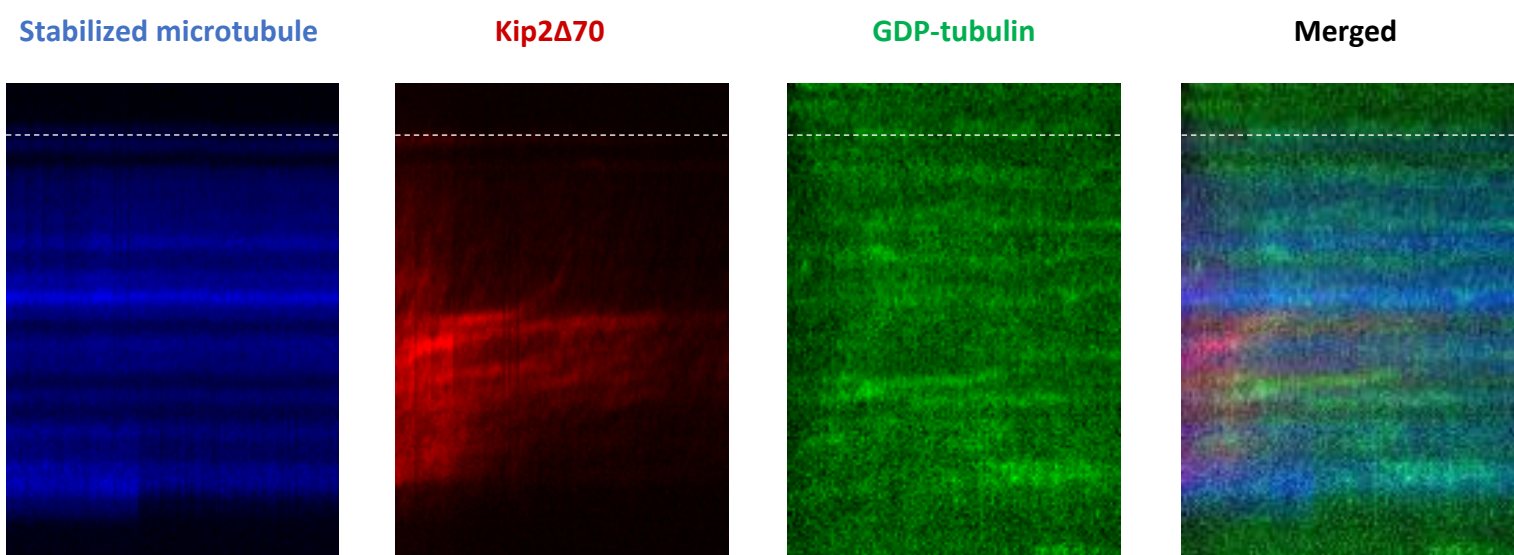
Figure 48. Kymograph of Kip2Δ70 and GDP-tubulin movements onto GMPCPP-stabilized microtubule. Although KipΔ70 moves processively to the plus end, same thing does not apply to GDP-tubulin. GMPCPP-stabilized microtubule in blue, Kip2 in red, free GDP-tubulin in green. White dotted line marks the plus end of the microtubule. Preliminary experiments in the lab.

Aim and importance of the study

The aim of this study is to provide, through *in vitro* experiments, data on the microtubule elongation activity of Kip2. We hypothesize that Kip2 attaches to microtubules through its motor domains, whereas its N-terminus unstructured areas bind to free tubulin dimers. Its processive movement along the microtubules, leads to transfer and accumulation of free tubulin dimers to the plus end. This results in a locally increased tubulin concentration, that promotes microtubule growth (**Figure 49**). There are very few kinesins known to transfer free tubulin dimers. Even the few examples that do so, do not interact directly with tubulin dimers, see **Kinesin-2**). Therefore, this mechanism is so far unprecedented for a kinesin.
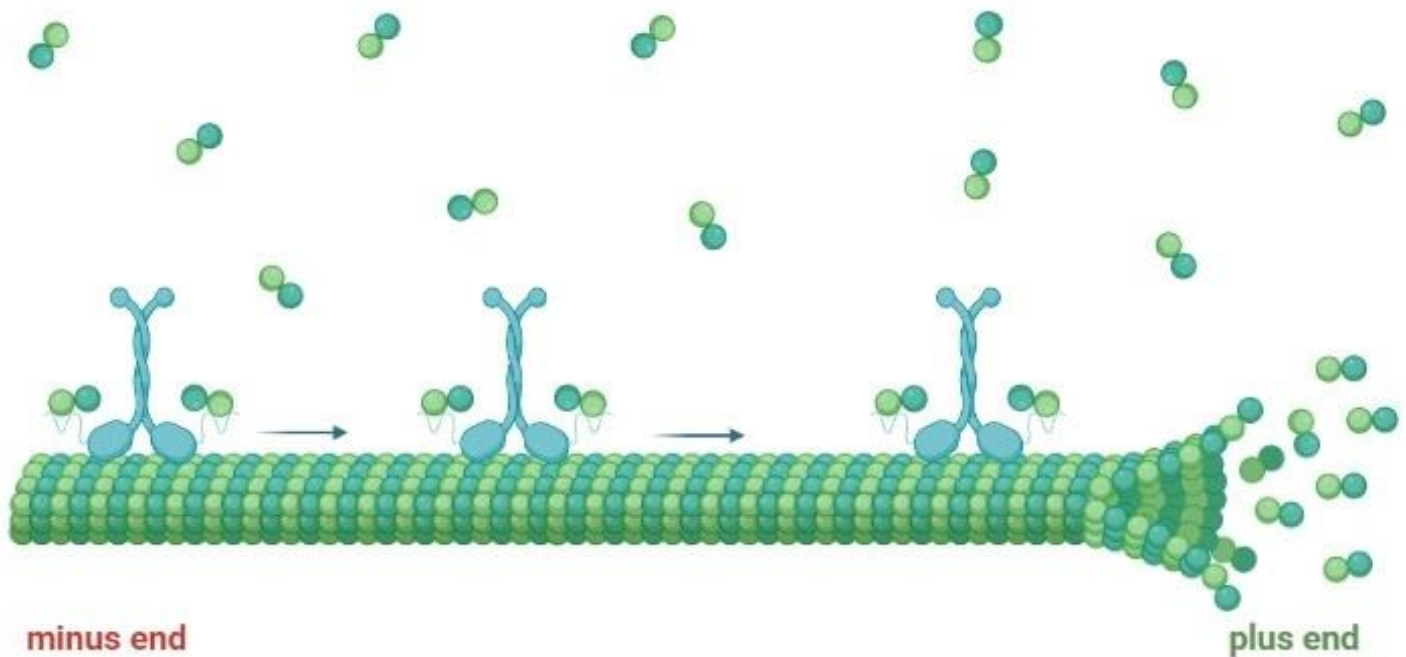
Figure 49. Cartoon depicting our hypothesis for microtubule elongation activity of Kip2. Tubulin dimers are in dark green-light green. Arrows indicate the plus end directed movement of Kip2. Created with BioRender.com

Experimental procedures

Construction of Kip2 expression vectors

Rationale of using two types of vectors

Full-length kinesins are often large and complex proteins that cannot be properly folded into bacteria. In the lab, there have been tries to produce full-length Kip2 (aa 1-706) in bacteria, but without success. It is believed that the α-helices of the C-terminus (**Figure 45**) cannot be properly folded; these helices are thought to form coiled coils and promote dimerization. So, production is restricted to eukaryotic cells, like SF9, an insect cell line. The main difficulties with protein production in that system are the difficult manipulations required and its duration; it takes at least four weeks to produce and isolate the desirable protein (Bac-to-Bac Baculovirus Expression System, Thermo Scientific, 10359016). On the other hand, in a recent study (Chen et al., unpublished data) it has been proven that the truncated version of Kip2 (aa 1-560, **Figure 45**), lacking part of the coiled coils (but still able to dimerize), can processively move along microtubules. The interest of this truncated version of Kip2 is that it can be successfully produced into bacteria.

In this study, vectors for fourteen different versions of Kip2 have been made: seven for bacterial and seven for insect cell expression (**Figure 50 - 53**). For each Kip2 version produced in bacteria, there is its counterpart for insect cell production. The vector chosen for bacterial production is the pET16 plasmid. In this, protein production is under the control of T7 promoter, allowing high transcription levels, whereas presence of *lac* operator allows inducible expression. Truncated Kip2 protein versions inserted into this vector bear two tags that can be exploited for purification. One is the 6xHis-tag, present at the C-terminus of the protein, whereas the other is the MBP (Maltose Binding Protein), present at the N-terminus of the protein (**Figure 53**). MBP, apart from acting as a purification tag, was added to increase the solubility of truncated protein (in case it was insoluble) (Rosano & Ceccarelli, 2014). Moreover, a PreScission site was added between MBP and Kip2 gene, in case the former impaired the N-terminus function (**Figure 53**). **Figures 50 - 52** show the seven different versions

of truncated Kip2. These are MBP-Kip2-His (without any fluorescent protein conjugated to it), MBP-Kip2-mCherry-His, MBP-Kip2Δ70-mCherry-His, MBP-Kip2Δ100-mCherry-His, MBP-Kip2P1-mCherry-His, MBP-Kip2P1Δ70-mCherry-His and MBP-Kip2P1Δ100-mCherry-His. "His" stands for the 6xHis-tag, Kip2Δ100 is a mutant at which the 100 first amino acids from the N-terminus have been removed (like in the Kip2Δ70 mutant) and Kip2P1 is the mutant at P1 region mentioned earlier. Finally, the last two (Kip2P1Δ70 and Kip2P1Δ100) are a combination between the two mutants.

The exact same versions were constructed for insect cell production (**Figure 50 - 53**) with four exceptions. First, Kip2 protein is full-length, second, the MBP tag is absent, third, the vector is pFastBac1 and fourth, PreScission site has been moved between Kip2 gene and the His tag.

MBP-**Kip2**   **MBP**-**Kip2**-**mCherry**   **MBP**-**Kip2Δ70**-**mCherry**

Kip2   **Kip2**-**mCherry**   **Kip2Δ70**-**mCherry**
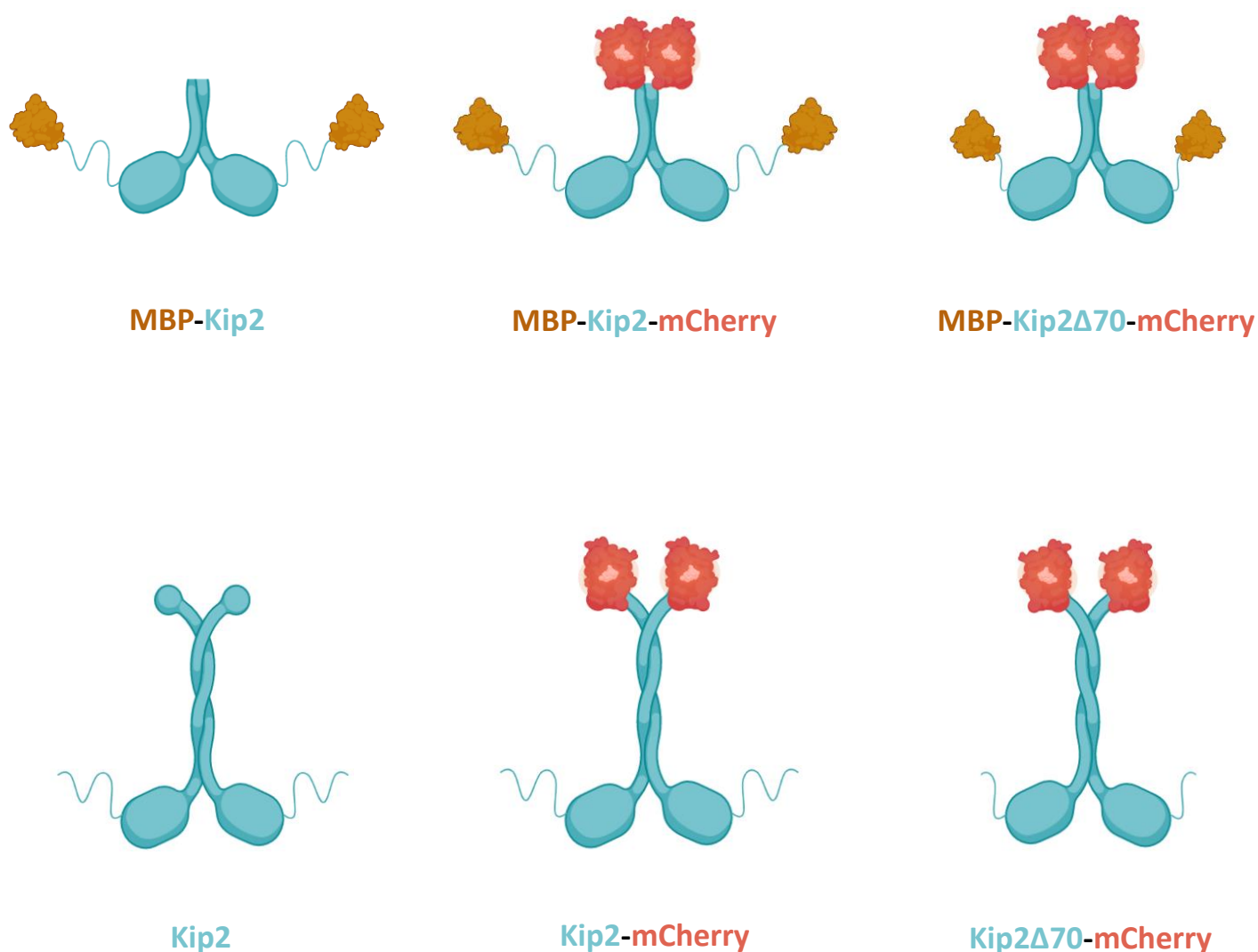
Figure 50. Cartoons of the different Kip2 proteins. Top; Kip2 versions for bacterial expression, bottom; Kip2 versions for insect cell expression. 6xHis-tag at the C-terminus of the proteins is not shown. Created with BioRender.com

MBP-Kip2Δ100-mCherry　　**MBP-Kip2P1-mCherry**　　**MBP-Kip2P1Δ70-mCherry**

Kip2Δ100-mCherry　　**Kip2P1-mCherry**　　**Kip2P1Δ70-mCherry**
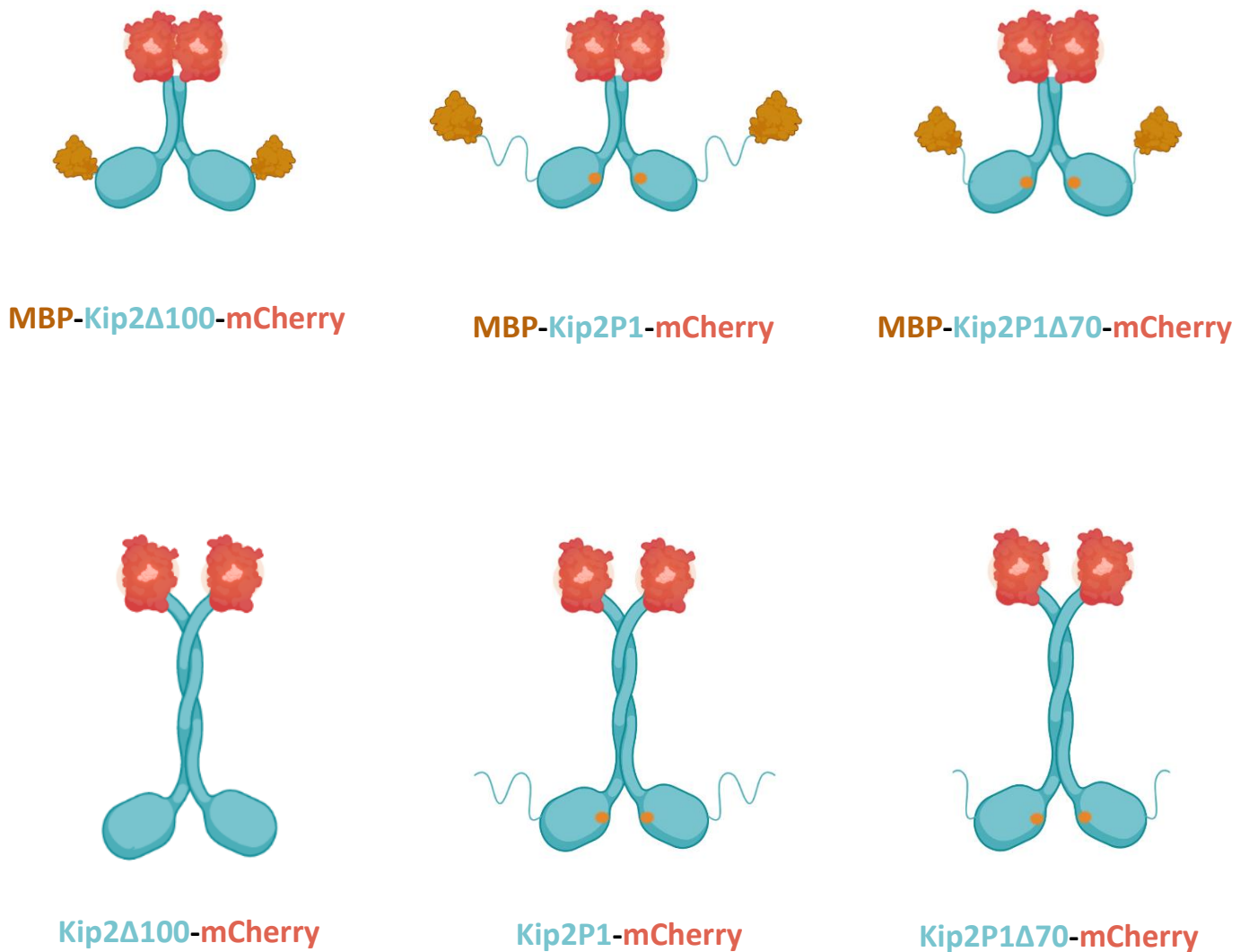
Figure 51. Cartoons of the different Kip2 proteins. Top; Kip2 versions for bacterial expression, bottom; Kip2 versions for insect cell expression.6xHis-tag at the C-terminus of the proteins is not shown. Small orange circles represent the P1 mutation (K294A, R296A). Created with BioRender.com
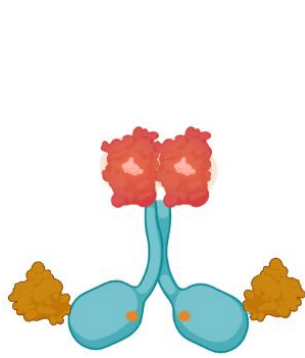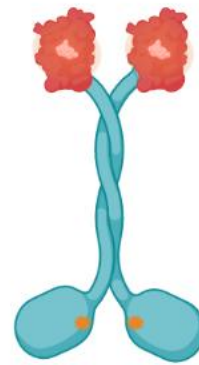
MBP-Kip2P1Δ100-mCherry   **Kip2P1Δ100-mCherry**

Figure 52. Cartoons of the fourteen different proteins. Left; Kip2 version for bacterial expression, right; Kip2 versions for insect cell expression. 6xHis-tag at the C-terminus of the proteins is not shown. Small orange circles represent the P1 mutation (K294A, R296A). Created with BioRender.com
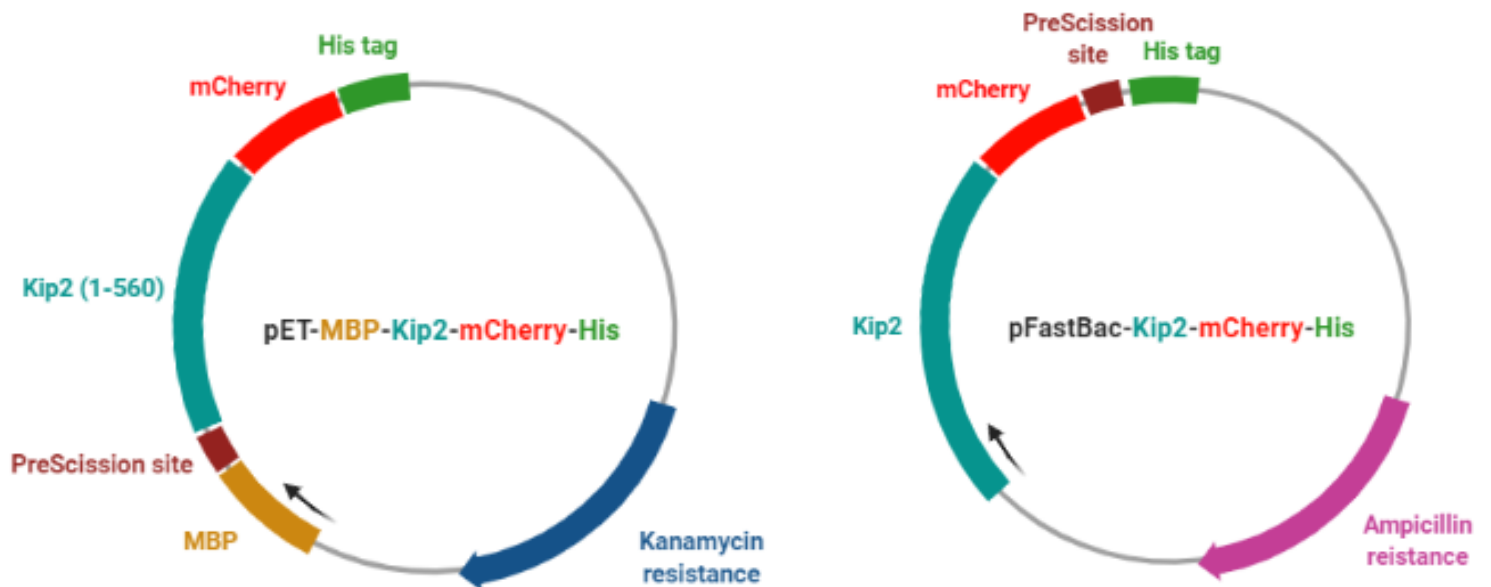
Figure 53. Cartoons of the vectors constructed for bacterial (MBP-Kip2-mCherry-His, left) and insect cell (pFastBac-Kip2-mCherry-His, right) production. Vectors constructed for the rest Kip2 versions have exactly the same structure. "His tag" stands for the 6xHis-tag. Only the genomic loci of interest are presented. Black arrow indicates the direction of transcription / translation. Created with BioRender.com

At PCR reactions, Q5 High-Fidelity DNA Polymerase (NEB, M0491) was used and the company protocol presented in **Table 1, 2** was followed. **Table 3** shows the collection of primers used in this study (primers were obtained from Sigma).

Components	20µl reaction
5x Q5 Reaction Buffer (NEB, B9027S)	4 µl
10 mM dNTPs	0.4 µl
10 µM Forward Primer	1 µl
10 µM Reverse Primer	1 µl
Template DNA	variable
Q5 High-Fidelity DNA Polymerase	0.2 µl
ddH$_2$O	up to 20 µl

Table 1. PCR reaction volumes, according to the NEB protocol

Step	Temperature (ºC)	Time
Initial Denaturation	98	30s
30 Cycles	98	5-10s
	65	10-30s
	72	20-30s/kb
Final Extension	72	2'
Hold	4-10	

Table 2. Thermocycler settings, according to the NEB protocol

Primer name	Sequence	Utility
mCherry_NotI_f	5'-aataGCGGCCGCgggagtgagcaagggcgaggagga-3'	mCherry gene amplification
mCherry_Rev_XhoI	5'-ggcCTCGAGcttgtacagctcgtccatgc-3'	mCherry gene amplification
Kip2FLFoSacI	5'-aacgcGAGCTCatgattcaaaaaatgagcccaagct-3'	Kip2 gene amplification for insertion into pFastBac
Kip2F1RevNotI	5'-aaggaaaaaaGCGGCCGCtttatcgttatccacgacaggg-3'	combination with forward primers for different Kip2 versions amplification and insertion into pFastBac
Kip2D70FoSacI	5'-aacgcGAGCTCatgtccgatcccttccttcaccca-3'	Kip2Δ70 mutant amplification for insertion into pFastBac
Kip2D100FoSacI	5'-aacgcGAGCTCatggggtcaatcactgtgaccatc-3'	Kip2Δ100 mutant amplification for insertion into pFastBac
5' kip2 BamHI	5'-gagGGATCCatgattcaaaaaatgagc-3'	Kip2 gene amplification for insertion into pET
kip2 561 NotIr	5'-aaaGCGGCCGCattgccggtggctttaatgtc-3'	combination with forward primers for different Kip2 versions amplification and insertion into pET
dBamHI 70 kip2f	5'-aaaGGATCCatccgatcccttccttcacccag-3'	Kip2Δ70 mutant amplification for insertion into pET
Kip2D100FoBamHI	5'-aaaGGATCCgatggggtcaatcactgtgaccatc-3'	Kip2Δ100 mutant amplification for insertion into pET
Q5SDM 7/23/19 F	5'-cgcagatgactctcagtatggg-3'	*Kip2 P1 region mutagenesis* (K294A, R296A)
Q5SDM 7/23/19 R	5'-atcgctaattctacgcccaatcc-3'	*Kip2 P1 region mutagenesis* (K294A, R296A)

Table 3. Collection of primers used in this study. Capital letter indicate the sites recognized by restriction enzymes

Digestion reactions were done at 37°C, for 1h. All restriction enzymes used were purchased from NEB. Two types of digestions were carried out. **Table 4** shows the volumes of components when digestion products were to be extracted from gel, purified and used for ligation reaction. **Table 5** shows the volumes of components when digestion products were only to be observed under UV light (e.g., verification of the desirable plasmid). The only difference between the two types of

digestions is the amount of DNA used: when digested DNA was to be isolated a greater amount of it was added, due to loss during the extraction and purification from agarose gel.

Components	20μl reaction
CutSmart Buffer (NEB, B7204S)	2 μl
DNA	10 μl
Enzyme	0.6 μl for each enzyme used
ddH$_2$O	up to 20 μl

Table 4. Digestion reaction volumes when digestion products were to be extracted from gel

Components	10μl reaction
CutSmart Buffer (NEB, B7204S)	1 μl
DNA	2 μl
Enzyme	0.3 μl for each enzyme used
ddH$_2$O	up to 10 μl

Table 5. Digestion reaction volumes when digestion products were only to be observed under UV light

For clean-up of PCR products and gel extraction, the NucleoSpin Gel and PCR Clean-up kit was used (Macherey-Nagel, 740609.50), according to the supplier protocol. Heat shock transformations were done by incubating chemically competent cells at 42°C, for 45s. Plasmid DNA was isolated by GenElute Plasmid Miniprep Kit (Sigma, PLN70), according to the supplier protocol. Gel electrophoresis was done in 0.7% agarose gels for 30', 100V. Mutagenesis PCRs were done according to the manual of QuikChange II Site-Directed Mutagenesis Kit (Agilent, 200523), but recommended materials were replaced with Pfu Turbo DNA

polymerase (Agilent, 600250), DpnI from NEB (R0176S), custom-made dNTP mix and XL1 Blue competent cells, and LB Broth.

At ligation reactions, T4 DNA Ligase (NEB, M0202) was used and the company protocol presented in **Table 6** was followed. Reactions were incubated at room temperature, for 1h.

Components	10μl reaction
T4 DNA Ligase Buffer (10x) (NEB, B0202S)	1 μl
Vector DNA (4 kb)	0.020 pmol
Insert DNA (1 kb)	0.060 pmol
T4 DNA Ligase	0.5 μl
Nuclease-free water	up to 10 μl

Table 6. Ligase reaction volumes, according to the NEB protocol

Insertion of mCherry gene into vectors

For the rest of the study, although PreScission site is included in the gene cassette (**Figure 53**), it will be omitted. Moreover, 6xHis-tag will be referred as "His". mCherry gene was PCR amplified from a plasmid with primers mCherry_NotI_f and mCherry_Rev_XhoI, followed by product clean-up. mCherry, pFastBac-linker-His and pET-MBP-linker-His were digested with restriction enzymes NotI, XhoI, extracted from agarose gel after electrophoresis, purified and ligated. Ligation products were transformed into chemically competent XL1 Blue cells. Cells transformed with the pFastBac vector were grown on LB agar with ampicillin (50 μg/ml) (Ampicillin sodium salt, Sigma, A9518), whereas cells transformed with the pET vector were grown in presence of kanamycin (50 μg/ml) (Kanamycin sulfate, Sigma, 60615). Both cell populations were grown overnight (O/N), at 37°C. Plasmid DNA was isolated from colonies and verification of desirable plasmids was done with proper

restriction enzyme digestions. pFastBac-mCherry-His and pET-MBP-mCherry-His vectors were created.

Construction of pFastBac gene cassettes for insect cell expression

Full-length Kip2 gene (named "Kip2") was isolated from *S. cerevisiae* genomic DNA, in a PCR reaction with primers Kip2FLFoSacI and Kip2F1RevNotI. PCR product was cleaned and used as template for two PCRs: one with primers Kip2Δ70FoSacI, Kip2F1RevNotI and one with primers Kip2Δ100FoSacI, Kip2F1RevNotI, to create Kip2Δ70 and Kip2Δ100 mutants respectively. After amplification, products were cleaned. pFastBac-mCherry-His, Kip2, Kip2Δ70 and Kip2Δ100 were digested with restriction enzymes NotI, SacI. Procedure followed afterwards is described above: pFastBac-Kip2-mCherry-His, pFastBac-Kip2Δ70-mCherry-His and pFastBac-Kip2Δ100-mCherry-His vectors were created.

pFastBac-Kip2-His was created after digestion of Kip2 and pFastBac-linker-His with NotI, SacI and ligation of the products.

pFastBac-Kip2P1-mCherry-His, pFastBac-Kip2P1Δ70-mCherry-His and pFastBac-Kip2P1Δ100-mCherry-His vectors have not yet been created, since all the mutagenesis PCR attempts have failed.

Construction of pET gene cassettes for bacterial expression

Full-length Kip2 gene was used as template in three PCRs: one with primers 5' kip2 BamHI, kip2 561 NotIr, one with dBamHI 70 kip2f, kip2 561 NotIr, and one with Kip2D100FoBamHI, kip2 561 NotIr. Kip2(1-560), Kip2Δ70(70-560) and Kip2Δ100(100-560) were the products of each reaction respectively. Products were cleaned and along with pET-MBP-mCherry-His, were digested in presence of restriction enzymes NotI, BamHI. Procedure followed afterwards is described above: pET-MBP-Kip2-mCherry-His, pET-MBP-Kip2Δ70-mCherry-His and pET-MBP-Kip2Δ100-mCherry-His vectors were created.

pET-MBP-Kip2-His was created after digestion of Kip2 and pET-MBP-linker-His with NotI, BamHI and ligation of the products.

pET-MBP-Kip2-mCherry-His, pET-MBP-Kip2Δ70-mCherry-His or pET-MBP-Kip2Δ100-mCherry-His vectors were mixed with primers Q5SDM 7/23/19 F and Q5SDM 7/23/19 R in a mutagenesis PCR. pET-MBP-Kip2P1-mCherry-His, pET-MBP-Kip2P1Δ70-mCherry-His and pET-MBP-Kip2P1Δ100-mCherry-His vectors were created. Mutagenesis creates a new restriction site recognized by the enzyme PvuI, allowing for detection of successful mutagenesis (sequence 5'-AAAATCAGA-3' mutates into 5'-GcgatcgCA-3', small letters indicate the site recognized by PvuI).

Proper insertion of Kip2 variations and mCherry gene was verified by sequencing of these areas, at all vectors created.

Buffers and media

The buffers and media used for the following experiments are presented in **Table 7**.

Buffer / Media	Components
2YT media (1L)	Tryptone (Formedium, TRP03) 16 gr, Yeast Extract (Formedium, YEA02) 10 gr, Sodium Chloride 5 gr
2xT buffer	40 mM Tris-Base pH 7.4 (Trizma base, Sigma, T1503), 400 mM KCl, 2.5 mM MgCl$_2$
4xT buffer	80 mM Tris-Base pH 7.4, 800 mM KCl, 5 mM MgCl$_2$
Lysis buffer	4xT buffer, 5 mM β-mercaptoethanol (Sigma, M6250), 0.1 mM ATP (Jena Bioscience, NU-1010), protease inhibitor (SigmaFAST, protease inhibitor Cocktail EDTA-Free, Sigma, S8830)
Purification buffer	2xT buffer, 5 mM β-mercaptoethanol, 0.1 mM ATP, protease inhibitor
Washing buffer	2xT buffer, 5 mM β-mercaptoethanol, 0.1 mM ATP, MilliQ water
Elution buffer	2xT buffer, 10 mM maltose, 5 mM β-mercaptoethanol, 0.1 mM ATP, MilliQ water, 5% glycerol
BRB80 1x pH 6.85	80 mM PIPES (Euromedex, 1124), 1 mM MgCl$_2$, 1 mM EGTA (Sigma, E4378)
BRB80 1x/BSA pH 6.85	BRB80 1x pH 6.85, 10 µl/ml BSA 10%

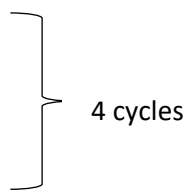|	
Elongation buffer pH 6.85	BRB20 1x (20 mM PIPES, 1 mM MgCl$_2$, 1 mM EGTA) supplemented with 100 mM KCl, 0.025% of 2% methyl cellulose, 50 µg/ml BSA, 1 mM GTP (Jena Bioscience, NU-1012), 1 mM ATP, 20 mM DTT (dithiothreitol, Euromedex EU0006-B), 4.5 mg/ml glucose, 0.35 mg/ml catalase, 0.2 mg/ml glucose oxidase, 10 µM porcine brain tubulin (95 % unlabeled, 5% ATTO-488-labeled), 50 nM Kip2 or Kip2Δ70 Kip2 and tubulins are added in the elongation buffer just before imaging

Table 7. Buffers and media used.

Production and purification of truncated Kip2

Due to time constraints, only the truncated forms of Kip2 (except from MBP-Kip2) could be purified. Moreover, only the MBP-Kip2-mCherry and MBP-Kip2Δ70-mCherry proteins could be tested for their effects on microtubule growth. Test of the remaining truncated versions as well as production and test of the full-length versions will be addressed in a future job.

Chemically competent Rosetta cells [*E. coli* strain BL21(DE3)] were heat shock-transformed with pET plasmids and grown on LB agar with kanamycin (50 µg/ml), O/N, at 37°C. 2-3 colonies from each transformation were picked and grown in 50 ml LB with kanamycin (50 µg/ml) O/N, at 180rpm, 37°C.

20 ml of that O/N culture were inoculated into 1L of 2YT media with kanamycin and chloramphenicol (Sigma, C0378) (50 µg/ml and 34 µg/ml respectively). Rosetta cells bear a plasmid encoding the chloramphenicol resistance gene and rarely used tRNAs in *E. coli*. So, by addition of chloramphenicol, it is ensured that bacteria will not lose this plasmid and codon bias will not affect protein quality (*E. coli* and *S. cerevisiae* have different codon usage; Gustafsson et al., 2004). Cells were grown at 37°C until 0.5<OD$_{600}$<0.6, then chilled on ice for 15', with shaking every 2'. Protein production was induced by addition of 0.2 mM IPTG (isopropyl 1-thio-β-D-galactopyranoside, Euromedex, EU0008). A sample of 50 µl was taken before IPTG addition, to check protein induction. Cells were grown O/N, at 180 rpm, 18°C.

After O/N induction, a sample of 50 μl and similar OD_{600} with the previous one was taken, to check protein induction. Cells were centrifuged at 3500rpm, for 20', at 4°C. Cell pellet was resuspended in 25 ml cold 4xT buffer and centrifuged at 4500G, for 10', at 4°C. Pellet was weighted and resuspended into 5 ml Lysis buffer/gr of cells, followed by lysis via sonication, with the following conditions:

> ➢ 0.8 seconds on/0.2 seconds off, for
>   a total time of 1' per sonication cycle
>
> ➢ 2' pause between each sonication cycle

4 cycles

First cycle was at 65% amplitude, whereas the other three at 75%. When cells could not be lysed easily, an 85% amplitude was used in the last cycle. A sample of 50 μl was taken, to check protein solubility (**crude lysate**). Cell lysate was centrifuged at 12,000 rpm, for 45', at 10°C. Supernatant was collected and a sample of 50 μl was taken (**clear lysate**). 1:1 dilution of the supernatant with MilliQ water followed: ATP, β-mercaptoethanol and protease inhibitor were added, to maintain their concentration stable (Purification buffer). Protein was purified using affinity chromatography with 2.25 ml of Amylose resin beads (NEB, E8021). Beads were washed two times with 10 ml MilliQ water and two times with 10 ml 2xT buffer before use. Supernatant was added to the amylose resin beads and the sample was gently rotated at 4°C, for 3 hours. Subsequently, sample was centrifuged at 1000 rpm, for 3-4', at 4°C. Before discarding supernatant, 50μl were taken, to check if all the protein was attached to amylose resin beads (**flow through**). Beads were washed with 10 ml Washing buffer, centrifuged at 1000 rpm, for 1-2', at 4°C. This was repeated 4-5 times more. Afterwards, protein was eluted: 1ml Elution buffer was added each time and sample was incubated for 5-10'. Centrifugation at 1000 rpm, for 1-2', at 4°C followed. After each centrifugation, supernatant was collected and 50μl were taken, to check the presence of the protein (**eluate**). Most of the times, three elutions were enough to collect all the protein.

Dialysis purification followed: All the supernatants collected, were added into a hydrated tube. The tube was sealed and incubated into 1L of 2xT, for 1h, at 4°C, with optional, gently rotation of the sample. After 1h, 2xT buffer was replaced with a new one and the sample was incubated for one more hour. Final product was supplemented with 0.1 mM ATP and centrifuged at max speed, for 10', at 4°C. Supernatant was collected and 5% glycerol was added. A sample of 50μl was taken, to check the presence of the protein (**after dialysis**). Protein was aliquoted in single-use aliquots, instantly frozen in liquid nitrogen and stored at -80 °C. Purification success was evaluated by SDS-PAGE electrophoresis. Protein concentration was measured using the Bradford assay and counting the absorbance at 280nm, on NanoDrop 2000 Spectrophotometer (Thermo Scientific, ND-2000).

SDS-PAGE

The 50μl samples collected from each step of purification (cells before and after induction, crude lysate, clear lysate, flow through and the eluates) were evaluated on SDS-PAGE (Sodium Dodecyl Sulfate-PolyAcrylamide Gel Electrophoresis). The first two samples (cells before and after induction) were centrifuged at max speed for 2' and supernatant was removed. Laemmli buffer 1x was added in all samples and boiling for 10', at 90°C followed. At some samples, addition of more Laemmli was required, to be fully soluble. 5μl from each sample were loaded. Electrophoresis of a 5% stacking/10% separation gel was done at 90V, for 10', then at 180V. Subsequently, gel was stained for 5' with Coomassie, destained in 7.5% acetic acid, 5% methanol buffer O/N and scanned.

In vitro reconstitution assay and TIRF microscopy

Porcine brain tubulin was purified as described in Castlodi & Popov (2003). NHS-Biotin- (Thermo Scientific, Ez-link NHS-LC-LC-Biotin, 21343), NHS-ATTO-488- (ATTO-TEC, AD488-31) and NHS-ATTO-647- (ATTO-TEC, AD647-31) labelled tubulins were prepared as described in Hyman et al. (1991). Biotinylated, ATTO-647-labelled

and GMPCPP- (Jena Bioscience, NU-405) stabilized microtubule seeds were prepared as described in Chen et al. (unpublished data). Silanized coverslips were prepared as described in Portran et al. (2017).

Flow chamber of ~11 μl was assembled from the silanized coverslip and coverslide, using double sided tape (LIMA, 70pc). The chamber was treated with 30μl of neutravidin (100 μg/ml) (Thermo Scientific, 31050) in PBS 1x for 1', then incubated with 100μl solution of 2% Pluronic F-127 (Sigma, P2443) for 1-5'. A wash with 100μl BRB80 1x/BSA followed, and 50μl microtubule seeds (0,2 μM) were allowed to attach to the neutravidin-coated surface for 1-5'. Chamber was washed with 100μl BRB80 1x/BSA and then 50μl elongation buffer were added. Chamber was fully sealed and immediately imaged under TIRF microscope (objective-based azimuthal ilas2 TIRF microscope, Nikon Eclipse Ti, modified by Roper Scientific) using an 100x/1.49NA Plan TIRF Apochromat, oil-immersive lens and 488, 561 and 642nm lasers for sample excitation. Emitted photons were collected by CMOS back-illuminater Prime95B Photometrics (1200x1200, 11 μm pixel size) (Eledyne Photometrics, Prime95B). Imaging was performed in a temperature-controlled chamber, at 30°C. Data was collected every 5s for 10', using Metamorph software. Analysis of microtubule dynamics and generation of kymographs were done using ImageJ software.

Experimental procedures can be summed up in the cartoons presented in **Figures 54, 55.**

Kymograph and statistical analysis

Generated kymographs were used to analyze seven parameters: growth time, growth speed, depolymerization speed, catastrophe and rescue frequency, time needed until the first growth and number of microtubules growing for the whole imaging period. For the first six parameters, calculation of statistically significant differences between the different conditions tested [control (absence of Kip2), MBP-Kip2-mCherry, MBP-Kip2Δ70-mCherry], was performed by Mann-Whitney test. For the last one, Fisher's exact test was used. Statistical analysis was performed using the Prism software.
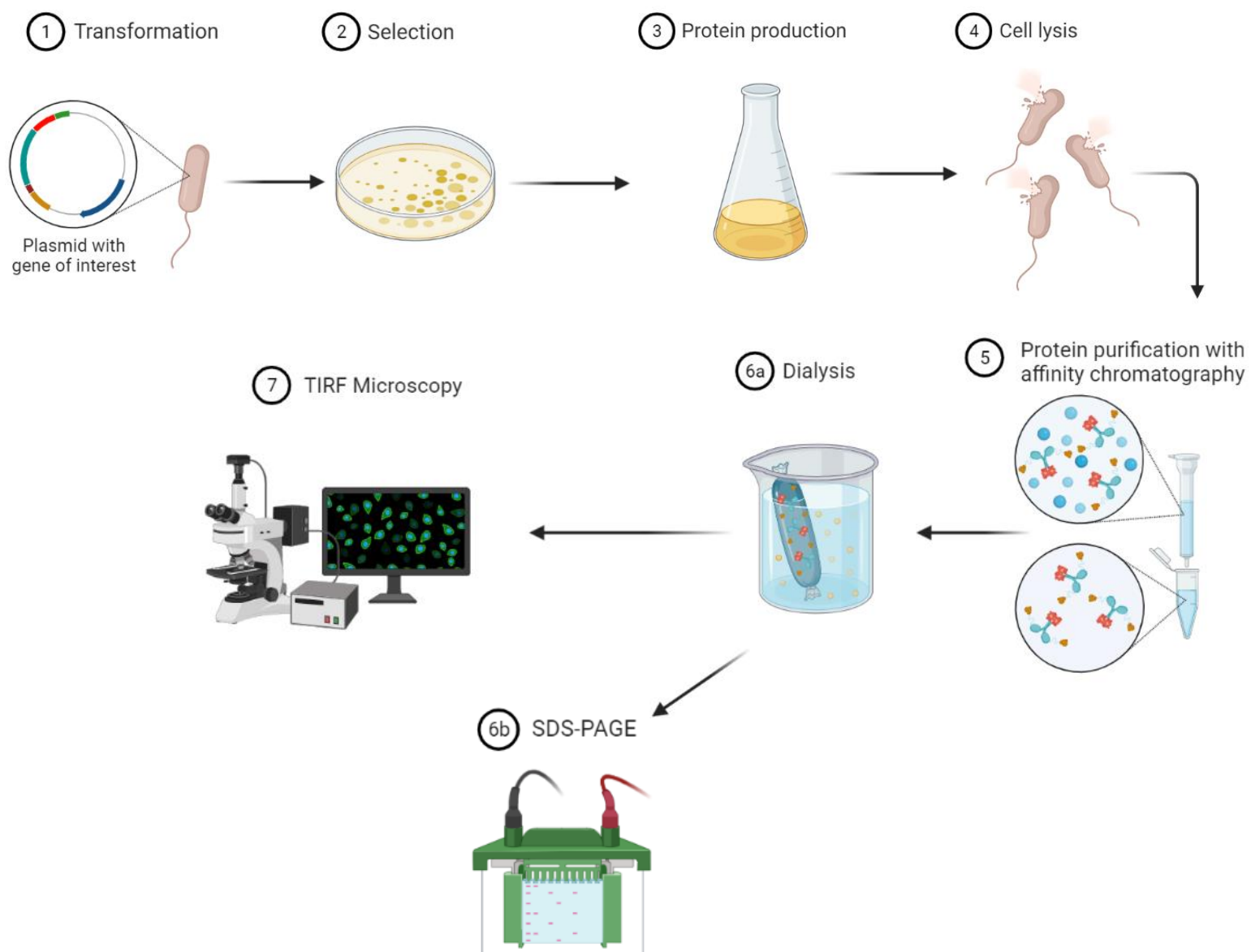
Figure 54. Cartoon depicting the experimental procedure. Created with BioRender.com
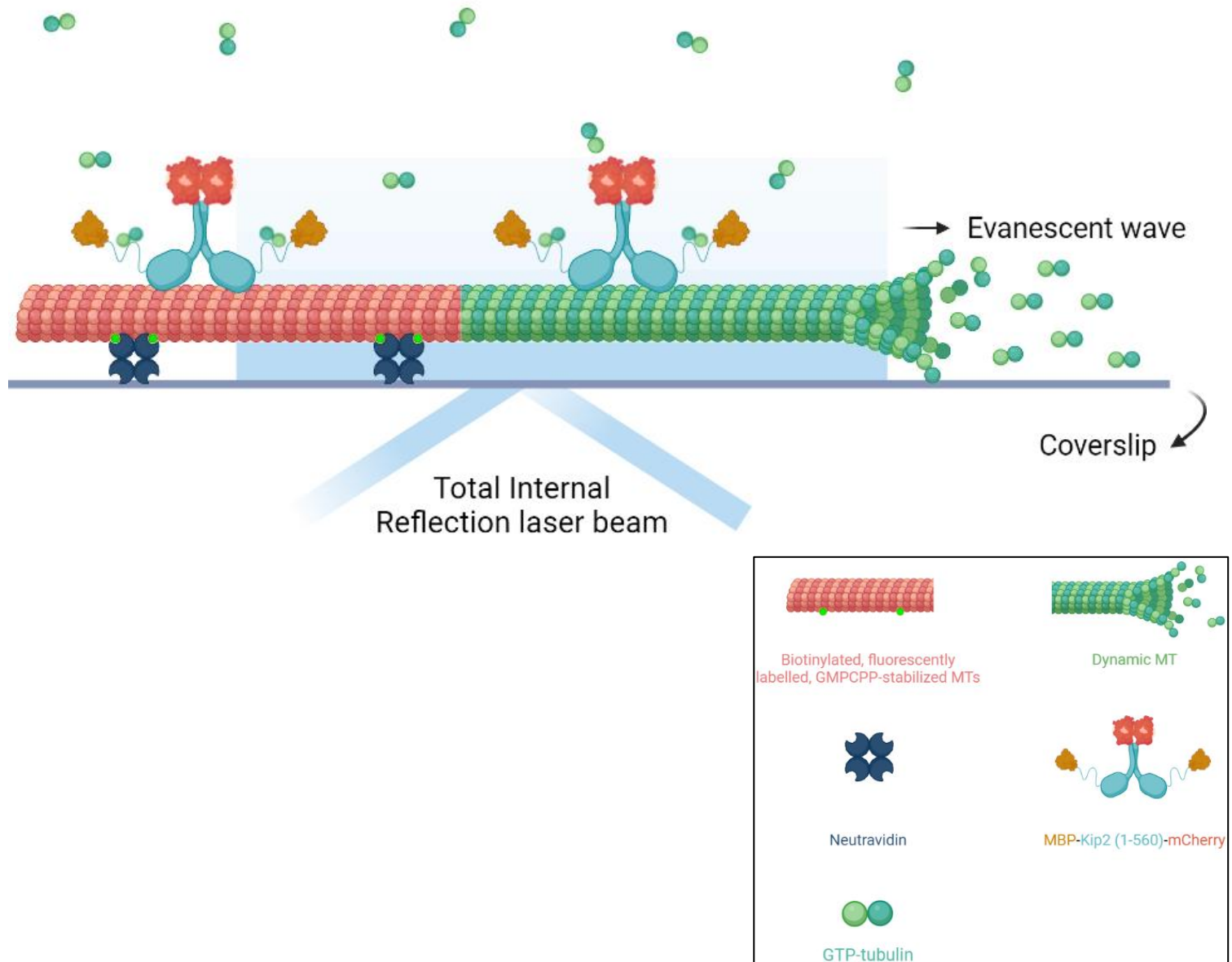
Figure 55. Stabilized microtubules were mixed with GTP-tubulin and Kip2 and observed using TIRF microscopy. Created with BioRender.com

Results

SDS-PAGE

SDS-PAGE results for the six purified proteins are presented below (**Figure 56-61**). The truncated form of Kip2 (1-560) has a molecular mass of approximately 62.4 kDa, whereas MBP is about 43 kDa and mCherry 26.7 kDa. Moreover, the PreScission site and the 6xHis tag have a molecular mass of 3.7 kDa (with the assumption that each amino acid weighs ~110 kDa). So, the MBP-Kip2-mCherry protein has a molecular mass of 135.8 kDa approximately. MBP-Kip2P1-mCherry has also the same molecular mass. MBP-Kip2Δ70-mCherry and MBP-Kip2P1Δ70-mCherry weigh about 128 kDa, whereas MBP-Kip2Δ100-mCherry and MBP-Kip2P1Δ100-mCherry 125 kDa (each amino acid weighs ~110 kDa).

Based on these, an intense band at ~130 kDa is expected. Indeed, in all cases (**Figure 56-61**) a very bright band at that weight is observed after protein induction. To verify the molecular mass difference between the six proteins, they should have been electrophoresed in a common gel. However, this experiment is missing.

Looking at the figures, one can observe that there is a considerable amount of protein lost at the "Flow through". However, when the volume of beads was increased from 2.25ml to 3ml (only at the purification of MBP-Kip2P1-mCherry and MBP-Kip2P1Δ100-mCherry), no differences were observed.

Purification quality is satisfactory but not excellent. At "Eluate" and "After dialysis" columns, proteins of low molecular mass can be observed (lower than 100 kDa). However, the biggest concern are the one or two bands that appear just below our protein. When columns "Cells before induction" and "Cells after induction" are observed in more detail, it is obvious that after induction the intensity of all bands is lower, except from the band that contains the protein of interest. However, one can also see that the bands appearing just below our protein are brighter too. That led us to think that these bands are just truncated forms of our protein (e.g. lacking a part from the mCherry protein. This can be observed in the cases of MBP-Kip2-mCherry, MBP-Kip2Δ70-mCherry, MBP-Kip2P1-mCherry and MBP-Kip2P1Δ100-mCherry, where

total protein production before and after induction is detectable). Since the brightness ratio between desirable/non-desirable bands is satisfactory, we proceeded.
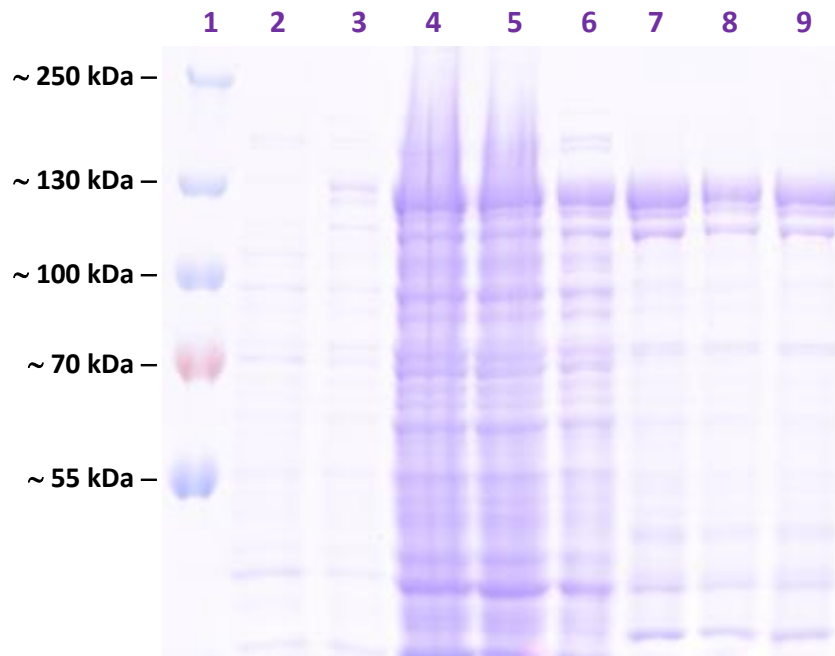
Figure 56. SDS-PAGE results from MBP-Kip2-mCherry purification. 1. Protein ladder, 2. Cells before induction, 3. Cells after induction, 4. Crude lysate, 5. Clear lysate, 6. Flow through, 7. Eluate 1, 8. Eluate 2, 9. After dialysis.
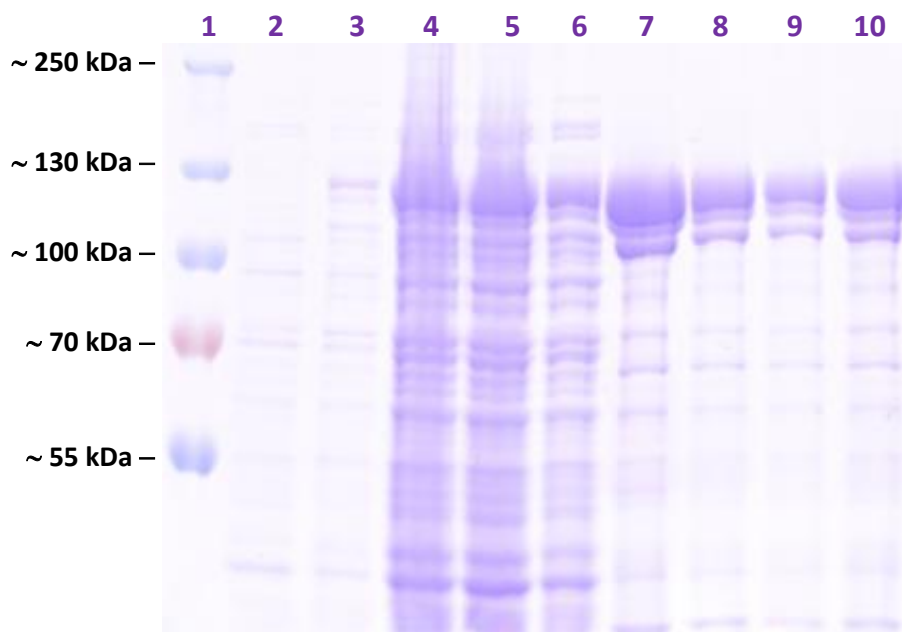
Figure 57. SDS-PAGE results from MBP-Kip2Δ70-mCherry purification. 1. Protein ladder, 2. Cells before induction, 3. Cells after induction, 4. Crude lysate, 5. Clear lysate, 6. Flow through, 7. Eluate 1, 8. Eluate 2, 9. Eluate 3, 10. After dialysis.
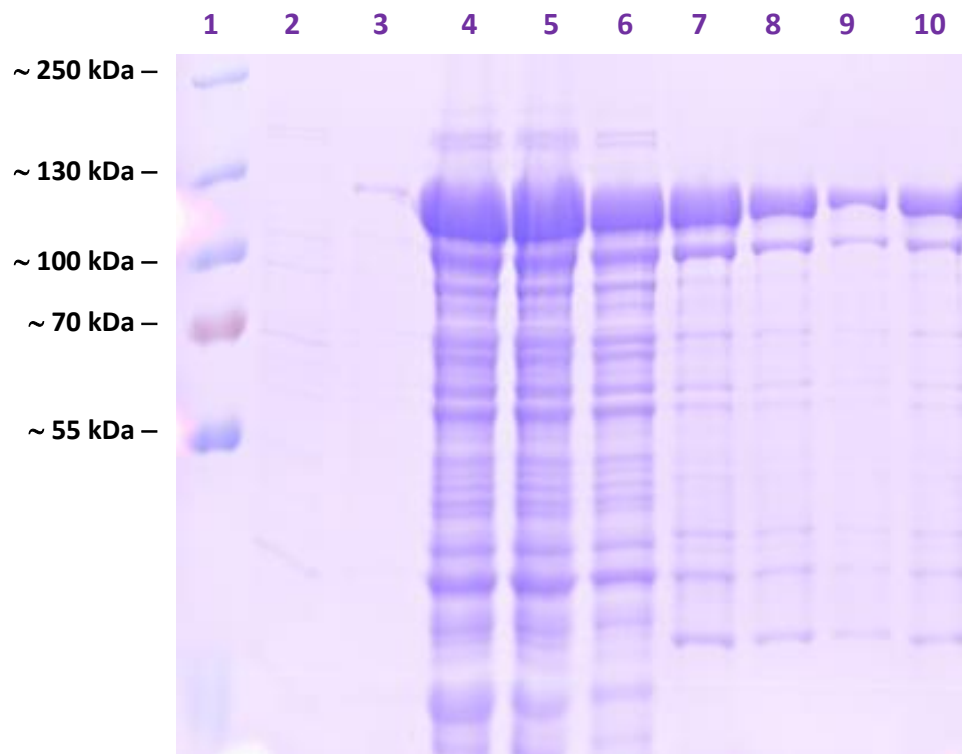
Figure 58. SDS-PAGE results from MBP-Kip2Δ100-mCherry purification. 1. Protein ladder, 2. Cells before induction, 3. Cells after induction, 4. Crude lysate, 5. Clear lysate, 6. Flow through, 7. Eluate 1, 8. Eluate 2, 9. Eluate 3, 10. After dialysis.

Figure 59. SDS-PAGE results from MBP-Kip2P1-mCherry purification. 1. Protein ladder, 2. Cells before induction, 3. Cells after induction, 4. Crude lysate, 5. Clear lysate, 6. Flow through, 7. Eluate 1, 8. Eluate 2.

Figure 60. SDS-PAGE results from MBP-Kip2P1Δ70-mCherry purification. 1. Cells before induction, 2. Cells after induction, 3. Crude lysate, 4. Clear lysate, 5. Flow through, 6. Eluate 1, 7. Eluate 2, 8. Eluate 3, 9. After dialysis, 10. Protein ladder.
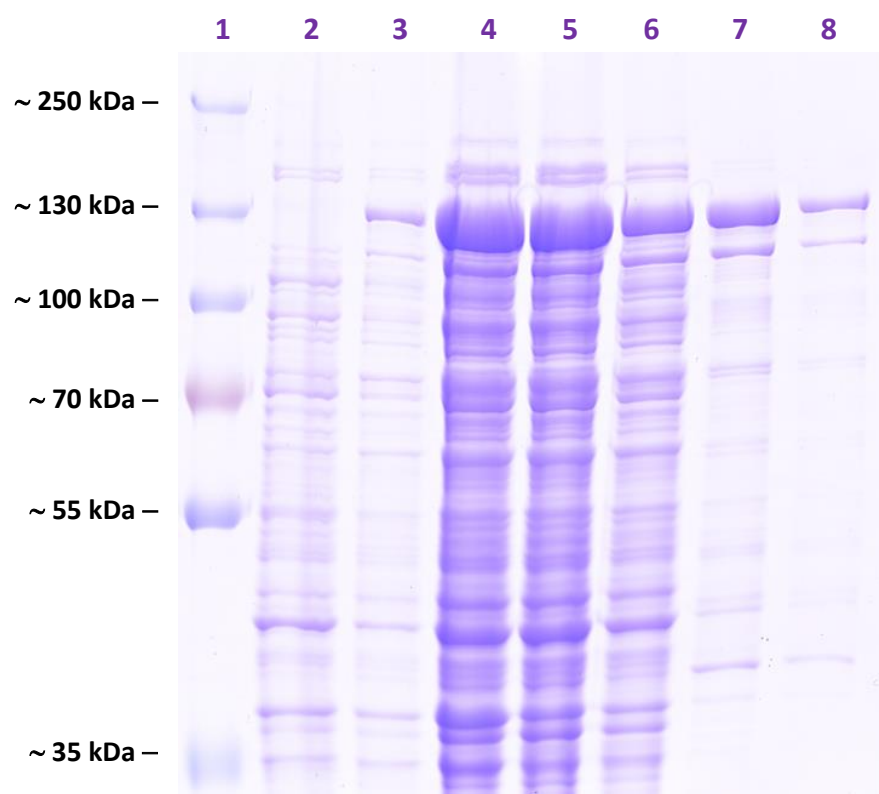

Figure 61. SDS-PAGE results from MBP-Kip2P1Δ100-mCherry purification. 1. Protein ladder, 2. Cells before induction, 3. Cells after induction, 4. Crude lysate, 5. Clear lysate, 6. Flow through, 7. Eluate 1, 8. Eluate 2, 9. After dialysis.
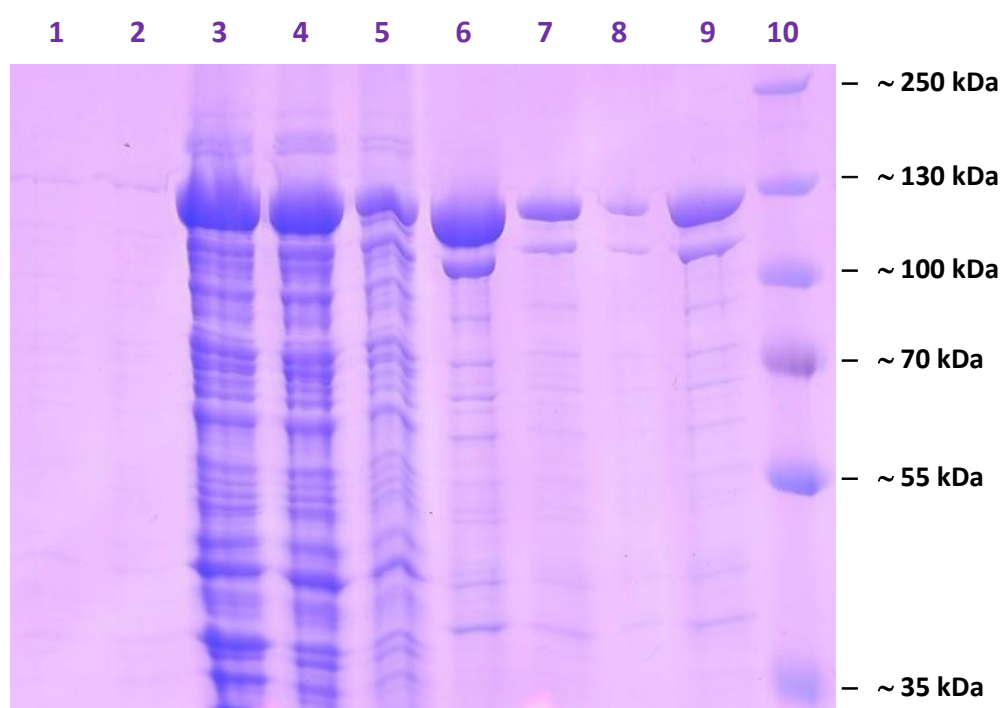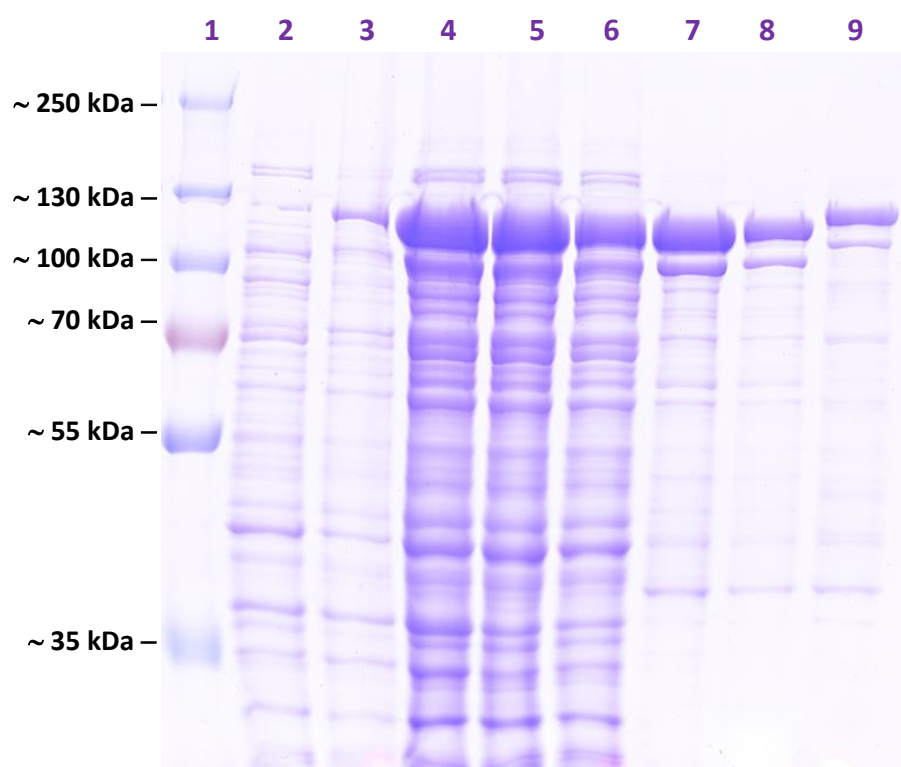
In vitro reconstitution assay results

As mentioned earlier, only the MBP-Kip2-mCherry and MBP-Kip2Δ70mCherry were tested in *in vitro* reconstitution assays (see Experimental procedures for details). Briefly, a flow chamber of ~11 µl was assembled from a silanized coverslip and a coverslide, using double sided tape. After treating the chamber sequentially with neutravidin (a streptavidin analogue) and 2% Pluronic F-127 solution, the chamber was washed with the assay buffer (BRB80 1x/BSA) and then biotinylated microtubule seeds were allowed to attach to the neutravidin-coated surface for 1-5'. Then the chamber was re-washed with the assay buffer and 50µl elongation mixture was added,

containing tubulin with or without Kip2 or Kip2Δ70. The chamber was fully sealed and immediately imaged under TIRF microscope in a temperature-controlled chamber, at 30°C. Data was collected every 5s for 10'. Under these conditions, 10µM of tubulin in the elongation buffer growth should occur even in absence of Kip2 (control). Therefore, in cases when microtubule growth was not observed, movies were not taken into account. Moreover, growing microtubules falling into one of the following categories were also not analyzed; microtubules with blurry kymographs (**Figure 62a**), microtubules which depolymerized upon contact with a neighbouring seed or dynamic microtubule (**Figure 62b, c**), microtubules whose growth was impaired upon contact with a neighbouring seed (**Figure 62d**), microtubules that presented unexpected structures (**Figure 63**) and microtubules that were consistently moving during imaging. Having set these criteria, 61 microtubules from 5 experiments with MBP-Kip2-mCherry, 62 microtubules from 2 experiments with MBP-Kip2Δ70-mCherry and 22 microtubules from 1 control experiment (absence of Kip2), were analyzed and kymographs were generated.
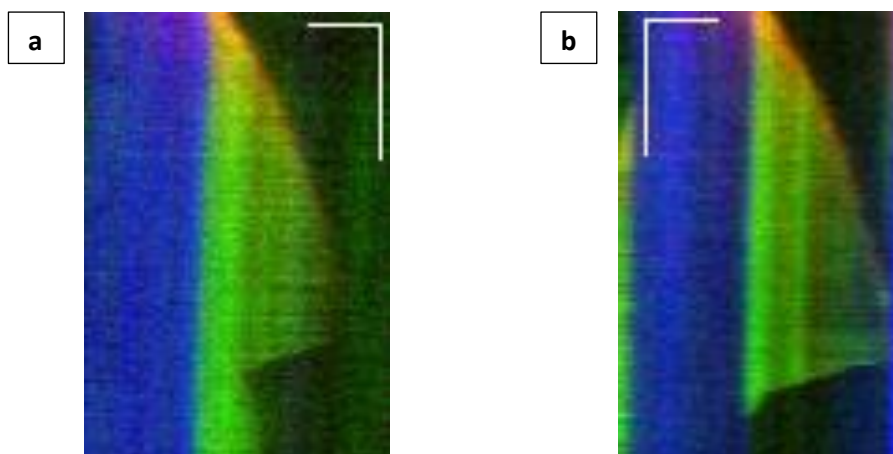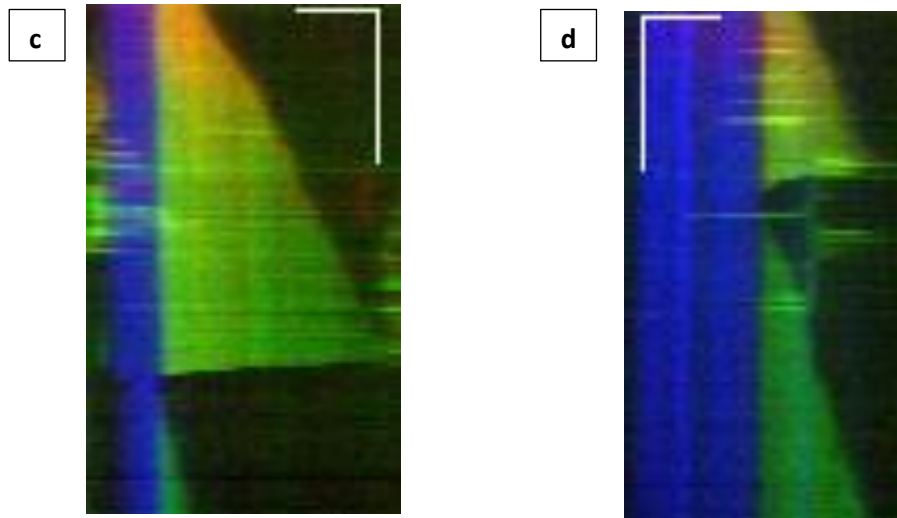
Figure 62. Kymographs falling into one of these categories were not analyzed. (**a**) Blurry kymograph. Microtubules depolymerizing upon contact with a neighbouring seed (**b**) or dynamic microtubule (**c**). Microtubules whose growth was impaired upon contact with a neighbouring seed (**d**). Blue; stabilized microtubule seed, Green; dynamic microtubule, Red; kinesin Kip2. Horizontal bar: 3µm, vertical bar: 3 min.
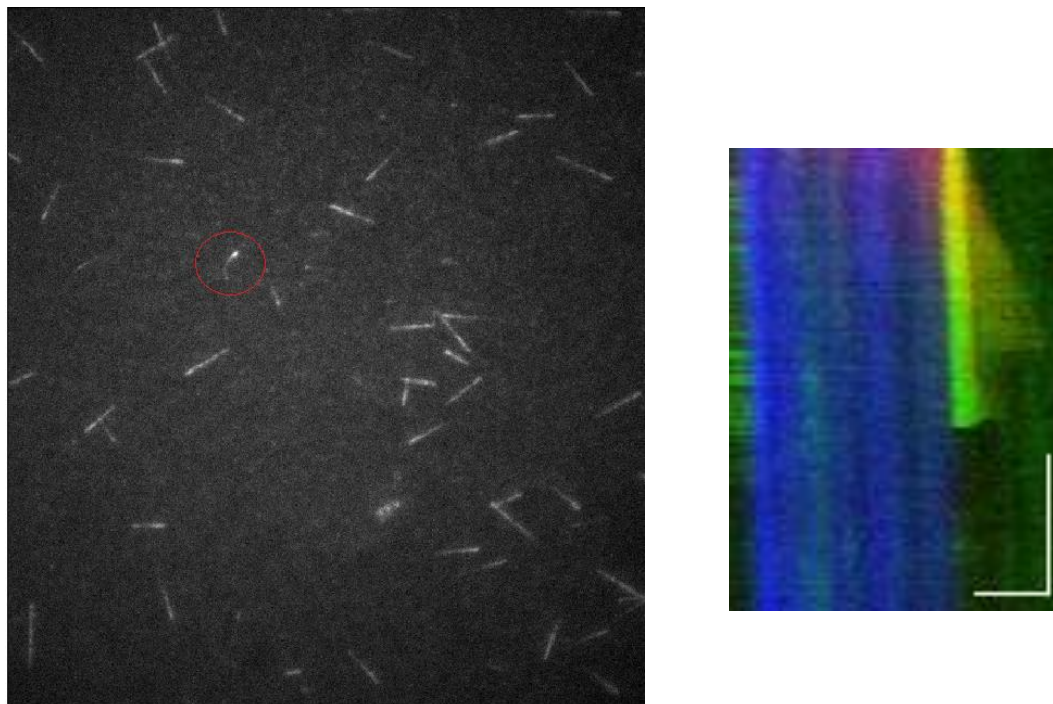
Figure 63. Microtubules presenting unexpected structure while growing. Left; picture of a microtubule presenting unexpected structure (red circle). Right; kymograph of this microtubule. Blue; stabilized

microtubule seed, Green; dynamic microtubule, Red; kinesin Kip2. Horizontal bar: 3µm, vertical bar: 3 min.

Kymographs from each condition tested were sorted into different categories. The aim of these categories was to better describe the variable kymographs generated and did not interfere with the calculations of statistical significance.

In the control experiment, kymographs were sorted into 3 different categories. 22.8% (5/22) of microtubules fell into the category "More than 5' until first growth"; in this category, microtubules did not show any growth for the first 5' of imaging (half a movie) (**Figure 64a**). 18.2% (4/22) fell into the category "More than 5' of growth"; here, microtubules were growing for at least 5' (**Figure 64b**). Lastly, 59% (13/22) fell into the category "Dynamic"; in this, microtubules had short periods of growing, followed by catastrophe events (**Figure 65**).
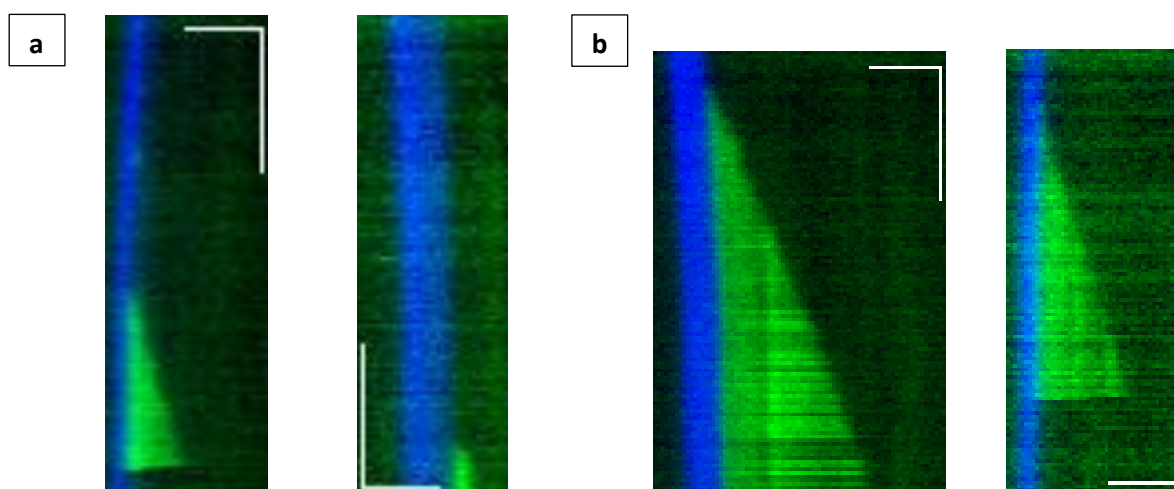
Figure 64. a. Microtubules growing for first time after five or more minutes of imaging. **b.** Microtubules growing for more than five minutes. Blue; stabilized microtubule seed, Green; dynamic microtubule. Horizontal bar: 3µm, vertical bar: 3 min.
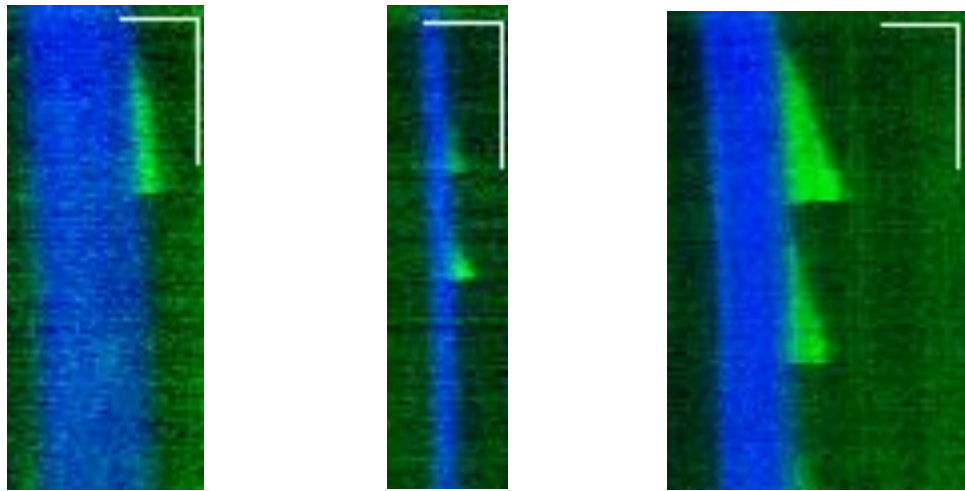
Figure 65. "Dynamic" microtubules. Blue; stabilized microtubule seed, Green; dynamic microtubule. Horizontal bar: 3µm, vertical bar: 3 min.

In presence of MBP-Kip2Δ70-mCherry, kymographs were sorted into 4 different categories. 11.3% (7/62) fell into the "More than 5' until first growth" (**Figure 66a**). 14.5% (9/62) fell into the "More than 5' of growth" (**Figure 66b**). 40.3% (25/62) fell into the "Dynamic" (**Figure 67a**). Lastly, 33.9% (21/62) fell into the category "Early growth", in which microtubule growth had already started growing before imaging (**Figure 67b**).

Figure 66. a. Microtubule growing for first time after five or more minutes of imaging. **b.** Microtubules growing for more than five minutes. Left kymograph was not rejected because seed did not affect microtubule growth. Blue; stabilized microtubule seed, Green; dynamic microtubule, Red; MBP-Kip2Δ70-mCherry. Horizontal bar: 3µm, vertical bar: 3 min.
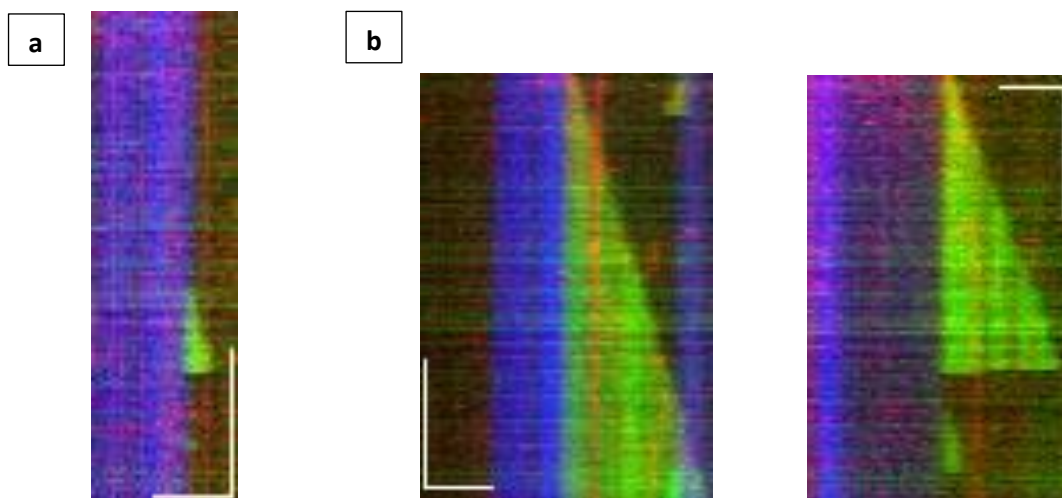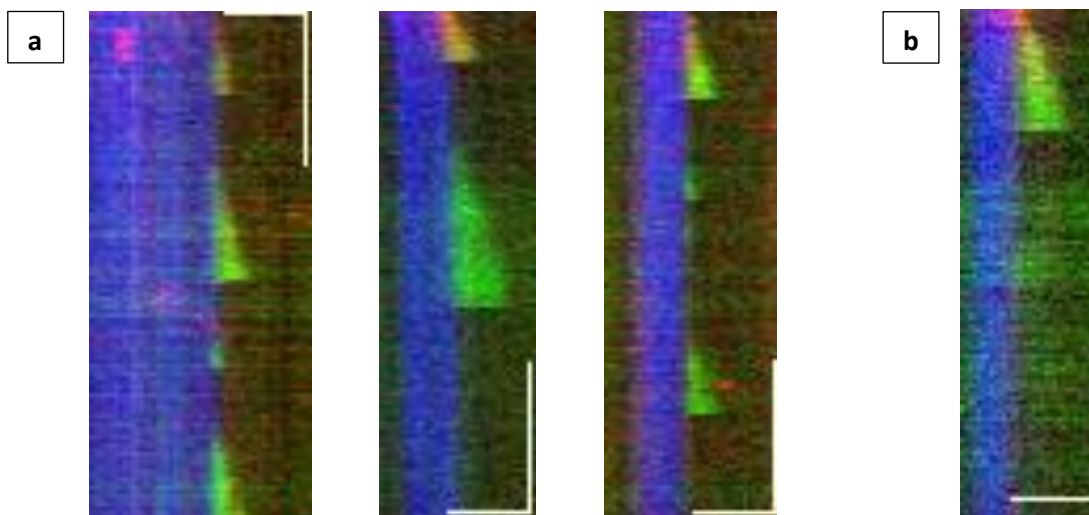

Figure 67. a. "Dynamic" microtubules. **b.** Microtubule growing before image acquisition started. Blue; stabilized microtubule seed, Green; dynamic microtubule, Red; MBP-Kip2Δ70-mCherry. Horizontal bar: 3µm, vertical bar: 3 min.

In presence of MBP-Kip2-mCherry, all microtubules had started growing before imaging. Kymographs were sorted into 5 different categories. 21.3% (13/61) fell into the "More than 5' of growth" (**Figure 68a**). 26.3% (16/61) fell into the "Dynamic" (**Figure 68b**). 32.7% (20/61) fell into the category "Growth for the whole movie", in which microtubules were growing for 10' (**Figure 69**). 14.8% (9/61) fell into the category "Slow catastrophe"; here catastrophe of microtubule was above 40s (**Figure 70a**). Lastly, in 4.9% (3/61) of microtubules a rescue event was observed (**Figure 70b**).
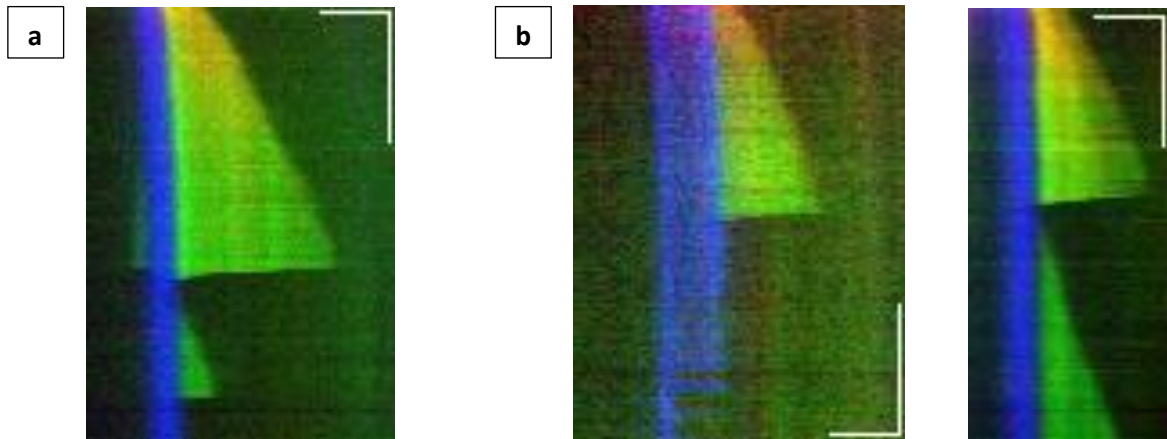
Figure 68. a. Microtubule growing for more than five minutes. **b.** "Dynamic" microtubules. Blue; stabilized microtubule seed, Green; dynamic microtubule, Red; MBP-Kip2-mCherry. Horizontal bar: 3µm, vertical bar: 3 min.
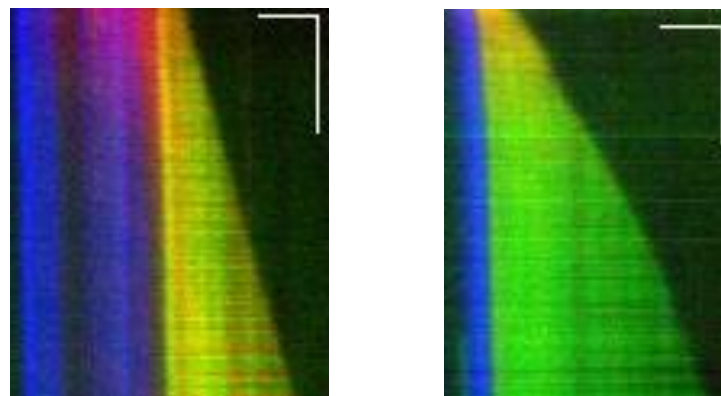
Figure 69. Microtubules growing for the whole imaging period. Blue; stabilized microtubule seed, Green; dynamic microtubule, Red; MBP-Kip2-mCherry. Horizontal bar: 3µm, vertical bar: 3 min.

Figure 70. a. Microtubules undergoing slow catastrophe. Note that the right one does not depolymerize completely. **b.** Microtubule with a rescue event. Blue; stabilized microtubule seed, Green; dynamic microtubule, Red; MBP-Kip2-mCherry. Horizontal bar: 3μm, vertical bar: 3 min.

Kymograph analysis

Generated kymographs were used to analyze seven parameters: growth time, growth speed, depolymerization speed (in cases it was possible to be measured), catastrophe and rescue frequency, time needed until the first growth and number of microtubules growing for the whole imaging period.
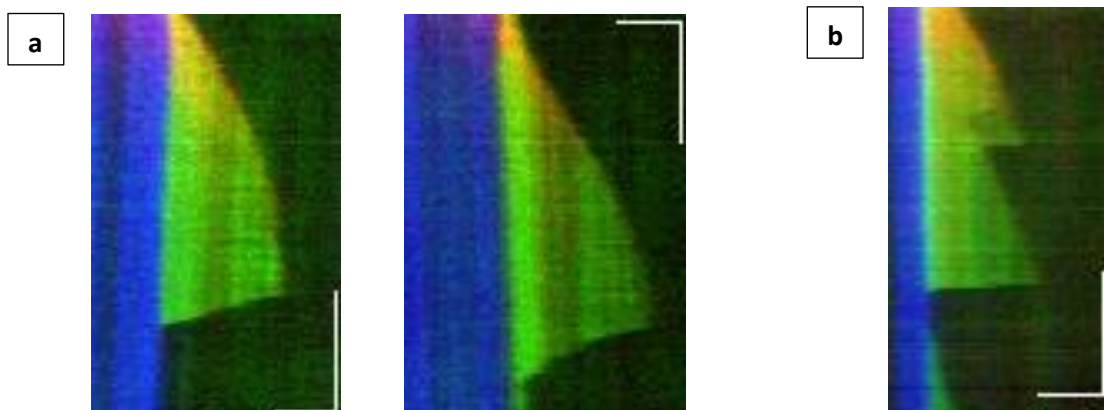
For the first six parameters, calculation of statistically significant differences between the different conditions tested [control (absence of Kip2), MBP-Kip2-mCherry, MBP-Kip2Δ70-mCherry], was performed by Mann-Whitney test. This test was used because data was not following a normal distribution. For the last parameter, the Fisher's exact test was used.

The first parameter analyzed is the growth time. This parameter answers the question "For how much time microtubules grow?". For each kymograph, the time a microtubule spent polymerizing was calculated. It is important to mention that in kymographs with two or more growing periods, the different growing times were not summed up to give an average of the growth time [e.g., in **Figure 68a**, two periods of growths (t_1 for the first, t_2 for the second) were calculated. However, they were not summed up to give the average growth time of the movie]. Results of the analysis are presented in **Figure 71**.
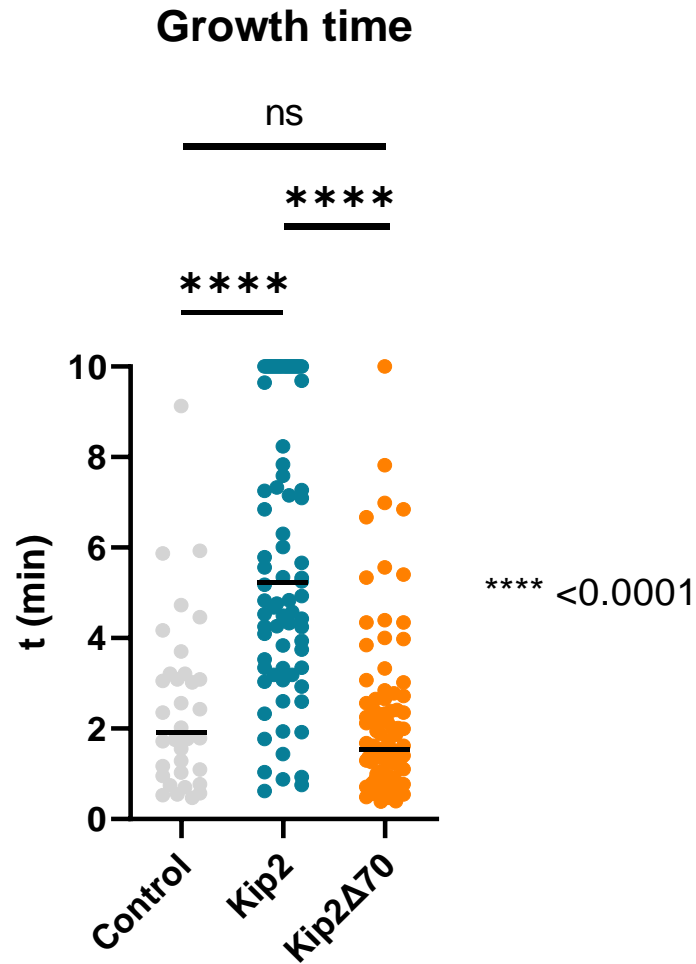
Growth time

	Control	Kip2	Kip2Δ70
# of values	34	78	91
Median	**1,902**	**5,217**	**1,542**
Mean	2,485	5,884	2,150
Std. Deviation	1,909	3,068	1,799

Figure 71. Growth time of microtubules in the different conditions tested. Black lines in the graph represent the median of the data, ns: not significant difference. Statistical analysis was performed using Mann-Whitney test.

Figure 71 clearly shows that Kip2 positively affects the time a microtubule spends growing. Importantly, this effect depends exclusively on the 70 amino acids of the N-terminus: when these are removed (Kip2Δ70), the time a microtubule spends growing is similar to the control.

Growth speed
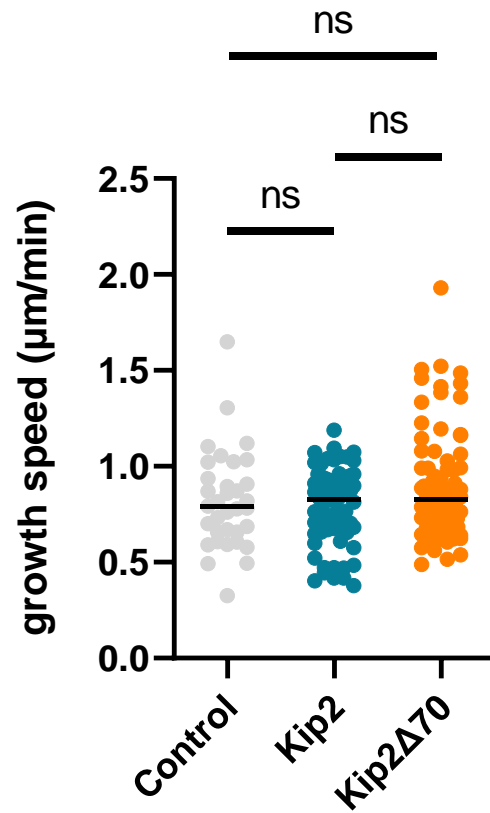
	Control	Kip2	Kip2Δ70
# of values	34	78	91
Median	**0,7881**	**0,8279**	**0,8256**
Mean	0,8175	0,7931	0,8816
Std. Deviation	0,2548	0,1870	0,2693

Figure 72. Growth speed of microtubules in the different conditions tested. Black lines in the graph represent the median of the data. Statistical analysis was performed using Mann-Whitney test.

Growth speed is a parameter answering the question "How fast does the microtubule grow?". Growth speed of microtubules were calculated from kymographs and the results are presented in **Figure 72**. Absence of difference on the growth speed between the different conditions was something unexpected. Similar growth speeds for control (absence of Kip2) and Kip2Δ70, whereas significantly increased growth speed for Kip2 were expected; with its N-terminus region, Kip2 would transfer tubulin to the plus end and increase the growth speed.

Depolymerization speed
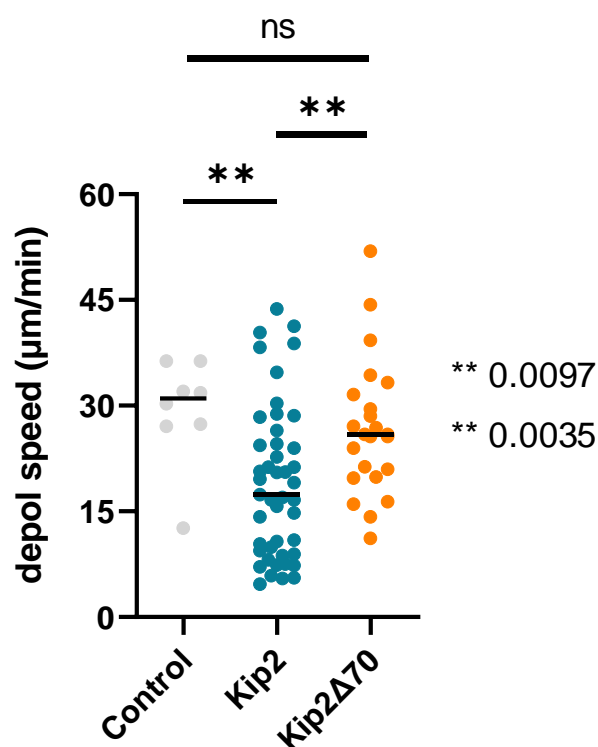
	Control	Kip2	Kip2Δ70
# of values	8	45	23
Median	**31,03**	**17,37**	**25,92**
Mean	29,23	19,08	26,68
Std. Deviation	7,556	10,88	9,597

Figure 73. Depolymerization speed of microtubules in the different conditions tested. Black lines in the graph represent the median of the data. 0.0097 value is between Control and Kip2 and 0.0035 value between Kip2 and Kip2Δ70. Statistical analysis was performed using Mann-Whitney test.

To address the question "How fast does the microtubule depolymerize?", the depolymerization speed was calculated. Very frequently, depolymerization speed could not be measured due to the instant depolymerization of the microtubule (e.g., **Figure 65**). As a result, in some cases, not many values for this parameter were acquired (**Figure 73**, # of values for control). **Figure 73** shows that in presence of Kip2, depolymerization speed is reduced compared to control (absence of Kip2) and Kip2Δ70. In particular, presence of Kip2 reduces depolymerization speed almost two

times compared to control. Similar results arise from the comparison between Kip2 and Kip2Δ70, whereas no difference is observed between Kip2Δ70 and the control.

Catastrophe frequency
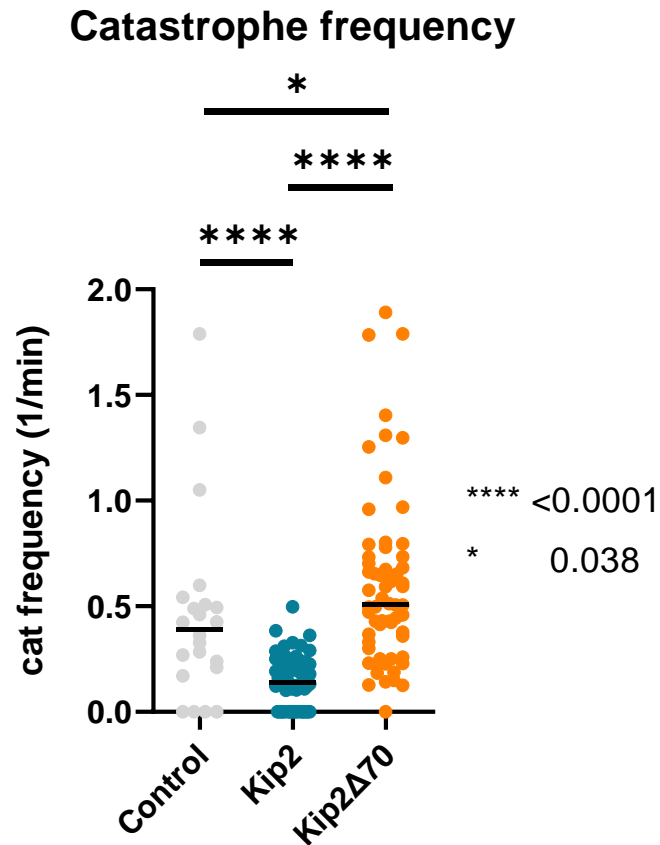
	Control	Kip2	Kip2Δ70
# of values	22	61	62
Median	**0,3932**	**0,1375**	**0,5097**
Mean	0,4545	0,1439	0,6066
Std. Deviation	0,4401	0,1238	0,4121

Figure 74. Catastrophe frequency of microtubules in the different conditions tested. Black lines in the graph represent the median of the data. Statistical analysis was performed using Mann-Whitney test.

Catastrophe frequency answers the question "How often a growing microtubule stops growing and starts to depolymerize?". It is calculated as the number of depolymerization events observed in a movie, divided by the time the microtubule spent polymerizing during the whole movie. **Figure 74** shows that Kip2 reduces catastrophe frequency compared to control (absence of Kip2) and Kip2Δ70. In

particular, presence of Kip2 reduces catastrophe frequency almost three times compared to the control.

Results from **Figure 74** suggest something unexpected: in presence of Kip2Δ70, microtubule disassembly is enhanced (catastrophe frequency of microtubule is increased significantly compared to the control). This is a puzzling result that we cannot interpret, at least for the moment.
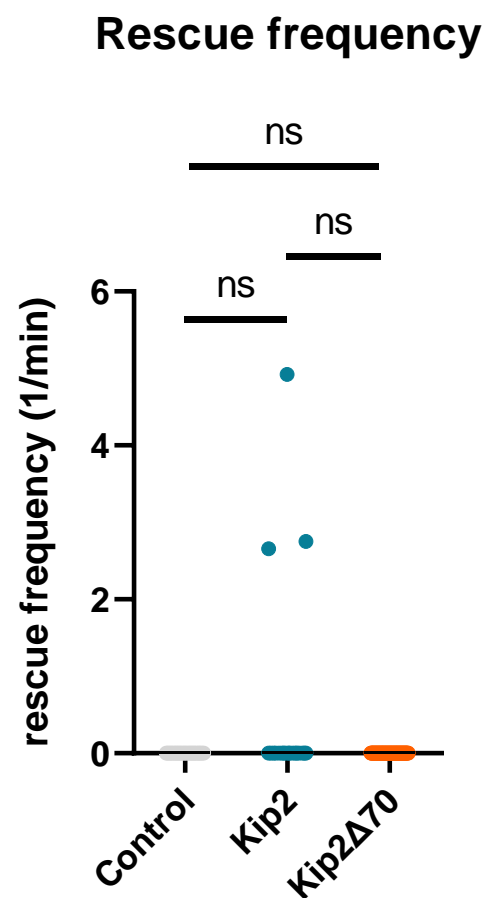
Rescue frequency

	Control	Kip2	Kip2Δ70
# of values	22	61	62
Median	**0,000**	**0,000**	**0,000**
Mean	0,000	0,1693	0,000
Std. Deviation	0,000	0,7864	0,000

Figure 75. Rescue frequency of microtubules in the different conditions tested. Black lines in the graph represent the median of the data. Statistical analysis was performed using Mann-Whitney test.

Rescue frequency answers the question "How often a depolymerizing microtubule stops depolymerization and starts to grow?". This parameter is calculated as the number of rescue events observed in a movie, divided by the time the microtubule spent depolymerizing during the whole movie. **Figure 75** shows that presence of Kip2 does not affect rescue frequency.
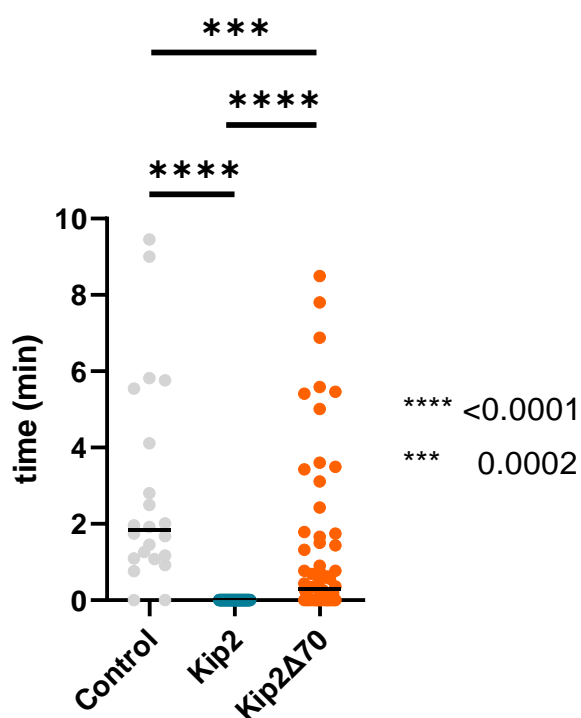
	Control	Kip2	Kip2Δ70
# of values	22	61	62
Median	**1,833**	**0,000**	**0,3050**
Mean	2,820	0,000	1,274
Std. Deviation	2,677	0,000	2,096

Figure 76. Time needed until the first microtubule growth, in the different conditions tested. Black lines in the graph represent the median of the data. Statistical analysis was performed using Mann-Whitney test.

Time needed until the first growth is presented in **Figure 76**. After mixing all the reagents [elongation buffer with tubulin and Kip2 or Kip2Δ70 (see Buffers and media) with the stabilized microtubules], coverslip was placed under the TIRF

microscope, a spot with many seeds was selected and then image acquisition started. Initiation of image acquisition is defined by the value "0" on the axis "time" in **Figure 76**. Time needed until the first growth measures the time a microtubule needs to start its first growth, after image acquisition has started. In all kymographs analyzed in presence of Kip2, microtubule growth had started before image acquisition. In absence of the kinesin (control), the average time until the first growth is almost two minutes, whereas in some cases it occurs after five or even eight minutes. Similar results arise from the comparison between Kip2 and Kip2Δ70: in presence of Kip2, microtubule growth starts significantly earlier. These results suggest that Kip2 accelerates growth initiation. An unexpected result is that in presence of Kip2Δ70 microtubules start to grow significantly earlier compared to the control.

Growth for the whole movie?
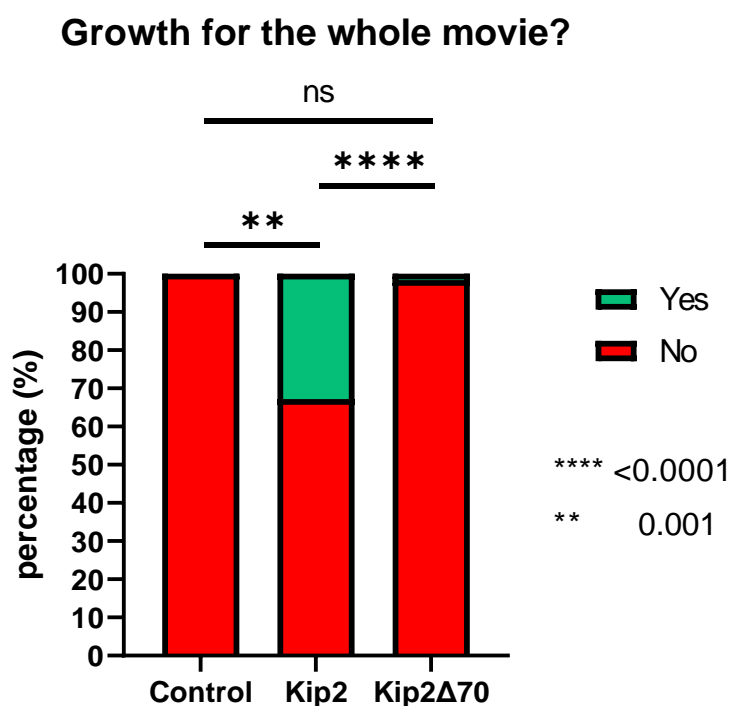
Figure 77. Percentage of microtubules in the different conditions tested, that grow for the whole imaging period (10 min). Black lines in the graph represent the median of the data. Statistical analysis was performed using Fisher's exact test.

Although **Figure 77** does not contain as much information as the previous graphs (it is a qualitative and not a quantitative graph: the answer is "Yes" or "No"), it

still shows the microtubule growth and anti-catastrophe features of Kip2. In presence of Kip2, one third (20/61) of the microtubules grow for the whole imaging time. On the contrary, none of the microtubules has this behaviour in the control, whereas only one microtubule shows same behaviour in presence of Kip2Δ70. The fact that difference is more significant between Kip2 and Kip2Δ70 rather than Kip2 and control may be due to the number of microtubules analyzed; 61 microtubules for Kip2, 62 for Kip2Δ70 and 22 for the control.

Discussion

In this study our aim was to provide, through *in vitro* experiments, data on the microtubule elongation activity of Kip2. We mixed Kip2 (1-560) or Kip2Δ70 (71-560) with free tubulin and stabilized microtubule seeds and imaged the results using a TIRF microscope. Seven parameters were measured to determine the effects of Kip2 on microtubules. Analysis of the data shows that the truncated Kip2 (1-560) retains microtubule elongation and anti-catastrophe activities of full-length Kip2. Moreover, it suggests that Kip2 acts as a nucleation factor.

Kip2 increases the time a microtubule spends growing, and this activity seems to depend on the N-terminus region (**Figure 71**). Moreover, it reduces depolymerization speed and catastrophe frequency in a N-terminus dependent manner (**Figures 73, 74**). The effect of Kip2 on the depolymerization speed is not in line with a previous study (Hibbel et al., 2015). However, it must be mentioned that in that study depolymerization speed was calculated for a 10nM concentration of full-length Kip2 (five times lower than in our case). The effect of Kip2 on the catastrophe frequency is in line with the previously reported anti-catastrophe feature of this kinesin (**Figure 42**, Hibbel et al., 2015), but here the effect is smaller, maybe due to the absence of the amino acids 561-706. Additionally, Kip2 seems to act as a nucleation factor, since microtubule growth starts shortly after its addition (**Figure 76**). These data seem to be in line with a previously reported nucleation activity of Kip2 (**Figure 42**, Hibbel et al., 2015) and with our model (**Figure 49**). In presence of the kinesin, tubulin is accumulated to the plus end, promoting growth initiation. In

absence of the kinesin, growth initiation depends on the diffusion of tubulin to the plus end, leading to a delay in growth initiation. Together, this data explains that in presence of Kip2, one third of the microtubules can grow for very long time (**Figure 77**).

As previously reported (Hibbel et al., 2015), Kip2 cannot act as a rescue factor (**Figure 75**). The absence of difference on the growth speed (**Figure 72**) can be due to the MBP presence at the N-terminus, which may interfere in interactions with tubulin. Another reason may be the fact that the truncated form was used. Finally, maybe the experimental conditions were not optimal; *in vitro* reconstitution experiments heavily depend on the conditions chosen (pH, buffer type, temperature, concentrations). A worth-mentioning comment is that a previous study (**Figure 42**, Hibbel et al., 2015) has found a slightly higher growth speed for 40nM of full-length Kip2 (in present experiments, 50nM of truncated Kip2 were used). However, in that experiments growth speed in control conditions was half of the one measured here. Comparing the two experiments, same tubulin origin and elongation buffer were used. The only differences were in the purification buffer, the protocol for GMPCPP stabilized microtubules and the Kip2 protein.

Results for the truncated Kip2Δ70 are not clear. The fact that Kip2Δ70 has same growth times as the control (**Figure 71**) is in line with our hypothesis, but at the same time it promotes microtubule growth significantly earlier than the control, contradicting our hypothesis (**Figures 49, 76**). Maybe the P1 region, which promotes microtubule growth (Chen et al., unpublished data) or the 27 remaining amino acids of the N-terminus (**Figures 45, 46**) play a role in this procedure. Adding to these observations, Kip2Δ70 seems to promote microtubule catastrophe (**Figure 74)**. Thus, Kip2Δ70 seems to be a very interesting mutant, but needs to be studied more extensively.

Comparing the data between Kip2 and Kip2Δ70, one can observe that in presence of Kip2 microtubules spend significantly more time growing (**Figure 71**). Moreover, Kip2 promotes microtubules growth significantly earlier, compared to Kip2Δ70 (**Figure 76**). As for the catastrophe speed and catastrophe frequency, Kip2

reduces significantly both parameters (**Figures 73, 74**). The only difference between the two proteins is the 70 amino acids of the unstructured N-terminus. Thus, this region seems to be responsible for the effects observed. No difference was observed in growth speed and rescue frequency between the two proteins (**Figures 72, 75**).

It must be mentioned that although the results seem convincingly, the number of microtubules analyzed is low. More experiments need to be done to acquire robust data.

Apart from the reproduction of the experiments above, other future aims are to test the other truncated versions of Kip2 created, to achieve a better purification, remove the MBP tag and check if the protein is functional. In addition, we could also repeat the experiments with the full-length proteins and optimize buffer conditions. Further experiments would be to purify the unstructured N-terminus region and test *in vitro* its interaction with tubulin dimers. We could also add that region to kinesin-1 (a kinesin known to not promote microtubule growth) to see if it enables kinesin-1 to promote microtubule growth. Finally, an important point is to perform the experiments using yeast tubulin instead of porcine brain tubulin, that is not the natural substrate for Kip2.

References

Papers

1. Akhmanova, A., & Steinmetz, M. O. (2015). Control of microtubule organization and dynamics: two ends in the limelight. *Nature reviews. Molecular cell biology*, *16*(12), 711–726. https://doi.org/10.1038/nrm4084

2. Alushin, G. M., Lander, G. C., Kellogg, E. H., Zhang, R., Baker, D., & Nogales, E. (2014). High-resolution microtubule structures reveal the structural transitions in αβ-tubulin upon GTP hydrolysis. *Cell*, *157*(5), 1117–1129. https://doi.org/10.1016/j.cell.2014.03.053

3. Boettcher, B., & Barral, Y. (2013). The cell biology of open and closed mitosis. *Nucleus (Austin, Tex.)*, *4*(3), 160–165. https://doi.org/10.4161/nucl.24676

4. Brouhard, G. J., & Rice, L. M. (2014). The contribution of αβ-tubulin curvature to microtubule dynamics. *The Journal of cell biology*, *207*(3), 323–334. https://doi.org/10.1083/jcb.201407095

5. Brouhard, G. J., & Rice, L. M. (2018). Microtubule dynamics: an interplay of biochemistry and mechanics. *Nature reviews. Molecular cell biology*, *19*(7), 451–463. https://doi.org/10.1038/s41580-018-0009-y

6. Brouhard, G. J., Stear, J. H., Noetzel, T. L., Al-Bassam, J., Kinoshita, K., Harrison, S. C., Howard, J., & Hyman, A. A. (2008). XMAP215 is a processive microtubule polymerase. *Cell*, *132*(1), 79–88. https://doi.org/10.1016/j.cell.2007.11.043

7. Carlier M. F. (1982). Guanosine-5'-triphosphate hydrolysis and tubulin polymerization. Review article. *Molecular and cellular biochemistry*, *47*(2), 97–113. https://doi.org/10.1007/BF00234410

8. Carvalho, P., Gupta, M. L., Jr, Hoyt, M. A., & Pellman, D. (2004). Cell cycle control of kinesin-mediated transport of Bik1 (CLIP-170) regulates microtubule stability and dynein activation. *Developmental cell*, *6*(6), 815–829. https://doi.org/10.1016/j.devcel.2004.05.001

9. Caudron, F., Andrieux, A., Job, D., & Boscheron, C. (2008). A new role for kinesin-directed transport of Bik1p (CLIP-170) in Saccharomyces cerevisiae. *Journal of cell science*, *121*(Pt 9), 1506–1513. https://doi.org/10.1242/jcs.023374

10. Chen, X., Portran, D., Widmer, L. A., Stangier, M. M., Liakopoulos, D., Stelling, J., Steinmetz, M. O., & Barral, Y. The motor domain of the kinesin Kip2 promotes microtubule polymerization at microtubule tips. Manuscript submitted for publication

11. Chen, Y., & Hancock, W. O. (2015). Kinesin-5 is a microtubule polymerase. *Nature communications*, *6*, 8160. https://doi.org/10.1038/ncomms9160

12. Cleary, J. M., & Hancock, W. O. (2021). Molecular mechanisms underlying microtubule growth dynamics. *Current biology: CB*, *31*(10), R560–R573. https://doi.org/10.1016/j.cub.2021.02.035

13. Drechsler, H., Tan, A. N., & Liakopoulos, D. (2015). Yeast GSK-3 kinase regulates astral microtubule function through phosphorylation of the microtubule-stabilizing kinesin Kip2. *Journal of cell science*, *128*(21), 3910–3921. https://doi.org/10.1242/jcs.166686

14. Erickson, H. P., & O'Brien, E. T. (1992). Microtubule dynamic instability and GTP hydrolysis. *Annual review of biophysics and biomolecular structure*, *21*, 145–166. https://doi.org/10.1146/annurev.bb.21.060192.001045

15. Findeisen, P., Mühlhausen, S., Dempewolf, S., Hertzog, J., Zietlow, A., Carlomagno, T., & Kollmar, M. (2014). Six subgroups and extensive recent duplications characterize the evolution of the eukaryotic tubulin protein family. *Genome biology and evolution*, *6*(9), 2274–2288. https://doi.org/10.1093/gbe/evu187

16. Gardner, M. K., Zanic, M., Gell, C., Bormuth, V., & Howard, J. (2011). Depolymerizing kinesins Kip3 and MCAK shape cellular microtubule architecture by differential control of catastrophe. *Cell*, *147*(5), 1092–1103. https://doi.org/10.1016/j.cell.2011.10.037

17. Gerson-Gurwitz, A., Thiede, C., Movshovich, N., Fridman, V., Podolskaya, M., Danieli, T., Lakämper, S., Klopfenstein, D. R., Schmidt, C. F., & Gheber, L. (2011). Directionality of individual kinesin-5 Cin8 motors is modulated by loop 8, ionic strength and microtubule geometry. *The EMBO journal*, *30*(24), 4942–4954. https://doi.org/10.1038/emboj.2011.403

18. Goodson, H. V., & Jonasson, E. M. (2018). Microtubules and Microtubule-Associated Proteins. *Cold Spring Harbor perspectives in biology*, *10*(6), a022608. https://doi.org/10.1101/cshperspect.a022608

19. Güttinger, S., Laurell, E., & Kutay, U. (2009). Orchestrating nuclear envelope disassembly and reassembly during mitosis. *Nature reviews. Molecular cell biology*, *10*(3), 178–191. https://doi.org/10.1038/nrm2641

20. Hartwell L. H. (1974). Saccharomyces cerevisiae cell cycle. *Bacteriological reviews*, *38*(2), 164–198. https://doi.org/10.1128/br.38.2.164-198.1974

21. Hawkins, T., Mirigian, M., Selcuk Yasar, M., & Ross, J. L. (2010). Mechanics of microtubules. *Journal of biomechanics*, *43*(1), 23–30. https://doi.org/10.1016/j.jbiomech.2009.09.005

22. Hibbel, A., Bogdanova, A., Mahamdeh, M., Jannasch, A., Storch, M., Schäffer, E., Liakopoulos, D., & Howard, J. (2015). Kinesin Kip2 enhances microtubule growth in vitro through length-dependent feedback on polymerization and catastrophe. *eLife*, *4*, e10542. https://doi.org/10.7554/eLife.10542

23. Hirokawa, N., Nitta, R., & Okada, Y. (2009b). The mechanisms of kinesin motor motility: lessons from the monomeric motor KIF1A. *Nature reviews. Molecular cell biology*, *10*(12), 877–884. https://doi.org/10.1038/nrm2807

24. Hirokawa, N., Noda, Y., Tanaka, Y., & Niwa, S. (2009a). Kinesin superfamily motor proteins and intracellular transport. *Nature reviews. Molecular cell biology*, *10*(10), 682–696. https://doi.org/10.1038/nrm2774

25. Holy, T. E., Dogterom, M., Yurke, B., & Leibler, S. (1997). Assembly and positioning of microtubule asters in microfabricated chambers. *Proceedings of the National Academy of Sciences of the United States of America*, *94*(12), 6228–6231. https://doi.org/10.1073/pnas.94.12.6228

26. Howard, J., & Hyman, A. A. (2007). Microtubule polymerases and depolymerases. *Current opinion in cell biology*, *19*(1), 31–35. https://doi.org/10.1016/j.ceb.2006.12.009

27. Howard, J., & Hyman, A. A. (2009). Growth, fluctuation and switching at microtubule plus ends. *Nature reviews. Molecular cell biology*, *10*(8), 569–574. https://doi.org/10.1038/nrm2713

28. Howes, S. C., Geyer, E. A., LaFrance, B., Zhang, R., Kellogg, E. H., Westermann, S., Rice, L. M., & Nogales, E. (2017). Structural differences between yeast and

mammalian microtubules revealed by cryo-EM. *The Journal of cell biology*, *216*(9), 2669–2677. https://doi.org/10.1083/jcb.201612195

29. Hyman, A. A., Salser, S., Drechsel, D. N., Unwin, N., & Mitchison, T. J. (1992). Role of GTP hydrolysis in microtubule dynamics: information from a slowly hydrolyzable analogue, GMPCPP. *Molecular biology of the cell*, *3*(10), 1155–1167. https://doi.org/10.1091/mbc.3.10.1155

30. Kapitein, L. C., Kwok, B. H., Weinger, J. S., Schmidt, C. F., Kapoor, T. M., & Peterman, E. J. (2008). Microtubule cross-linking triggers the directional motility of kinesin-5. *The Journal of cell biology*, *182*(3), 421–428. https://doi.org/10.1083/jcb.200801145

31. Katsuki, M., Drummond, D. R., & Cross, R. A. (2014). Ectopic A-lattice seams destabilize microtubules. *Nature communications*, *5*, 3094. https://doi.org/10.1038/ncomms4094

32. Kim, A. J., & Endow, S. A. (2000). A kinesin family tree. *Journal of cell science*, *113 Pt 21*, 3681–3682. https://doi.org/10.1242/jcs.113.21.3681

33. Konjikusic, M. J., Gray, R. S., & Wallingford, J. B. (2021). The developmental biology of kinesins. *Developmental biology*, *469*, 26–36. https://doi.org/10.1016/j.ydbio.2020.09.009

34. Koshland, D. E., Mitchison, T. J., & Kirschner, M. W. (1988). Polewards chromosome movement driven by microtubule depolymerization in vitro. *Nature*, *331*(6156), 499–504. https://doi.org/10.1038/331499a0

35. Lawrence, C. J., Dawe, R. K., Christie, K. R., Cleveland, D. W., Dawson, S. C., Endow, S. A., Goldstein, L. S., Goodson, H. V., Hirokawa, N., Howard, J., Malmberg, R. L., McIntosh, J. R., Miki, H., Mitchison, T. J., Okada, Y., Reddy, A. S., Saxton, W. M., Schliwa, M., Scholey, J. M., Vale, R. D., … Wordeman, L. (2004). A standardized kinesin nomenclature. *The Journal of cell biology*, *167*(1), 19–22. https://doi.org/10.1083/jcb.200408113

36. Lichtman, J. W., & Conchello, J. A. (2005). Fluorescence microscopy. *Nature methods*, *2*(12), 910–919. https://doi.org/10.1038/nmeth817

37. Liu, A. P., & Fletcher, D. A. (2009). Biology under construction: in vitro reconstitution of cellular function. *Nature reviews. Molecular cell biology*, *10*(9), 644–650. https://doi.org/10.1038/nrm2746

38. Maekawa, H., Usui, T., Knop, M., & Schiebel, E. (2003). Yeast Cdk1 translocates to the plus end of cytoplasmic microtubules to regulate bud cortex interactions. *The EMBO journal*, *22*(3), 438–449. https://doi.org/10.1093/emboj/cdg063

39. Magiera, M. M., & Janke, C. (2014). Post-translational modifications of tubulin. *Current biology: CB*, *24*(9), R351–R354. https://doi.org/10.1016/j.cub.2014.03.032

40. Mandelkow, E. M., Mandelkow, E., & Milligan, R. A. (1991). Microtubule dynamics and microtubule caps: a time-resolved cryo-electron microscopy study. *The Journal of cell biology*, *114*(5), 977–991. https://doi.org/10.1083/jcb.114.5.977

41. Maney, T., Hunter, A. W., Wagenbach, M., & Wordeman, L. (1998). Mitotic centromere-associated kinesin is important for anaphase chromosome segregation. *The Journal of cell biology*, *142*(3), 787–801. https://doi.org/10.1083/jcb.142.3.787

42. Martin-Fernandez, M. L., Tynan, C. J., & Webb, S. E. (2013). A 'pocket guide' to total internal reflection fluorescence. *Journal of microscopy*, *252*(1), 16–22. https://doi.org/10.1111/jmi.12070

43. Mattheyses, A. L., Simon, S. M., & Rappoport, J. Z. (2010). Imaging with total internal reflection fluorescence microscopy for the cell biologist. *Journal of cell science*, *123*(Pt 21), 3621–3628. https://doi.org/10.1242/jcs.056218

44. McKean, P. G., Vaughan, S., & Gull, K. (2001). The extended tubulin superfamily. *Journal of cell science*, *114*(Pt 15), 2723–2733. https://doi.org/10.1242/jcs.114.15.2723

45. McNally F. J. (2013). Mechanisms of spindle positioning. *The Journal of cell biology*, *200*(2), 131–140. https://doi.org/10.1083/jcb.201210007

46. Miki H., Hirokawa N. (2013) Kinesin Superfamily Classification. In: Roberts G.C.K. (eds) Encyclopedia of Biophysics. Springer, Berlin, Heidelberg. https://doi.org/10.1007/978-3-642-16712-6_762

47. Miki, H., Okada, Y., & Hirokawa, N. (2005). Analysis of the kinesin superfamily: insights into structure and function. *Trends in cell biology*, *15*(9), 467–476. https://doi.org/10.1016/j.tcb.2005.07.006

48. Miki, H., Setou, M., Kaneshiro, K., & Hirokawa, N. (2001). All kinesin superfamily protein, KIF, genes in mouse and human. *Proceedings of the National Academy of Sciences of the United States of America*, *98*(13), 7004–7011. https://doi.org/10.1073/pnas.111145398

49. Miller, R. K., Heller, K. K., Frisèn, L., Wallack, D. L., Loayza, D., Gammie, A. E., & Rose, M. D. (1998). The kinesin-related proteins, Kip2p and Kip3p, function differently in nuclear migration in yeast. *Molecular biology of the cell*, *9*(8), 2051–2068. https://doi.org/10.1091/mbc.9.8.2051

50. Mitchison, T., & Kirschner, M. (1984). Dynamic instability of microtubule growth. *Nature*, *312*(5991), 237–242. https://doi.org/10.1038/312237a0

51. Mostowy, S., & Cossart, P. (2012). Septins: the fourth component of the cytoskeleton. *Nature reviews. Molecular cell biology*, *13*(3), 183–194. https://doi.org/10.1038/nrm3284

52. Nitta R., Hirokawa N. (2013) Kinesin: Fundamental Properties and Structure. In: Roberts G.C.K. (eds) Encyclopedia of Biophysics. Springer, Berlin, Heidelberg. https://doi.org/10.1007/978-3-642-16712-6_767

53. Nogales E. (2015). An electron microscopy journey in the study of microtubule structure and dynamics. *Protein science: a publication of the Protein Society*, *24*(12), 1912–1919. https://doi.org/10.1002/pro.2808

54. Nogales, E., Wolf, S. G., & Downing, K. H. (1998). Structure of the alpha beta tubulin dimer by electron crystallography. *Nature*, *391*(6663), 199–203. https://doi.org/10.1038/34465

55. Nsamba, E. T., Bera, A., Costanzo, M., Boone, C., & Gupta, M. L. (2021). Tubulin isotypes optimize distinct spindle positioning mechanisms during yeast mitosis. *The Journal of cell biology*, *220*(12), e202010155. https://doi.org/10.1083/jcb.202010155

56. Portran, D., Schaedel, L., Xu, Z., Théry, M., & Nachury, M. V. (2017). Tubulin acetylation protects long-lived microtubules against mechanical ageing. *Nature cell biology*, *19*(4), 391–398. https://doi.org/10.1038/ncb3481

57. Rice, L. M., Montabana, E. A., & Agard, D. A. (2008). The lattice as allosteric effector: structural studies of alphabeta- and gamma-tubulin clarify the role of GTP in microtubule assembly. *Proceedings of the National Academy of Sciences of the United States of America*, *105*(14), 5378–5383. https://doi.org/10.1073/pnas.0801155105

58. Rice, L. M., Moritz, M., & Agard, D. A. (2021). Microtubules form by progressively faster tubulin accretion, not by nucleation-elongation. *The Journal of cell biology*, *220*(5), e202012079. https://doi.org/10.1083/jcb.202012079

59. Roostalu, J., & Surrey, T. (2017). Microtubule nucleation: beyond the template. *Nature reviews. Molecular cell biology*, *18*(11), 702–710. https://doi.org/10.1038/nrm.2017.75

60. Roostalu, J., Thomas, C., Cade, N. I., Kunzelmann, S., Taylor, I. A., & Surrey, T. (2020). The speed of GTP hydrolysis determines GTP cap size and controls microtubule stability. *eLife*, *9*, e51992. https://doi.org/10.7554/eLife.51992

61. Schliwa, M., & Woehlke, G. (2003). Molecular motors. *Nature, 422*(6933), 759–765. https://doi.org/10.1038/nature01601

62. Sept, D., Baker, N. A., & McCammon, J. A. (2003). The physical basis of microtubule structure and stability. *Protein science: a publication of the Protein Society*, *12*(10), 2257–2261. https://doi.org/10.1110/ps.03187503

63. Taschner, M., & Lorentzen, E. (2016). The Intraflagellar Transport Machinery. *Cold Spring Harbor perspectives in biology*, *8*(10), a028092. https://doi.org/10.1101/cshperspect.a028092

64. Walczak, C. E., Gayek, S., & Ohi, R. (2013). Microtubule-depolymerizing kinesins. *Annual review of cell and developmental biology*, *29*, 417–441. https://doi.org/10.1146/annurev-cellbio-101512-122345

65. Walker, R. A., O'Brien, E. T., Pryer, N. K., Soboeiro, M. F., Voter, W. A., Erickson, H. P., & Salmon, E. D. (1988). Dynamic instability of individual microtubules analyzed by video light microscopy: rate constants and transition frequencies. *The Journal of cell biology*, *107*(4), 1437–1448. https://doi.org/10.1083/jcb.107.4.1437

66. Zhang, R., Alushin, G. M., Brown, A., & Nogales, E. (2015). Mechanistic Origin of Microtubule Dynamic Instability and Its Modulation by EB Proteins. *Cell*, *162*(4), 849–859. https://doi.org/10.1016/j.cell.2015.07.012

Books

1. Keiser, G. (2016). Basic Principles of Light. In: Biophotonics. Graduate Texts in Physics. Springer, Singapore. https://doi.org/10.1007/978-981-10-0945-7_2

2. Lodish, Harvey et al. (2016). *Molecular Cell Biology*. W.H. Freeman (8th ed., pp. 777; 782; 836).

3. Pollard, Thomas D. et al. (2017). *Cell Biology*. Elsevier (3rd ed., pp. 574; 593-612; 623-647; 659-669).

Other sources

1. Britannica, T. Editors of Encyclopaedia (2021, December 21). *cytoskeleton. Encyclopedia Britannica*. https://www.britannica.com/science/cytoskeleton